

DEVELOPMENT OF RARE EARTH-FREE NEGATIVE ELECTRODE
MATERIALS FOR NiMH BATTERIES

A THESIS SUBMITTED TO
THE GRADUATE SCHOOL OF NATURAL AND APPLIED SCIENCES
OF
MIDDLE EAST TECHNICAL UNIVERSITY

BY

EZGİ ONUR ŞAHİN

IN PARTIAL FULFILLMENT OF THE REQUIREMENTS
FOR
THE DEGREE OF MASTER IN SCIENCE
IN
METALLURGICAL AND MATERIALS ENGINEERING

AUGUST 2016

Approval of the thesis:

**DEVELOPMENT OF RARE EARTH-FREE NEGATIVE ELECTRODE
MATERIALS FOR NiMH BATTERIES**

submitted by **EZGİ ONUR ŞAHİN** in partial fulfilment of the requirements for the degree of **Master in Science in Metallurgical and Materials Engineering Department, Middle East Technical University** by,

Prof. Dr. Gülbin Dural Ünver
Dean, Graduate School of **Natural and Applied Sciences** _____

Prof. Dr. C. Hakan Gür
Head of Department, **Metallurgical and Materials Engineering** _____

Prof. Dr. Tayfur Öztürk
Supervisor, **Metallurgical and Materials Engineering Dept., METU** _____

Examining Committee Members:

Prof. Dr. M. Kadri Aydınol
Metallurgical and Materials Engineering Dept., METU _____

Prof. Dr. Tayfur Öztürk
Metallurgical and Materials Engineering Dept., METU _____

Assoc. Prof. Dr. H. Emrah Ünalın
Metallurgical and Materials Engineering Dept., METU _____

Assoc. Prof. Dr. Y. Eren Kalay
Metallurgical and Materials Engineering Dept., METU _____

Assist. Prof. Dr. Gülhan Çakmak
Metallurgical and Materials Engineering Dept., MSKU _____

Date: 8/24/2016

I hereby declare that all information in this document has been obtained and presented in accordance with academic rules and ethical conduct. I also declare that, as required by these rules and conduct, I have fully cited and referenced all material and results that are not original to this work.

Name, Last Name: Ezgi ONUR ŞAHİN

Signature:

ABSTRACT

DEVELOPMENT OF RARE EARTH-FREE NEGATIVE ELECTRODE MATERIALS FOR NiMH BATTERIES

Onur Şahin, Ezgi

M.Sc., Department of Metallurgical and Materials Engineering

Supervisor: Prof. Dr. Tayfur Öztürk

August 2016, 94 pages

Ni/MH battery negative electrodes normally make use of rare earth AB₅ compounds. Development of rare earth-free negative electrode materials for Ni/MH batteries is desirable so as to lower the cost, and widen the availability. Although there are a number of alternatives, of these AB₂ alloys are particularly attractive, as they offer better capacities than AB₅. A major problem in this group of alloys is that they are difficult to activate, i.e. they require a large number of cycles before they could reach their full capacity.

The present work concentrates on a Laves phase C14 AB₂ alloy, (TiZr)(VNiMnCrSn)₂, and aims to develop methods for their rapid activation. The study examines the methods in two groups. In one, the methods aim to increase the surface area of the powders and in the other the methods aim for surface modifications.

Pristine alloy had zero initial capacity, which has increased to and saturated at 220 mAh/g after 14 cycles. So as to examine the effect of surface area on activation two methods were used; sieving and ball milling. AB₂ powder was sieved into different particle sizes, namely d(0.5)=37.3, 62.7 and 82.5 µm. It was found that with coarse particles, the activation was relatively fast reaching a capacity of 245 mAh/g after 7-8 cycles. The fast activation of coarse particles was attributed to the ease of particle fragmentation which led to the generation of new fresh surfaces. Electrodes with fine powders (e.g. d(0.5) = 37.3 µm) activates later with a lower saturation capacity. The low saturation capacity was attributed

to ineffective utilization of the active powder, i.e. a fraction of powders not in contact with the electrode.

Ball milling was more effective in improving the activation behaviour of the alloy. Milling of powders leads initially to a decrease in particle size. But with prolonged milling the particles do agglomerate yielding particle sizes similar to the initial one. A saturation capacity of 330 mAh/g was obtained after 5-6 cycles, which is slightly above the expected capacity of the powder based on the PCI curve measured with gas phase storage. The saturation capacity was less with prolonged milling.

For surface modifications, the main method used involved hot alkaline treatment. This included treating the AB₂ powder in boiling 6M KOH solution for various periods of time before the electrode was prepared. KOH treatment was effective in all cases, as the electrode was fully active after 1-2 cycles. SEM examination of treated alloy has shown that KOH treatment results in the leaching of powders leaving behind a nickel rich surface layer.

The saturation capacity has steadily increased with increased duration of the treatment reaching a maximum value of 390 mAh/g after 80 minute-treatment. This capacity is very much higher than the gas phase storage capacity of the alloy expected at 1 atm hydrogen pressure, i.e. 1.2 wt. % H corresponding to 320 mAh/g. This was attributed to the formation of rough surfaces generated by the treatment, as such surfaces could stabilize hydrogen bubbles whereby allowing an increase in local hydrogen evolution pressure.

Another method under investigation in the current study was NiO coating of AB₂ powders. For this purpose, using sol-gel approach pristine particles were coated with NiO which upon charging in the electrode would be reduced to Ni, thus aiming for the formation of Ni rich surfaces as in KOH treatment. Two routes were employed; one with the use NiCl₂, and the other with the use of NiNO₃. Of these, with details used in the present work, only the second route gave a capacity, but overall activation performance in all samples were poor.

Keywords: electrochemical hydrogen storage, AB₂ Laves phase alloys, (Ti_{0.36}Zr_{0.64})(V_{0.15}Ni_{0.58}Mn_{0.20}Cr_{0.07})₂, activation, sieving, ball milling, boiling KOH treatment, NiO coating, pressed electrode, pasted electrode, particle drop-out

ÖZ

NiMH BATARYALAR İÇİN NADİR TOPRAK ELEMENTİ İÇERMEYEN NEGATİF ELEKTROTLARIN GELİŞTİRİLMESİ

Onur Şahin, Ezgi

Y. Lisans, Metalurji ve Malzeme Mühendisliği Bölümü

Tez Yöneticisi: Prof. Dr. Tayfur Öztürk

Ağustos 2016, 94 sayfa

Ni/MH batarya negatif elektrotlarında yaygın olarak nadir toprak elementi içeren AB₅ bileşikleri kullanılmaktadır. Ni/MH bataryalar için nadir toprak elementi içermeyen negatif elektrot malzemelerinin geliştirilmesi, malzemelerin temin edilebilirliği ve düşük maliyet açısından önemlidir. Birkaç alternatif olmakla beraber, bu alternatifler arasında AB₂ alaşımları AB₅ bileşiklerine göre daha yüksek kapasite sunmaları nedeniyle özellikle caziptir. Bu alaşım grubunun en önemli problemi zor aktive olmaları, başka bir deyişle tam kapasiteye ulaşılması için nispeten fazla sayıda şarj-deşarj döngüsü gerektirmeleridir.

Bu çalışma, Laves fazlı C14 yapısında (TiZr)(VNiMnCrSn)₂ kompozisyonlu AB₂ alaşımını konu almakta ve hızlı aktivasyonu için yöntemlerin geliştirilmesini amaçlamaktadır. Çalışmada yöntemler iki grupta incelenmektedir. İlkinde parçacıkların yüzey alanındaki artışın etkisi incelenmekte, ikincisinde ise yüzey modifikasyonunun etkileri incelenmektedir.

İşlem görmemiş alaşım elektrokimyasal ölçümlerinde sıfır olan başlangıç kapasitesi 14 döngü ile artarak 220 mAh/g'lık doyum kapasitesine ulaşmıştır. Yüzey alanının etkisini incelemek amacıyla eleme ve öğütme olmak üzere iki farklı metot kullanılmıştır. AB₂ alaşım tozu d(0.5)=37.3, 62.7 ve 82.5 µm olmak üzere farklı parçacık boyutları elde edilecek şekilde elenmiştir. Ölçümler sonucunda iri parçacıklarla aktivasyonun daha hızlı olduğu ve 7-8 döngü sonrasında 245 mAh/g'lık bir kapasiteye ulaşıldığı görülmüştür. İri

parçacıkların hızlı aktivasyonu taze yüzeylerin açığa çıkmasına yol açan parçacık ufalanması ile açıklanmıştır. İnce toz ($d(0.5) = 37.3 \mu\text{m}$) ise daha geç aktive olmakta ve düşük doyum kapasitesi vermektedir. Düşük doyum kapasitesinin aktif tozun bir kısmının elektrotla teması kaybetmesinden kaynaklandığı düşünülmektedir.

Öğütme, alaşımın aktivasyon davranışını iyileştirmede daha etkindir. Tozun kısa süreli öğütülmesi parçacık boyutunda düşüşe neden olmuştur. Fakat uzayan öğütme süresi ile parçacıklar topaklanmakta ve böylelikle parçacık boyutu nispi bir artış göstermektedir. 5-6 döngü ile 330 mAh/g 'lık bir doyum kapasitesi elde edilmiştir. Bu kapasite tozun beklenen kapasitesi, yani gaz fazında ölçülmüş basınç-kompozisyon-eşsıcaklık eğrisinden beklenen olan kapasiteden bir miktar yüksektir. Uzayan öğütme süresi ile doyum kapasitesinde düşme oluşmaktadır.

Yüzey modifikasyonu olarak kullanılan ana yöntem sıcak KOH işlemidir. Bu yöntemde elektrot hazırlama öncesi AB_2 tozu değişen süreler ile kaynayan 6M KOH çözeltisi içerisinde bekletilmektedir. İncelenen tüm durumlarda sıcak KOH işlemi etkili olmuştur. 1-2 döngü içerisinde alaşımın aktive olduğu görülmüştür. Yapılan işlemde alaşım parçacıklarının nikelce zengin bir yüzey bırakarak liç olduğu gözlemlenmiştir.

İşlem süresinin artması ile doyum kapasitesi artarak 80 dakikalık işlem ile en yüksek kapasiteye, 390 mAh/g 'a ulaşmıştır. Bu değer, alaşımın 1 atm hidrojen basıncı altında gaz fazı depolama değeri olan kütlece $1.2 \% \text{ H}$ 'in (320 mAh/g) üzerindedir. Bu iyileşme sonucu pürüzlü yüzey oluşumuna bağlanmış ve pürüzlü yüzeylerin hidrojen baloncuklarını kararlı hale getirerek yerel hidrojen basıncını arttırdığı sonucuna varılmıştır.

İncelenen bir diğer metot AB_2 alaşım tozunun NiO ile kaplanmasıdır. Bu amaçla işlem görmemiş parçacıklar sol-jel yöntemi ile NiO ile kaplanmış ve elektrotun şarj edilmesi ile Ni'e dönüşmesi hedeflenmiş ve bu şekilde KOH işleminde olduğu gibi nikelce zengin yüzey oluşturması amaçlanmıştır. İzlener iki yöntemden birinde NiCl_2 , diğerinde ise NiNO_3 kullanılmıştır. İçeriği detaylı olarak anlatılmış olan bu yöntemlerden yalnızca ikincisi ile kapasite elde edilmiş fakat her iki örneğin de aktivasyon performansı zayıf bulunmuştur.

Anahtar kelimeler: elektrokimyasal hidrojen depolama, AB_2 Laves fazlı alaşımlar, $(\text{Ti}_{0.36}\text{Zr}_{0.64})(\text{V}_{0.15}\text{Ni}_{0.58}\text{Mn}_{0.20}\text{Cr}_{0.07})_2$, aktivasyon, eleme, öğütme, kaynayan KOH işlemi, NiO kaplama, preslenmiş elektrot, sıvalı elektrot, parçacık dökülmesi

To my late uncle, Cumhuriyet...

ACKNOWLEDGEMENTS

I would like to mention that part of this thesis was published as “Activation behavior of an AB₂ type metal hydride alloy for NiMH batteries” *International Journal of Hydrogen Energy*, 41, 9948-9953, co-authored by Semra Tan, Yang Shen, Dag Noréus and Tayfur Öztürk. Financial support for this study by the Scientific and Technological Research Council of Turkey (TÜBİTAK) under Grant No. 112M193 was gratefully acknowledged.

Firstly, for his supervision, advice, support and for his contributions in this thesis; I would like to express my gratitude to my supervisor Prof. Dr. Tayfur Öztürk. I feel lucky to be his student since my undergraduate years.

Thanks to my labmates Fatih Pişkin, Cavit Eyövgü, Hatice Gözde Yıldırım, Doğançan Sarı, Necmi Avcı and earlier members Burak Aktekin, Alptekin Aydınli, Assist. Prof. Dr. Gülhan Çakmak and Dr. Semra Tan and to all my friends in this department.

Thanks to my life-long friends who were with me throughout many years and who will always be there.

Finally, thanks for the ones who have paved the way for my education and all the skills I have obtained until now; my brother Mustafa Can Onur, mother Canan Onur, father İbrahim Ersin Onur, my husband Alper Şahin and to my whole family with my respect and gratitude for supports in the path of being me.

TABLE OF CONTENTS

ABSTRACT.....	v
ÖZ.....	vii
ACKNOWLEDGEMENTS.....	x
TABLE OF CONTENTS.....	xi
LIST OF TABLES.....	xiii
LIST OF FIGURES	xiv
CHAPTERS	
1. INTRODUCTION	1
2. LITERATURE REVIEW	3
2.1. Overview of Negative Electrode Materials for Ni/MH Batteries	3
2.1.1. AB ₅ alloys	6
2.1.2. AB compounds.....	7
2.1.3. BCC solid solutions	8
2.1.4. Mg alloys	9
2.1.3. AB ₂ alloys	11
2.2 Activation Methods for AB ₂ Based Alloys.....	16
2.2.1 Activation via new surfaces	17
2.2.2 Activation via surface modification.....	19
2.3 Measurement of Electrochemical Performance	22
2.3.1 Architecture of negative electrodes in Ni/MH batteries	22
2.3.2 Architecture of negative electrodes for electrochemical measurements ..	26
3. EXPERIMENTAL.....	31
3.1 Materials	31
3.2 Processing	31
3. 2. 1 Sieving	31
3.2.2 Ball milling	32
3.2.3 KOH treatment.....	33

3.2.4 NiO coating.....	33
3.3 Electrochemical Measurements	34
3.4 Material Characterization.....	38
4. RESULTS AND DISCUSSION.....	39
4.1 Characterization of AB ₂ Alloy.....	39
4.2 Activation via Increased Surface Area	42
4.2.1 Ball milling	42
4.2.2 Sieving	45
4.3 Activation via Surface Modification.....	47
4.3.1 KOH treatment.....	48
4.3.2 NiO coating.....	54
4.4 Discussion.....	60
5. CONCLUSIONS	67
REFERENCES	69
APPENDICES	77
APPENDIX A: EFFECT OF PLASMA PROCESSING ON ELECTROCHEMICAL BEHAVIOUR OF AN AB ₂ ALLOY.....	77
APPENDIX B: Mg-Cu ALLOYS AS NEGATIVE ELECTRODES FOR Ni/MH BATTERIES.....	87

LIST OF TABLES

TABLES

Table 2.1: Negative electrode materials studied in Ni/MH batteries and their capacities (Adapted from Chandra et al., 1996)	5
Table 2.2: Electrochemical hydrogen capacities of Laves phases (Cuevas & Joubert, 2001)	13
Table 2.3: Electrochemical properties of C14 dominated, C14/C15 equal abundance and C15 dominated alloys (Young et al., 2010)	13
Table 2.4: Electrochemical measurement details from different studies	29
Table 4.1: Composition of the alloy according to the results of the EPMA analysis.	39
Table 4.2: EDS analysis of a lamellar region in AB ₂ alloy.....	41

LIST OF FIGURES

FIGURES

Figure 2.1: Ni/MH battery operation scheme (Liu et al., 2011)	3
Figure 2.2: Electrochemical reactions at the electrode/electrolyte surface during charge (a) and discharge (b) (Young, et al., 2011).	4
Figure 2.3: Comparison of the rechargeable battery technologies as a function of volumetric and specific energy densities (Landi et al., 2009)	5
Figure 2.4: Crystal structure of LaNi ₅ alloy (a) and the tetrahedral sites and (b) octahedral sites (c) for hydrogen occupancy (Liu et al., 2011)	6
Figure 2.5: Crystal structures of cubic TiNi (a) and monoclinic TiNi (b) (Cuevas & Joubert, 2001)	7
Figure 2.6: Crystal structures of Mg ₂ Ni (a) and Mg ₂ Cu (b)	9
Figure 2.7: Crystal structures of C14 (a) and C15 (b) Laves phases and the possible sites for hydrogen occupancy (Liu et al., 2011).....	12
Figure 2.8: Partial isothermal section (at. %) at 1000 ⁰ C of the Zr-Cr-Ni phase diagram (Joubert et al., 1996)	14
Figure 2.9: The surface of the metal hydride must be able to transport hydrogen to the interior of the particle, provide catalytic activation helping to break and form an O–H bond and protect the particle from further oxidation (Ye et al., 2013).	16
Figure 2.10: Ellingham diagram for oxides (Shen et al., 2015). Note that Zr and Ti are located far below as compared to others.	17
Figure 2.11: Surface morphology of the 5 min 1% HF treated bulk sample before (a) and after (b) the treatment (Sun et al., 2002).	20

Figure 2.12: Change in surface composition with respect to time. Note that the composition becomes Ni rich as duration of treatment increases (Choi et al., 1999).	21
Figure 2.13: The negative electrode, separator and the positive electrode of the battery	23
Figure 2.14: Binder, conductive additive and active particle in a slurry (Roscher et al., 2011)	24
Figure 2.15: Images of sintered (a) and pasted (b) electrodes under SEM-BEI (Linden & Reddy, 2011)	25
Figure 2.16: SEM micrograph of Ni foam.....	25
Figure 3.1: Particle size distribution of the unsieved AB ₂ alloy.....	31
Figure 3.2: The sieve shaker with the sieves	32
Figure 3.3: (a) Retsch planetary ball mill and the (b) 50 cc vial	32
Figure 3.4: (a) AB ₂ powder and 6M KOH solution and (b) KOH treatment	33
Figure 3.5: (a) NiCl ₂ .6H ₂ O and (b) NiNO ₃ .6H ₂ O which were used in the first and second routes respectively.	34
Figure 3.6: Illustration of single compartment cell. Note that the working electrode is a pressed electrode, counter electrode is a Ni mesh and reference electrode is a Zn rod.	35
Figure 3.7: Illustration of double compartment cell. Note that the working electrode is a foam electrode, counter electrode is a Ni sheet and reference electrode is a Hg/HgO.....	35
Figure 3.8: Photographs of (a) negative electrode prepared with pellet and mesh and (b) corresponding counter electrode for electrochemical measurements.	36
Figure 3.9: Photographs of (a) cell used in the electrochemical charge-discharge measurement for electrode prepared by pellet and mesh and b) Lanhe CT2001A battery tester.....	36

Figure 3.10: Photographs of (a) negative electrode prepared with paste and foam and (b) corresponding counter electrode for electrochemical measurements.	37
Figure 3.11: Photographs of (a) the electrochemical charge-discharge measurement setup for electrode prepared by paste and foam and (b) Gamry Interface 1000 potentiostat/galvanostat/ZRA.	38
Figure 4.1: Fitted XRD pattern of AB ₂ powder. Note that the alloy contains a secondary phase besides predominant C14 phase.	40
Figure 4.2: Phase distribution in AB ₂ alloy under SEM (powder mounted in epoxy, polished and etched) at (a) 2000x and (b) 16000x.....	40
Figure 4.3: Pressure-composition isotherm of pristine AB ₂ alloy at 30°C. Note that the alloy shows 1.2 wt. % gaseous phase hydrogen storage capacity at 1 atm which corresponds to 320 mAh/g (Young, personal communication, May 19, 2015).....	41
Figure 4.4: SEM images of (a) unmilled and ball milled AB ₂ powder after (b) 1, (c) 3 and (d) 5 hours of milling.	42
Figure 4.5: Particle size distribution of powders resulting from 1h, 3 h and 5 h milling. The distribution of starting powder was also included for comparison.	43
Figure 4.6: Discharge capacity vs. cycle number for pressed electrodes prepared from AB ₂ powders milled for 1, 3 and 5 hours. Data for pristine alloy is included for comparison.....	44
Figure 4.7: Particle size distributions for AB ₂ particles: +38/-45 μm, +53/-63 μm and +75/-90 μm. Note that d(0.5) values for these intervals are 37.3 μm, 62.7 μm and 82.5 μm respectively.....	45
Figure 4.8: Discharge capacity-cycle number plot of pressed electrodes of powders sieved into separate batches yielding average particle sizes of d(0.5) of 37.3, 62.7 and 82.5 μm. Data for the unsieved powder is also included for comparison.....	46
Figure 4.9: Discharge capacity-cycle number plot of foam electrodes of powders sieved into separate batches yielding average particle sizes of d(0.5) of 37.3, 62.7 and 82.5 μm. Data for the unsieved powder is also included for comparison.....	47

Figure 4.10: SEM images of the surfaces of (a) untreated powder and powders subjected to hot KOH treatment for (b) 20, (c) 60 and (d) 80 minutes.....	48
Figure 4.11: Discharge capacity vs. cycle number plot of the pressed electrodes prepared from powders treated in boiling KOH solution for 20, 60 and 80 minutes. Data of pristine powder is also included for comparison (Tan et al., 2016).....	49
Figure 4.12: SEM image of the surface of AB ₂ powder subjected to hot KOH treatment for 100 minutes.	50
Figure 4.13: Change in amount of present elements by increasing KOH treatment duration obtained by EPMA.	51
Figure 4.14: SEM images of the mixture collected over 80 minute KOH treated AB ₂ powders observed at (a) 2000x and (b) 8000x. Note that mixture also contains some AB ₂ particles.	51
Figure 4.15: (a) EDS analysis and (b) XRD pattern of the mixture collected over 80 minute KOH treated AB ₂ powders. Note that the angles at which Ni(OH) ₂ peaks and C14 peaks are given on the XRD pattern.....	52
Figure 4.16: SEM images of AB ₂ powders mounted in epoxy and KOH treated for (a and b) 20 minutes, (c and d) 60 minutes, (e and f) 80 minutes and (g and h) 100 minutes. Note that the images for 100 minute treated powders are at 10000x and 60000x magnification and the rest is at 60000x and 120000x.....	53
Figure 4.17: Discharge capacity vs. cycle number plot of the foam electrodes prepared from powders treated by boiling KOH solution for 20, 60 and 80 minutes. Note that the data of pristine powder is also included for comparison.....	54
Figure 4.18: SEM image of NiO coating in the absence of AB ₂ powders using NiCl ₂ precursor.	55
Figure 4.19: XRD pattern of NiO coating by sucrose and NiCl ₂ precursors. Note that the pattern is compatible with NiO.	55
Figure 4.20: SEM image of AB ₂ powder coated using NiCl ₂ precursor. The gelled mixture was calcined at 650°C.....	56

Figure 4.21: Discharge capacity vs. cycle number plot of the pressed electrodes prepared from powders coated by sol-gel methods that use NiCl ₂ as precursor. Data of pristine powder is also included for comparison.	56
Figure 4.22: Discharge capacity vs. cycle number plot of the foam electrodes prepared from powders coated by sol-gel methods that use NiCl ₂ as precursor. Data of pristine powder is also included for comparison.	57
Figure 4.23: SEM image of NiO coating in the absence of AB ₂ powders using NiNO ₃ precursor.	58
Figure 4.24: XRD pattern of NiO coating by EG and NiNO ₃ precursors. Note that the material contains Ni peaks.	58
Figure 4.25: SEM image of AB ₂ powder coated using NiNO ₃ as precursor. The gelled mixture was calcined at 200°C.	58
Figure 4.26: Discharge capacity vs. cycle number plot of the pressed electrodes prepared from powders coated by sol-gel methods that use NiNO ₃ as precursor. Note that the data of pristine powder is also included for comparison.	59
Figure 4.27: Discharge capacity vs. cycle number plot of the foam electrodes prepared from powders coated by sol-gel methods that use NiNO ₃ as precursor. Note that the data of pristine powder is also included for comparison.	60
Figure 4.28: PCI curve of the AB ₂ alloy. Note that at 1 bar the alloy gives a gas phase capacity of 1.2 wt. % hydrogen which corresponds to 320 mAh/g electrochemical storage capacity.	64
Figure 4.29: Discharge capacity vs. cycle number of the foam and pressed electrodes prepared from coarse powders.	65
Figure 4.30: 3D structure of (a) unpressed nickel foam and (b) resulting 2D structure after pressing.	65

CHAPTER 1

INTRODUCTION

As the fossil fuel reserves are being depleted, development of strong alternatives that are renewable, clean, and safe is becoming more important. One of the most important activities in energy research concentrates on transportation as it is a must for the daily life but contribute quite substantially to environmental pollution. Development of pure electric vehicles (EV) attract more and more attention as they can be improved to use easy, clean and abundant fuelling. Regarding environmental concerns EV development necessitate powerful design of energy storage materials and devices like fuel cells and batteries (Yu et al., 2001).

Hydrogen, being the lightest element in the periodic table, plays a very important role in providing clean and useful energy carriage. When hydrogen is burnt only water (H_2O) forms. Due to its high gravimetric specific energy, storing hydrogen and using it when needed could be a solution to energy needs. It can be stored in different ways; gaseous storage which necessitate compression -that might be hazardous in some applications. It can be stored in liquid form where the temperature would be 20 degrees above the absolute zero. The small atoms of hydrogen can also be stored “in” materials. Metal hydrides can hold up to 7% hydrogen by weight. Considering the volumetric efficiency, storing hydrogen as metal hydride is considered more efficient when compared to other forms of hydrogen storage. Ability to be stored within the material makes hydrogen storage a wide research area that opens up new horizons for many different applications. It is possible to burn hydrogen in internal combustion engine, but it can be made use of more efficiently either in fuel cells or batteries. One of the most practical and safe methods of using hydrogen is in nickel/metal hydride battery where the energy is stored and retrieved electrochemically.

Since the initial development in 1970's Ni/MH batteries have come a long way from small electronic devices to hybrid electric vehicles. In fact, first application of batteries in electric car is Toyota Prius which makes use 28 modules that have 6500 mAh capacity and are composed of (1.2 V) 6 NiMH cells (Taniguchi et al., 2001). Although recently emphasis has shifted away from NiMH batteries, where the safety is important it is still the battery of choice. In fact, there is a revival of Ni/MH batteries recently as it offers charge and discharge cycles more than 2000, fast charging ability, and full recyclability. Current designs enable the utilization rate of the active materials yielding 95% of the theoretical capacity (Yartys et al., 2016). In fact, there is an increasing demand for such batteries for tailoring wind and solar energy. Successful applications have been reported both for solar and wind energy reaching a power rating of as high as 10 MW (Nishimura et al., 2013).

Commercial Ni/MH batteries have traditionally been based on AB₅ alloys as negative electrode material. This compounds are based on rare-earth elements, as exemplified by (La_{0.65}Ce_{0.25}Pr_{0.03}Nd_{0.07})(Ni_{0.73}Co_{0.15}Mn_{0.06}Al_{0.06})₅ (Peng et al., 2013). However rare earth elements are subject to price fluctuation (Schüler et al., 2011). For instance, the price on average have increased 9 fold in 2012 (Y. Li et al., 2013). Due to such fluctuations it is desirable to find alternatives which are rare earth free.

Alternatives to AB₅ include AB alloys, V-based BCC alloys, Mg alloys and AB₂ alloys. Each has its own problems (Cuevas & Joubert, 2001). Of these AB₂ alloys are particularly attractive and come close to satisfy many of the requirements in negative electrode material. The difficulty in AB₂ alloys is that they are difficult to activate, i.e. a number of charge-discharge cycles need to be applied so as for the alloy to reach their full capacity.

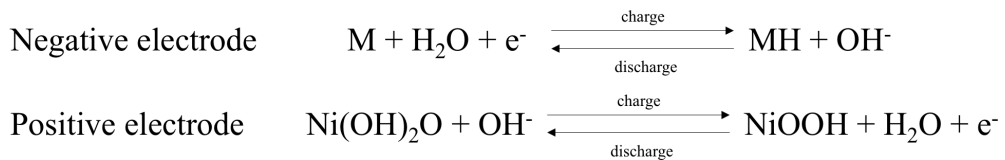
The current study therefore concentrates on treatments that could be applied to powders so that they are fully active once the battery is manufactured. The study focuses on AB₂ alloy, namely (Ti_{0.36}Zr_{0.64})(V_{0.15}Ni_{0.58}Mn_{0.20}Cr_{0.07})₂. The methods used in the current study fall into two groups. In one, processes were applied so as to increase the surface area of the powders. In the other the surface was modified with such methods as by hot alkaline treatment and NiO coating by sol-gel.

CHAPTER 2

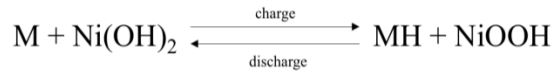
LITERATURE REVIEW

2.1. Overview of Negative Electrode Materials for Ni/MH Batteries

Ni/MH battery is composed of a negative electrode that is able to store hydrogen, a positive electrode (Ni(OH)₂), and alkaline electrolyte (Cuevas & Joubert, 2001). A typical Ni/MH battery operation scheme is given in Figure 2.1. Half-cell reactions during charging and discharging in Ni/MH batteries are as follows;



Thus the net reaction is



During charging hydrogen forms by the electrolysis of water at the electrode-electrolyte interface. H⁺ is then absorbed by the metal hydride negative electrode. (OH⁻) formed as a result of this electrolysis react with Ni(OH)₂ forming NiOOH, Figure 2.2.

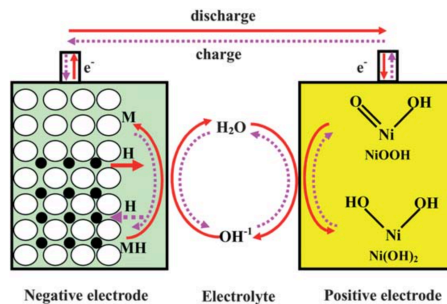


Figure 2.1: Ni/MH battery operation scheme (Liu et al., 2011)

Absorption of hydrogen by the negative electrode occurs in two stages. In the first stage hydrogen is attached (i.e. adsorption) to the surface. This adsorption of hydrogen to the electrode surface is of crucial importance regarding the performance of negative electrode. Surface exchange current density is a measure of the kinetics of this process which can be measured by special techniques (Zhao & Ma, 2009).

Following adsorption, hydrogen diffuses into the the lattice of the negative electrode material. Adsorption together with hydrogen diffusion in the lattice determines the kinetics of the process during charging. Diffusion coefficient in negative electrode material could be measured electrochemically as described by Yuan & Xu (2001). The diffusion rate is also relevant to the storage capacity. High diffusion rate of hydrogen at the electrode would promote the hydrogen diffusion into the lattice rather than the bubbling which might be caused when this is not the case.

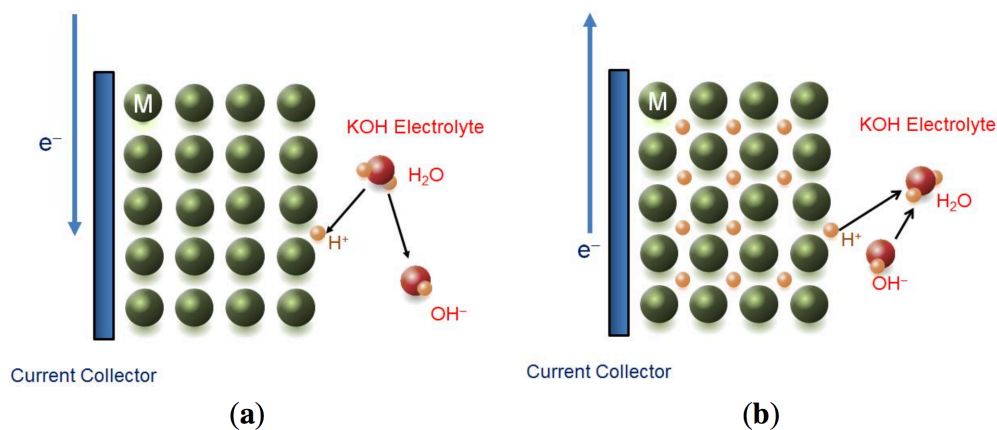


Figure 2.2: Electrochemical reactions at the electrode/electrolyte surface during charge (a) and discharge (b) (Young, et al., 2011).

A negative electrode for Ni/MH battery should meet a number of requirements. One of these refer to the amount of hydrogen that could be stored in the alloy. This is directly related to the discharge capacity of the battery. Equally important is that the alloy must be able to be charged and discharged hydrogen at the operating, i.e. normally ambient, conditions. In the strong oxidizing alkaline medium, the alloy should be stable, i.e. it must resist corrosion.

First studies with regard to hydrides within the context of Ni/MH batteries started in early 1970's with the alloy system Ti-Ni with Batelle-Geneva Research Center and

Daimler-Benz -Volkswagen AG group (Sakai et al., 1999). In 1970's research on AB₅ alloys was initiated by Phillips Laboratories. CNRS researchers have diversified AB₅ alloy by varying the rare-earth elements. Besides they applied surface treatments to alloy powders to obtain better performance. The negative electrode materials studied in Ni/MH batteries are given in Table 2.1.

Table 2.1: Negative electrode materials studied in Ni/MH batteries and their capacities (Adapted from Chandra et al., 1996)

Type of hydride	Metal/Alloy	Structure	Capacity (wt. % H)	Capacity (mAh/g)
Elemental	Pd	Fm3m	0.56	165
AB ₅	LaNi ₅	P6/mmm	1.37	372
AB ₂	TiNi ₂	Fd3m	1.70	460
A ₂ B	Mg ₂ Ni	P6mm	3.59	961
AB	TiFe	Pm3m	1.89	506
BCC	TiV ₂	BCC	2.6	696

Commercialization of Ni/MH batteries started in Japan in 1990. Comparing to Ni/Cd batteries, their counterparts in that time, Ni/MH batteries offered higher energy density, less environmental concerns but higher cost, Figure 2.3. With regulations for disposal of Ni/Cd batteries, usage of Ni/MH batteries expanded. In a five year-period, yearly production reached 310 million units (Uehara et al., 1997). Following these developments from 1991 to the present large-scale production of Ni/MH batteries is continued.

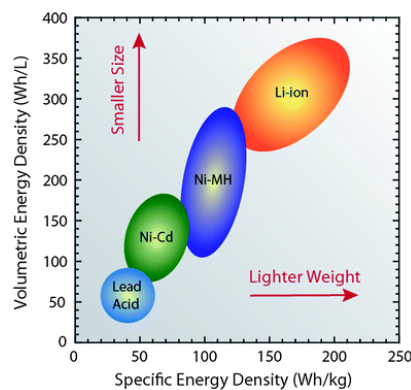


Figure 2.3: Comparison of the rechargeable battery technologies as a function of volumetric and specific energy densities (Landi et al., 2009)

2.1.1. AB₅ alloys

AB₅ alloys typified by LaNi₅ are widely used in commercial NiMH batteries. A site is normally occupied by La, Ce, Pr or Nd. La content was decreased starting from mid 1980's by replacement of mixed rare-earth elements called *mischmetal* (Mm) resulting in cost reduction as well as improvement in the electrochemical performance. The modification of B side started with the usage of Co besides Ni. This modification increases long term cyclic stability of the alloy at the expense of a decrease in storage capacity. In order to improve the capacity elements Mn and Al were added in addition to Co. Satisfactory results were obtained with MmNi_{3.55}Mn_{0.4}Al_{0.3}Co_{0.75} (Cuevas & Joubert, 2001).

AB₅ alloys have CaCu₅ hexagonal structure, Figure 2.4. The prototype LaNi₅ when hydrogenated it absorbs 1.43 wt. % hydrogen and forms LaNi₅H₆. It experiences 27.3 % volume expansion during hydrogenation. LaNi₅ gives discharge capacity of 372 mAh/g but the capacity decreases with cycling only, 12 % remains after 400 cycles. The decrease in capacity is observed due to formation of lanthanum hydroxide and decomposition of the alloy by cycling (Cuevas & Joubert, 2001). Improved version MmNi_{3.55}Mn_{0.4}Al_{0.3}Co_{0.75} on the other hand displays 332 mAh/g and retains half of its capacity at the end of 400 cycles (Adzic et al., 1995).

One of the main drawbacks of AB₅ alloys is their high rate discharge behaviour. When the alloy MmNi_{3.55}Mn_{0.4}Al_{0.3}Co_{0.75} is discharged at a rate of C/2, a discharge capacity is only half of the one that with C/10. When the discharge rate is increased to C/1 the capacity is nearly zero (Kaabi et al., 2016).

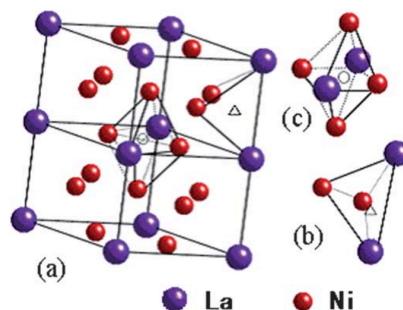


Figure 2.4: Crystal structure of LaNi₅ alloy (a) and the tetrahedral sites and (b) octahedral sites (c) for hydrogen occupancy (Liu et al., 2011)

LaNi₅ and other combinations of rare-earth metals with Co or Ni is claimed to have a positive effect on hydrogen evolution reaction in alkaline media and have exchange current densities comparable to Pd and Pt electrodes. According to Bocutti et al. (2000), this ease of hydrogen absorption in rare earth metals originates from their semi-empty d-orbitals.

2.1.2. AB compounds

There are a number of Ti and Zr-based AB alloys offering low specific weight and reasonable cost. They are mainly two groups; Ti-based; TiFe, TiCo and TiNi, and Zr-based; ZrNi and ZrCo. As an example, TiFe hydrogenates to TiFeH₂ with 2 wt. % hydrogen storage capacity resulting in lattice expansion of by 18.8 % (Cuevas & Joubert, 2001).

The most interesting AB compound is TiNi which undergoes a martensitic transformation at around ambient temperature. This alloy therefore shows shape memory behaviour. At high temperatures the compound has CsCl type cubic structure which upon cooling transforms into monoclinic martensite phase, Figure 2.5.

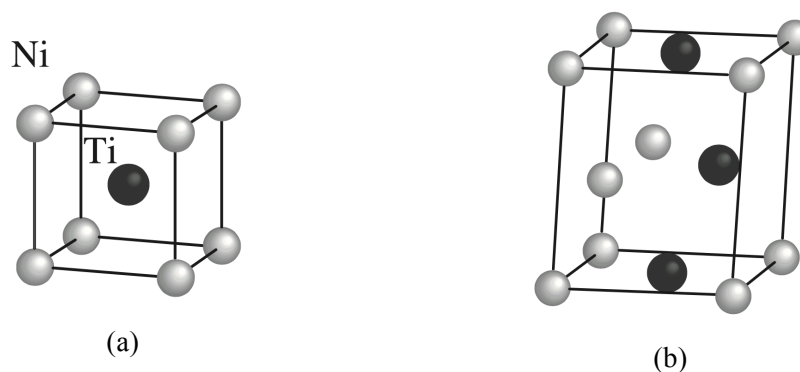


Figure 2.5: Crystal structures of cubic TiNi (a) and monoclinic TiNi (b) (Cuevas & Joubert, 2001)

Cubic TiNi when hydrided forms tetragonal TiNiH. Apart from expansion due to hydrogen, Ti atoms are also displaced. The alloy shows a sloping plateau in gas phase storage yielding 1.4 wt. % hydrogen storage capacity. This corresponds to an electrochemical capacity of 355 mAh/g. TiNi alloy however when electrochemically tested gives a much lower capacity of 245 mAh/g. Moreover, the cycle life is limited

where for instance 60 % of 245 mAh/g is lost after 300 cycles. The poor cycle life was attributed to a low corrosion resistance of the alloy. According to Cuevas & Joubert (2001), partial substitution of Ti with Zr increases both capacity up to 370 mAh/g and the cycle life.

On the positive side the exchange current density in this alloy is very high and electrocatalytic activity is similar to LaNi_5 . This was attributed to presence of metallic nickel clusters on the alloy surface.

Ti_2Ni phase is a secondary phase that could be present in Ti-Ni alloys. The two phase alloy containing both TiNi and Ti_2Ni was the earliest hydrogen storage material that was investigated. Presence of Ti_2Ni causes an increase in hydrogen storage capacity even if the phase itself has a low discharge capacity (i.e. 170 mAh/g). With 45 wt. % TiNi , the capacity of the two-phase alloy reaches 330 mAh/g. Ti_2Ni with its good electrocatalytic activity acts as a gate for hydrogen discharge.

2.1.3. BCC solid solutions

BCC hydrogen storage alloys differ from others due to their high hydrogen storage capacities (around 3 wt. %) which is nearly twice as high as that of LaNi_5 (Akiba & Okada, 2002). However, the reversible capacity is less than this value. The alloys normally display two plateaus in pressure-composition isotherm, the lower being far below 1 atm. Therefore, two hydrides are formed: first hydride that cannot be desorbed and the second one being responsible for the reversible capacity. In order to improve the capacity either the first hydride could be destabilized or the reversible capacity of the second hydride could be increased by tuning the amount of the elements (Tamura et al., 2003).

Examples to this type of alloys cover V-based compositions; V-Ti-Fe, V-Ti-Mn, V-Ti-Co, V-Ti-Cr, V-Ti-Ni. Tsukahara et al. (1996) reported that the single phase V-based solid solution could not give electrochemical discharge capacity due to its lack of electrocatalytic activity. For electrochemical activity they benefit from the presence of second phase (Akiba, 1999). The second phase, depending on the composition and alloy preparation method, may be TiNi or Laves phase. Okada et al. (2002) emphasize

the catalytic effect of TiNi which occur at grain boundaries. Similar effect was reported for Laves phase which when present besides the BCC phase in V-Ti-Ni and V-Zr-Ti-Ni alloys yields better activation performance and a high capacity (Tsukahara et al., 1996).

2.1.4. Mg alloys

Mg based alloys are also attractive materials for hydrogen storage due to their low density, abundance, and their high hydrogen capacity (7.6 wt. %). However, the problem with Mg-based hydrogen storage alloys is their high stability and poor hydrogenation-dehydrogenation kinetics (M. Zhu et al., 2013). These severe thermodynamic and kinetic limitations result in high desorption temperatures around 300°C to release the stored hydrogen at atmospheric pressure. Unless the necessary precautions are taken, Mg-based alloy oxidizes irreversibly in alkaline medium as is the case in Ni/MH batteries. This causes a decrease in the amount of active material and therefore lowers the capacity (Ruggeri & Roué, 2003).

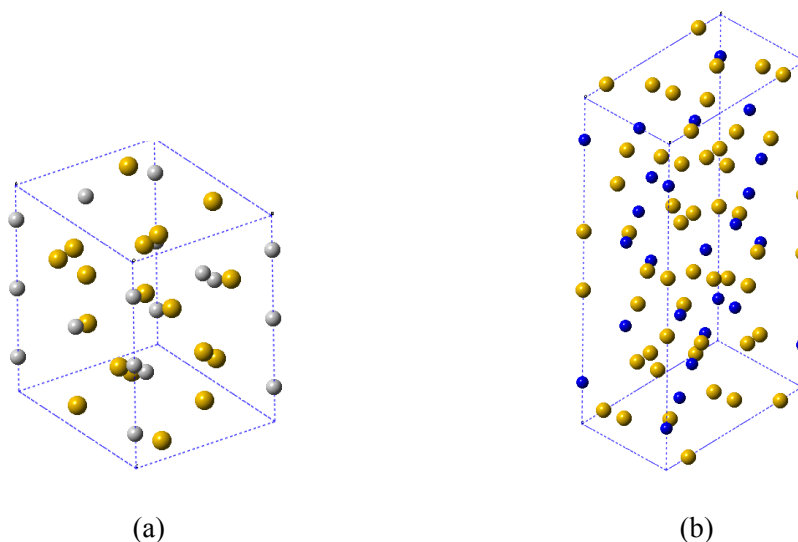
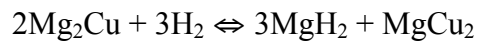


Figure 2.6: Crystal structures of Mg₂Ni (a) and Mg₂Cu (b)

Mg-alloys may be produced by mechanical alloying, melting or via solution based techniques. The most important representatives in this alloy system are hexagonal (C36) Mg₂Ni and orthorhombic (C15) Mg₂Cu as given in Figure 2.6. Mg₂Ni compound hydrogenates to Mg₂NiH₄ having 3.59 wt. % hydrogen storage capacity

which corresponds to an electrochemical capacity of 1080 mAh/g. This leads to an expansion of 32.1 % in the lattice (Chandra et al., 1996).

Similar to Mg-Ni system, Mg and Cu form Mg₂Cu (43.3 wt. % Mg) but as reported by Zhu et al. (2013) hydrogenation of this compound is not easy to reverse. Mg₂Cu undergoes disproportionation reaction during hydriding:



Hydrogen storage capacity depends on Mg and Cu contents. By increase in Mg content from 44.1 wt. % to 90.5 wt. %, the hydrogen content was increased from 2.72 to 6.62 wt. % (Sun et al., 1999). Electrochemically these values correspond to 729 mAh/g and 1775 mAh/g respectively. In a study by Akyıldız et al. (2006), 5.9 wt. % hydrogen capacity is obtained with Mg₉₀Cu₁₀ thin films at the desorption temperature around 100°C.

Jurczyk et al. (2008) used mechanical alloying in order to prepare the nanocrystalline Mg₂Ni and Mg₂Cu alloys with the average crystallite size of 20 nm. Electrochemical measurements showed 100 mAh/g discharge capacity for Mg₂Ni whereas 25 mAh/g was measured with Mg₂Cu alloy. In a separate study, Jurczyk et al. (2008) examined the effect of Pd addition to Mg₂Cu and Mg₂Ni. For Mg₂Cu alloy, the capacity remained the same with Pd addition (i.e. 25 mAh/g), with improvement in cyclic stability. In the case of Mg₂Ni the capacity was much higher and reached a value of 360 mAh/g.

In recent years a new family of alloys emerged, i.e. AB₃ or A₂B₇, containing some fraction of Mg which combine AB₂ with AB₅ alloys. Actually La-Mg-Ni alloys were studied a long time ago (Oesterreicher & Bittner, 1980). However, they did not attract much attention due to their low hydrogen desorption rates. In A₂B₇ the structure is composed of stacking of units of MgZn₂ (C14) i.e. AB₂ with CaCu₅, i.e. AB₅. The compositions were diversified with the addition of elements like Co, Mn, Al, Ni, Mo. The composition La_{0.7}Mg_{0.3}Ni_{2.8}Co_{0.5} gives a discharge capacity of 410 mAh/g. Unfortunately, this alloy had a low cyclic stability in alkaline electrolyte. Increase in Mg content, while giving rise to capacity, deteriorates cyclic stability. Cyclic stability can be improved by partial substitution of La with Ce. This is due to smaller change

in lattice volume with Ce upon hydriding and more importantly due to the formation of a protective surface film. However, this decreases the discharge capacity dramatically. For optimization Co and Al addition is proposed. These alloys still need to be improved to be used as negative electrode materials in Ni/MH batteries (Liu et al., 2011).

The main problem is corrosion of Mg-rich compositions. Therefore, Mg-alloys cannot be used as negative electrodes in Ni/MH batteries without anti-corrosion surface modifications. Maybe the most practical way of protecting the Mg-alloy particles from corrosion is coating with NAFION. NAFION solution (perfluorosulfonic acid-PTFT copolymer) is used either to coat the powder particles or the whole electrode. It forms a rough but continuous film on the surface that prevents direct contact of Mg-alloy particles with alkaline medium. As reported by Kim et al. (2013), NAFION coated pellets of MgNi composite give much higher capacity (408 mAh/g) than the bare pellets (156 mAh/g). The increase in discharge capacity is attributed due to protection of the alloy powders thus including all the active mass in hydrogenation process.

2.1.3. AB_2 alloys

Investigations on AB_2 -based alloys started quite early in 1970's with Ti-Ni alloys. This alloy has a stoichiometry of Ti:Ni = 1:2 that is equivalent to $TiNi_2$, which formed by combining TiNi and $TiNi_3$. Development of AB_2 alloys continued by compositional modifications with introduction of a number of common elements. Here A-side can be Ti, Zr or Hf while the B-side may be occupied by Ni, V, Cr, Cu, Co, Mn, Fe, Al, Sn. The use of abundant elements in AB_2 alloys make them economically attractive. AB_2 alloys are now the closest candidates to replace AB_5 alloys in Ni/MH batteries due to the capacity they offered, e.g. 438 mAh/g (Young et al., 2008). AB_2 alloys also have lower equilibrium pressures than AB_5 -type and they also have lower volume change when hydrogenated without a change in crystal structure. In addition to these they offer higher cyclic stability than AB_5 alloys (Du et al., 2001).

AB_2 alloys have Laves phase crystal structures. This is a close-packed structure with ratio of atomic radii, r_A/r_B , ideally 1.225 (Stein et al., 2004). There are three types of Laves phases: hexagonal C14, cubic C15 and again hexagonal C36 (intergrowth of

C14 and C15). In all of the structures A atom is surrounded by four A and twelve B atoms. The B atom is surrounded by six A and six B atoms. The hexagonal layers are differently stacked in each of these structures. C14 (prototype MgZn_2) and C15 (prototype MgCu_2) are the most frequently observed structures in AB_2 alloys (Huot et al., 1995), Figure 2.7.

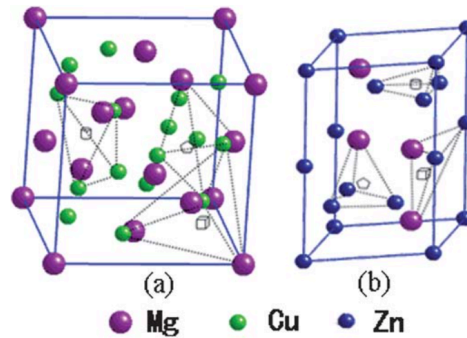


Figure 2.7: Crystal structures of C14 (a) and C15 (b) Laves phases and the possible sites for hydrogen occupancy (Liu et al., 2011)

Electrochemical hydrogen capacities of binary Laves phases are given in Table 2.2. The C14 and C15 phases contribute differently to the hydrogen storage properties. Modification in chemical composition, rapid quench or annealing yields different C14 and C15 amounts and performance. Due to difficulties in production, AB_2 alloys most of the time cannot be monophasic in the as-cast condition. Therefore, secondary phases are almost always present in AB_2 alloys.

As seen in the Table 2.2, ZrMn_2 has C14 crystal structure. As titanium is added to this alloy and the content increases, the average A-atom radius decreases from 1.694 to 1.675 Å due to the smaller size of the Ti-atom which stabilizes C14 further. For Zr–Ti–V–Ni system when the r_A/r_B ratio is less than 1.225, the crystal structure is C14-dominated (Young et al., 2008). For the formation of stable C14 phase electron-atom ratio ranges between 1.80-2.32 (Zhang et al., 1999). Huot et al. (1995) investigating NbM_2 and $\text{Zr}_{0.5}\text{Ti}_{0.5}\text{M}_2$ which are pure C14, observed improved high rate dischargeability, i.e. little drop in capacity with high rate of discharge.

ZrV_2 has C15 crystal structure. For the stable C15 phase to be formed the electron-atom ratio is either between 1.50-1.80 or higher than 2.32 (Zhang et al., 1999). This

structure occurs in $Zr_{1-x}Ti_x(Ni_{0.6}Mn_{0.3}V_{0.1}Cr_{0.05})_2$ with low Ti content (Du et al., 2001). This particular alloy as well as other C15 has higher hydrogen storage capacity, better high rate dischargeability but the alloys have low cycle life (Young et al., 2011). Young et al. (2010) comparing C15 with C14 pointed out that C14 could have superior performance in terms of high rate dischargeability.

Table 2.2: Electrochemical hydrogen capacities of Laves phases (Cuevas & Joubert, 2001)

Compound	Crystal structure	Capacity (mAh/g)
ZrV ₂	C15	750
ZrCr ₂	C15	520
ZrMn ₂	C14	480
TiCr _{1.9}	C14	640
TiMn _{1.6}	C14	390

Young et al. (2010) investigated alloys where both C14 and C15 were present. By modifying the amount of Co, Cr and Mn in Ti-Zr-V-Ni-Co-Cr-Mn-Al-Sn alloys they found that C14 was dominant in $Ti_{12}Zr_{21.5}V_{10}Ni_{40.2}Co_{1.5}Cr_{8.5}Mn_{5.6}Al_{0.4}Sn_{0.3}$, whereas in $Ti_{12}Zr_{21.5}V_{10}Ni_{40.2}Co_{5.0}Cr_{5.5}Mn_{5.1}Al_{0.4}Sn_{0.3}$ there were equal abundance of C14/C15 and in $Ti_{12}Zr_{21.5}V_{10}Ni_{40.2}Co_{8.0}Cr_{3.5}Mn_{4.1}Al_{0.4}Sn_{0.3}$ alloy was the C15 was dominant phase. The electrochemical performance of these alloys are reported in Table 2.3.

Table 2.3: Electrochemical properties of C14 dominated, C14/C15 equal abundance and C15 dominated alloys (Young et al., 2010)

Dominant crystal structure	Capacity (mAh/g)	Cycle life (70 %)	% HRD at 10 th cycle (100 mA/g)	Diffusion coefficient (cm ² /s)	Exchange current density (A/cm ²)
C14	401	615	89 %	5.6×10^{-10}	750
C14/C15	360	675	94 %	11.1×10^{-10}	640
C15	335	545	90 %	12.1×10^{-10}	390

Phases and intermetallics which occur in Zr-Cr-Ni system were determined by Joubert et al. (1996) in the form of ternary phase diagram given in Figure 2.8. Here it is interesting to follow the case of $ZrCr_2$. This alloy has C15 structure, but with addition of nickel it transforms into C14 and with further addition it transforms back to C15 (Cuevas & Joubert, 2001).

Multi-component AB_2 alloys often contain minor secondary phases besides Laves phases (Zhang et al., 1999). In Laves phase compounds $ZrMn_2$, $ZrCr_2$ and ZrV_2 atoms residing in A site can partially be replaced by Ti. It was reported that this partial substitution of zirconium with titanium results in a decrease in lattice parameter and leads to the formation of an additional BCC phase.

In AB_2 alloys BCC phase could be present as an additional phase. Akiba and Iba (1998) name these alloys Laves-phase related BCC solid solutions where the main phase is either C14 or C15. The alloys could have quite high capacity. For instance, (Young et al., 2016) reports a value for an Ti-V-Cr alloy which is as high as 938 mAh/g.

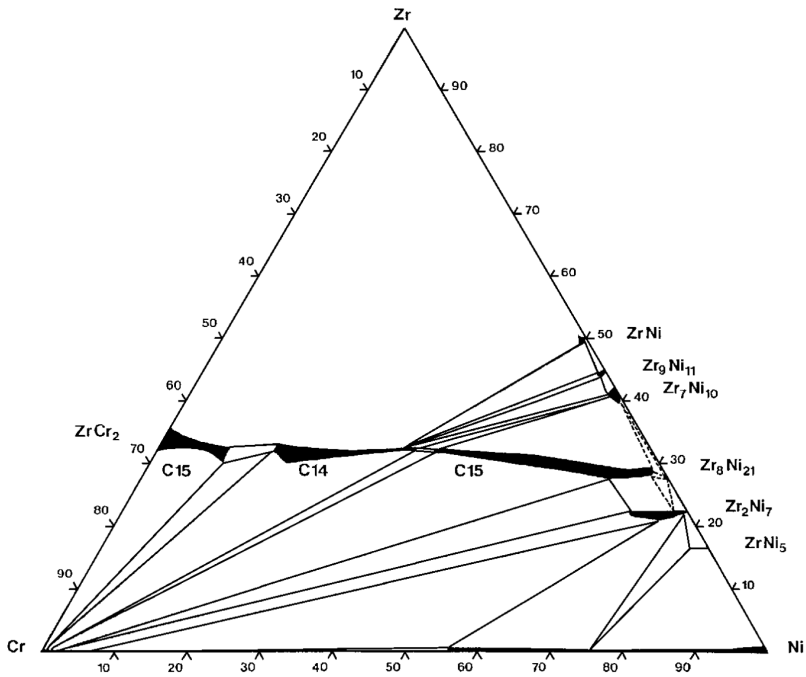


Figure 2.8: Partial isothermal section (at. %) at 1000⁰C of the Zr-Cr-Ni phase diagram (Joubert et al., 1996)

In a study by Homma et al. (2002) the alloy $V_{77.8}Zr_{7.4}Ti_{7.4}Ni_{7.4}$ with a phase ratio of Laves:BCC=4:1 was electrochemically charged and the hydrogen content in the alloy was determined by the change in lattice parameters of each phase. It was observed that before hydride is formed, hydrogen is dissolved in Laves phase rather than the BCC phase. As a result of this study it was concluded that hydrogen diffuses into the material via Laves phase but the phase offering main storage is BCC phase. Therefore, even if the main abundant phase is not BCC, a wide and effective distribution of BCC phase is important for hydrogen storage in these alloys. Thus this composition when compared to compositions such as $V_{54.5}Zr_{18.25}Ti_{11.25}Ni_{16}$ and $V_{17}Zr_{36}Ti_{17}Ni_{30}$, (with a decrease in vanadium content) where the phase ratio Laves: BCC increases there is a decrease in maximum amount of stored hydrogen (Homma et al., 2002).

Minor phases which could be present in AB_2 alloys include two AB phases, namely ZrNi and TiNi (Young et al., 2011). ZrNi phase or similar other phases Zr_9Ni_{11} and Zr_7Ni_{10} display different characteristics. Zr_7Ni_{10} has a good hydrogen storage capability whereas Zr_9Ni_{11} was considered to act as a very good catalyst in hydrogen sorption. Young et al. (2011), reported that the abundance of the latter phase, i.e. Zr_9Ni_{11} increases with Co, Al, Fe addition to the alloy and decreases with Sn, while the effect is just reverse for the former phase.

According to Young et al. (2011), at Zr:Ti = 32.3:9 only ZrNi is formed. However, when the ratio decreases from 26:9 to 21.5:12 only TiNi structure is observed. These two phases are very fine and the occupancy of the A-site was determined by the measurement of lattice parameters. Young et al. (2011) further concluded that Sn content was very effective in which AB minor phase is to be formed in the alloy. It was also stated the causes that suppress C14, TiNi and Zr_9Ni_{11} promotes the formation of C15, ZrNi and Zr_7Ni_{10} .

Despite superior discharge capacity and the other related properties, AB_2 alloys suffer from sluggish activation, i.e. alloys would develop their full capacity after a number of cycles. This is attributed to the presence of the dense oxide layer on the surface of the alloy particles. This layer prevents the use of the whole active mass, thus yielding

capacity less than that available. For the alloy to reach full capacity, the particles must somehow crack and eliminate this layer which requires charge-discharge cycles.

According to Züttel et al. (1995) in C15 dominated (with Zr_7Ni_{10} minor phase) $Zr(V_xNi_{1-x})_2$ alloys, partial substitution of zirconium with titanium results in a decrease in plateau pressure and provides better activation. This was due to the surface oxide layer which becomes loose when the composition was titanium rich. However, Kim et al. (1994) studying a C14 dominated $ZrCrNi$ alloy, did not observe any improvement with partial substitution of Zr with Ti. No improvement was observed in hydrogen storage properties, cycle life and activation. In this study, the decrease in cycle life was considered to result from high polarization resistance of titanium oxide formed on the alloy surface. Still, coexistence of Ti and Zr normally considered to have positive effect on the electrochemical performance, as well as in the corrosion resistance of the alloy.

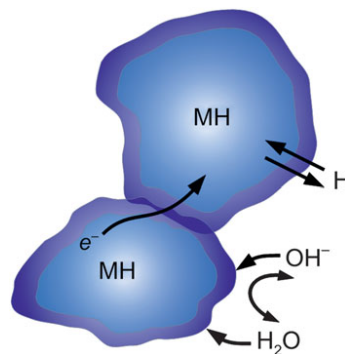


Figure 2.9: The surface of the metal hydride must be able to transport hydrogen to the interior of the particle, provide catalytic activation helping to break and form an O–H bond and protect the particle from further oxidation (Ye et al., 2013).

2.2 Activation Methods for AB_2 Based Alloys

As mentioned previously, AB_2 type alloys are promising negative electrode materials for rechargeable Ni/MH batteries. Such alloys, when compositions were optimized, offer high electrochemical discharge capacity and good cycle life compared to the rare earth containing AB_5 alloys (Liu & Lee, 1997). However, AB_2 alloys suffer from slow activation. It is known that particle surface is of vital importance regarding activation. The alloys in question contain elements like Zr and Ti which can oxidize relatively

easily, as can be seen from the Ellingham Diagram given in Figure 2.10. Thus the alloy particles are normally wrapped by an oxide layer. Therefore, AB₂ alloys require many charge-discharge cycles to break these oxide layers and to obtain the full charge capacity.

Many methods are employed for easy and early activation of these alloys. These methods may be examined in two major groups: the one aims for generation of new fresh surfaces, the other aims for surface modifications.

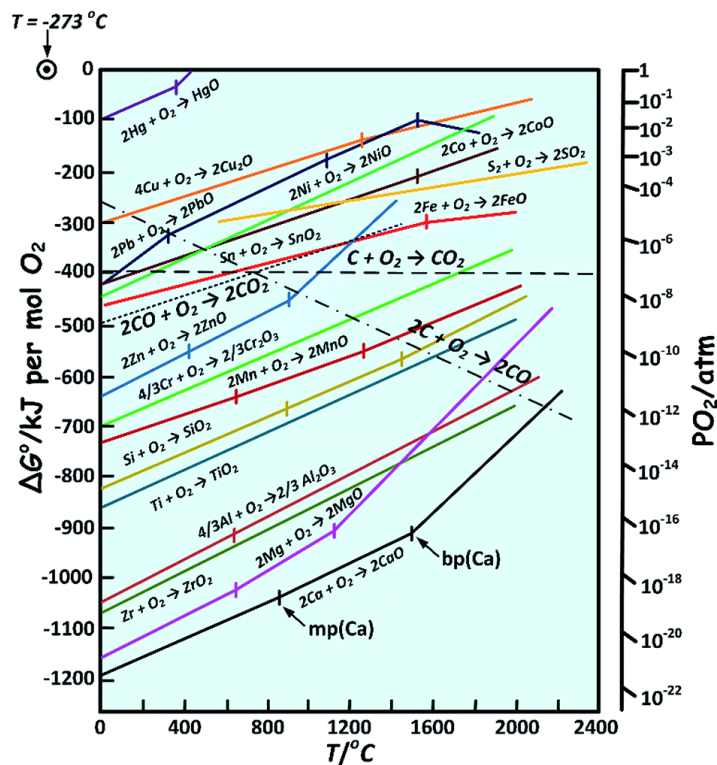


Figure 2.10: Ellingham diagram for oxides (Shen et al., 2015). Note that Zr and Ti are located far below as compared to others.

2.2.1 Activation via new surfaces

Effect of generation of new surfaces on activation was discussed in a number of studies. Liu and Lee (1997), used hydriding-dehydriding cycles on $Zr_{0.7}Ti_{0.3}V_{0.4}Mn_{0.3}Cr_{0.3}Ni_{1.0}$ C14 alloy for 5 times so as to produce new fresh surfaces. While electrode made using unmodified powder required more than 15 cycles to reach full capacity (275 mAh/g), the cycled alloy reached its full capacity only after the 6th

cycle. But the cycling was not altogether successful since the capacity was not as high. This was attributed to a decreased utilization of the active material caused by fine particle size.

Liu and Lee (1997), in an earlier study compared Zr-Ti-V-Cr-Mn-Ni C14 alloy of two different particle sizes. They came up with the conclusion that larger initial particle size provides higher saturation capacity while alloys of both sizes reach their maximum capacities in approximately 10 cycles. They also observed higher rate capability when compared to finer sized particles. They assigned this behaviour to ineffective distribution of conductive additive which increased the contact resistance between the particles and resulted in less-efficient use of active material. Moreover, easier disintegration by cycling was observed with large particles.

Matsuoka and Tamura (2007) studied the effect of mechanical grinding on the activation of $Zr_{0.9}Ti_{0.1}Ni_{1.1}Co_{0.1}Mn_{0.5}V_{0.2}Cr_{0.1}$ alloy of initially 65 μm in size. It was reported that specific surface area increases to 0.8 m^2/g with milling time up to 1 hour and then decreases with further milling dropping down to 0.25 m^2/g after 10 h. Mechanical grinding at up to 1 h was reported to improve discharge capacity and provide rapid activation, the best result was obtained with 1 h (particle size 2 μm) yielding the nominal capacity of 350 mAh/g in the fifth cycle. They attributed this to the particle disintegration and formation of nanocrystallites which led to shortened diffusion path for hydrogen. The discharge capacity was reduced to 180 mAh/g after 10 h milling (particle size 30 μm). They found that the charge transfer resistance increases with this prolonged grinding.

Sun et al. (1997), milled the $Zr(Cr_{0.4}Ni_{0.6})_2$ C15 alloy with the addition of Ni. They observed a capacity of 140 mAh/g without the additive at fifth cycle. This capacity was increased to 195 mAh/g, reached in two cycles. In a similar study Sun et al. (2002) milled the Laves phase $ZrCr_{0.7}Ni_{1.3}$ alloy with the addition of 5 % amorphous MgNi alloy powder. The alloy reached the maximum capacity in 10 cycles instead of 20 cycles.

Wu et al. (2000), examined the effect of application of voltage pulses on activation of $Ti_{0.35}Zr_{0.65}Ni_{1.2}V_{0.6}Mn_{0.2}Cr_{0.2}$. During this practice, the electrochemical hydriding and

dehydriding potentials are controlled at -1.2 and -0.8 V (vs. Hg/HgO reference) respectively. With pulsing for 24 hours, a capacity of 235 mAh/g (where maximum capacity is 280 mAh/g) was obtained in the first cycle while the unprocessed alloy displayed zero initial capacity. They reported that the alloy particles are cracked by repeated hydriding-dehydriding thus enhanced activation behavior was obtained. Similarly, McCormack et al. (1996), used voltage pulses to activate Zr_7Ni_{10} and ZrCrNi in two forms; single phase C14 and two-phase C14 and Zr_7Ni_{10} . During the process the voltage pulses of 50 s intervals between (-1.7) - (-1.0) V (vs. NiOOH/Ni(OH)₂ positive electrode) were applied to the negative electrode for 24h. This treatment produced no improvement in single phase C14 ZrCrNi. While it leads to the maximum capacity of Zr_7Ni_{10} (120 mAh/g) and 90% of the capacity of the two-phase ZrCrNi (234 mAh/g instead of 260 mAh/g in the first cycle. McCormack et al. (1996) attributes this fast activation to the presence of internal microcracks caused by voltage pulses. They further state that these microcracks are different than the decrepitation cracks and do not lead the reduction in particle size.

2.2.2 Activation via surface modification

There are two approaches in surface modification; one is to deeply oxidize the powders (Wang et al., 1994, Ye et al., 2013) and the other one is to etch the surface with some reducing agents. The latter method is discussed in some details below.

Gao et al. (1996) studied the fluorination of $Zr(V_{0.4}Ni_{0.6})_{2.4}$ using HF. As a result of this treatment they obtained a nickel-rich layer on the surface of the alloy particles. The treated alloy displayed 80 mAh/g initial capacity (the untreated one did not show any capacity) which increased to a value of 230 mAh/g after 10 cycles. The improvement in activation performance was attributed to change in surface composition and to an increase in specific surface area. In a study by Sun et al. (2002) reported above, Laves phase $ZrCr_{0.7}Ni_{1.3}$ was subjected to HF treatment. The powders were treated in 1 % HF for different time periods., it was observed that with 5 min treatment, the activation was complete in 2-3 cycles. The treatment remained microcracks on the bulk alloy surface, Figure 2.11. Li et al. (1999) proposed an advanced fluorination technique where they treat the annealed C15

$Zr_{0.9}Ti_{0.1}Mn_{0.6}V_{0.2}Co_{0.1}Ni_{1.1}$ alloy particles in Ni ion containing complex fluoride solution at 50-80°C. With this treatment the alloy reached a capacity of 300 mAh/g in 2-3 cycles. This compares to 160 mAh/g reached in the untreated alloy at the sixth cycle.

Jiansheng et al. (2001) applied a fluorination treatment using NH_4F and $NiCl_2$ which produced activation at the first cycle. The alloys in question were single phase C15 $Zr(V_{0.1}Mn_{0.3}Ni_{0.6})_2$, $Zr(V_{0.1}Mn_{0.3}Ni_{0.6}Co_{0.05})_2$, $ZrTi_{0.1}(V_{0.1}Mn_{0.3}Ni_{0.6}Co_{0.05})_2$ alloys and multiphase (comprising C15 and Zr_7Ni_{10}) $ZrTi_{0.1}(V_{0.1}Mn_{0.3}Ni_{0.6}Co_{0.05}Cr_{0.05})_2$ alloy. The untreated alloy showed initial capacities of 40, 75 110 and 150 mAh/g respectively, which reached values of 250, 300, 350 and 370 mAh/g after 5 cycles or more. Treated alloys on the other hand displayed nearly their maximum capacities (all between 350-400 mAh/g) at the first cycles. This enhancement in activation behaviour was due to Ni-rich fresh surfaces whose presence were confirmed with EDS and XPS measurements.

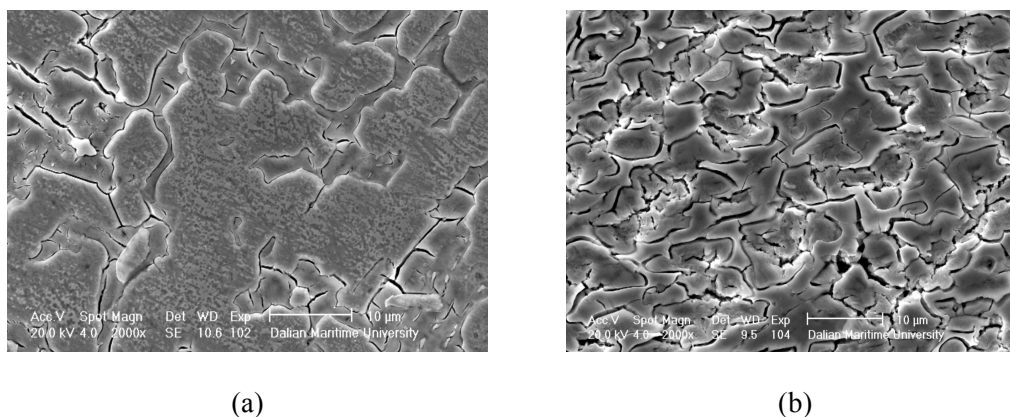


Figure 2.11: Surface morphology of the 5 min 1% HF treated bulk sample before (a) and after (b) the treatment (Sun et al., 2002).

Another approach is to treat the particles in hot alkaline solutions rather than in weak acid. Choi et al. (1999) applied 6 M boiling KOH solution to electrode made using $Zr_{0.9}Ti_{0.1}Ni_{1.1}Co_{0.1}Mn_{0.6}V_{0.2}$ alloy for different periods of time: 15 min, 1 h and 2 h. With 15 min and 1 h treatments the activation behaviour was not significantly improved. However, with 2 h boiling KOH solution treatment the zero initial capacity was increased to 320 mAh/g and the cycles needed to activate the alloy was decreased

from 20 to 2. It was confirmed that the treatment only affects the particles surface where the composition starting from the original one changes to a Ni rich one, Figure 2.12. Similar studies have been carried out in a number of cases for AB₂ alloys (e.g., Yan et al., 1995, Kuriyama et al. 1996, Wu et al. 2000, Martinez et al. 2013).

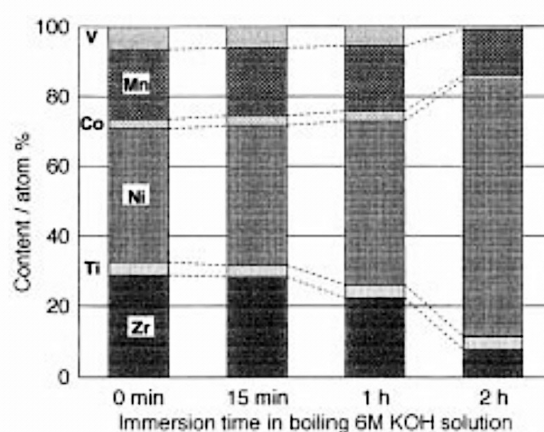


Figure 2.12: Change in surface composition with respect to time. Note that the composition becomes Ni rich as duration of treatment increases (Choi et al., 1999).

Jung et al. (1998), while in KOH solution have studied the effect of charging on the activation of the alloy. The alloy was $Zr_{0.7}Ti_{0.3}Cr_{0.3}Mn_{0.3}V_{0.4}Ni$ alloy which was immersed in 6 M KOH solution at 50-80°C and the charging was carried out at current densities varying from 50 to 300 mA/g for 2-8 hours. As a result of this treatment, the capacity and the ease of activation were improved with increasing treatment time. They reported that the treatment (80°C) with simultaneous charging at 50 mA/g for 8 h, the alloy electrode reached the maximum capacity of 350 mAh/g at the first cycle. They reported that the reductive condition caused by application of negative potential during charging lead to the formation of Ni layer in the surface. A similar study was reported by Liu et al. (1996) for C14 Zr-Ti-V-Cr-Mn-Ni alloy.

Iwakura et al. (1995) used a KOH solution containing KBH_4 as reducing agent. $ZrV_{0.5}Mn_{0.5}Ni$ electrodes were immersed into 6M KOH solutions containing up to 0.1 M KBH_4 , at 40°C-80°C. Of these, the electrode modified with 6M KOH, 0.01 M KBH_4 resulted in the fastest activation and yielded highest capacity. The alloy was activated in the first cycle and has reached a capacity of 300 mAh/g. According to Iwakura et al. (1995) this treatment results in pre-hydrogenation of the alloy and changes

pulverization mode. The particles forms cracks ranging from fine to coarse depending on the treatment time. They have attributed improvement in the activation to the extraction rate of hydrogen from BH_4^- and diffusion rate of hydrogen in the alloy.

The surface of the particles may also be modified by forming a metallic layer. Such metallic coatings were applied by Bocutti et al. (2001) and Suciu et al. (2006). (Bocutti et al., 2001) modified the surface of Mm or LaNi_5 using a sol-gel method. They have deposited copper oxides on the surface in ethylene glycol solution containing copper sulfate hexahydrate. The electrochemical measurements conducted in KOH solution at 70°C yielded initial discharge capacity of 200 mAh/g which doubled the initial capacity for the pristine powder. They have also indicated that for 200 charge/discharge cycles no surface deterioration was detected. They proposed that formation of the porous copper framework during charging step would improve the mechanical support and would ease the hydrogen absorption.

Suciu et al. (2006) have used a similar approach in the context of fuel cells. They used organic precursors sucrose and pectin as the gelling agent. In order to produce ZrO_2 nanoparticles they have used with $\text{Zr}(\text{NO}_3)_4 \cdot 5\text{H}_2\text{O}$ dissolved in water and the gelation ingredients. The two solutions were mixed and under 90°C approximately for 5 hours. The gel was calcined at 650°C for 3 hours with $200^\circ\text{C}/\text{hour}$ heating rate. It was indicated that with this sol-gel method chemically pure nanosized oxide powders would be produced with a narrow size distribution.

2.3 Measurement of Electrochemical Performance

2.3.1 Architecture of negative electrodes in Ni/MH batteries

Ni/MH cells as mentioned previously are composed of a stack of negative, positive electrode and a separator between them that was soaked in electrolyte, Figure 2.13. The negative electrode contains the active material, i.e. metal hydride, optionally binders or additives, and a porous substrate as a current collector. At this point electrical conductivity of the porous substrate is important. The substrate can be in the form of mesh, grid, foil, foam or knit, made of materials like nickel, copper, their coatings or alloys.

There are two routes in preparation of the negative electrode for batteries, namely sintering and pasting. The first route involves direct dry-compaction of the powders without the use of any binder. However, for conductivity considerations the active powder can be mixed with conductivity enhancers e.g. Ni, Cu powder or carbon black. In another approach, pressing is done in a die without the substrate. With this method, the resulting pellet is wrapped with the current collector. The current collector used as an envelope should be flexible enough as in the case of expanded metal or metal foam. Again in order to enhance conductivity, this pellet could be sintered after pressing.



Figure 2.13: The negative electrode, separator and the positive electrode of the battery

In pasted electrodes, a slurry is formed by mixing the active material, conductivity enhancer both in powder form with a suitable binder, Figure 2.14. The binder provides strength and durability to the electrode and eliminate structural disintegrations that might occur during charging and discharging cycles. The binder must have certain bond strength and flexibility, resistance to alkaline electrolyte and should be permeable to hydrogen. Suitable materials for this purpose cover PVA, MC, CMC, PTFE, FEP, PVB, HPMC (Yan & Cui, 1999). One of the most important characteristics of binders is their affinity to water. There are hydrophilic and hydrophobic binder materials. Hydrophilic binder surfaces are more active and have less electrical resistance. But, this high surface activity is problematic as it results in the absorbance of the electrolyte at the same time. Hydrophobic binders, on the other hand, increases the electrical resistance while providing a good corrosion resistance. Most of the time a combination of these binders is preferred (Ma et al., 2012). the

amount and combination of the binder materials is important with respect to the conductivity of the electrode.

Electrodes without a binder is also possible. One of the most important concerns in binder-free electrodes is dropping out of the active material from the porous substrate. (Yan & Cui, 1999) proposes high pressure rolling to prevent the particle drop-out. After the addition of the powder mixture, a pressure of 600 MPa was applied to the pre-rolled Ni foam.

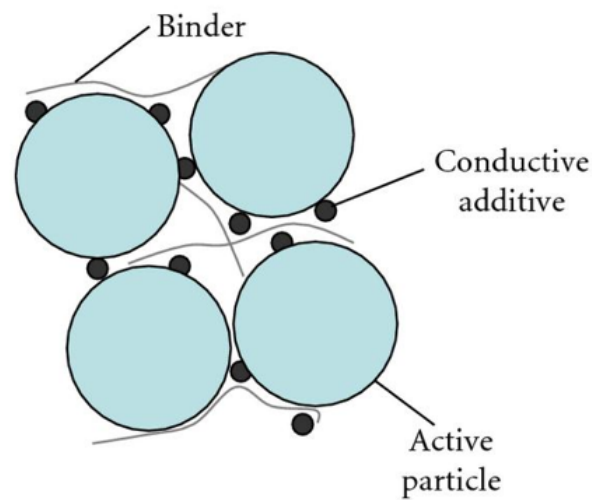


Figure 2.14: Binder, conductive additive and active particle in a slurry (Roscher et al., 2011)

Yan and Cui (1999) also compared the performance of the electrodes with and without binders in terms of internal resistances and activation. Their results showed that binder usage leads higher internal resistance in the battery and lower capacity at the first cycle. Young et al. (2009, 2010) used an 0.2 mm thick negative electrode which was obtained by pressing the active powder under 10 tons directly on to 1 cm² nickel mesh using 75 μm powder sieved from the induction melted powder.

The essential ingredient of the electrode is the conductive additive. Their role is to improve the electrical contact between the active powders so that the active mass is efficiently utilized. Nickel, graphite and acetylene black are among frequently used conductivity enhancers. According to Ma et al. (2012), up to 5 % conductive additive is sufficient to change the capacity obtained and the resistance significantly.

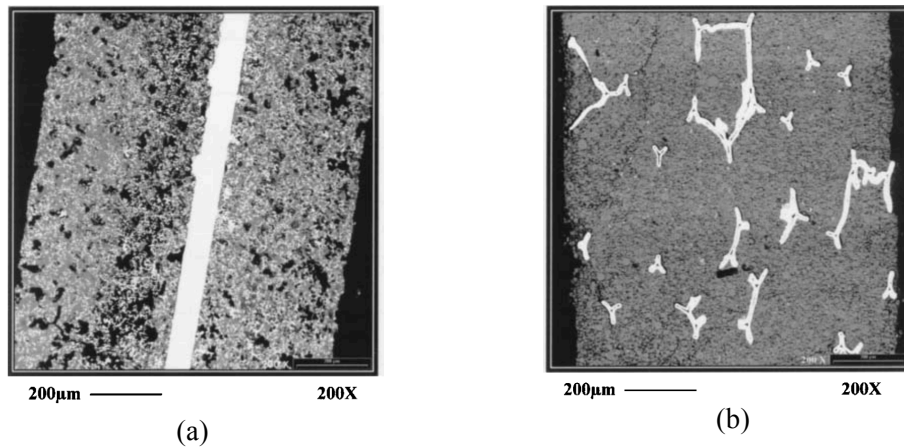


Figure 2.15: Images of sintered (a) and pasted (b) electrodes under SEM-BEI (Linden & Reddy, 2011)

The positive electrodes used in Ni/MH batteries are always make use nickel hydroxide as active ingredient. The nickel hydroxide used in recent batteries contains additives like Co, Zn, Ca and Mg. The powder is in high density and spherical form with particle size in the order of a few microns. Surface area and the shape is important the charge-discharge reactions at the particle surface, especially in high rate discharge condition. The positive electrode is either sintered or pasted, as shown in Figure 2.15. The sintered type is preferred in applications where rate and power capability is the major concern, though this is more expensive than the pasted type (Linden & Reddy, 2011). In the more common applications, the nickel hydroxide is pasted into Ni foam, Figure 2.16. The conductivity of the electrode depends on the pore size of Ni foam which would normally vary between 200-400 μm .

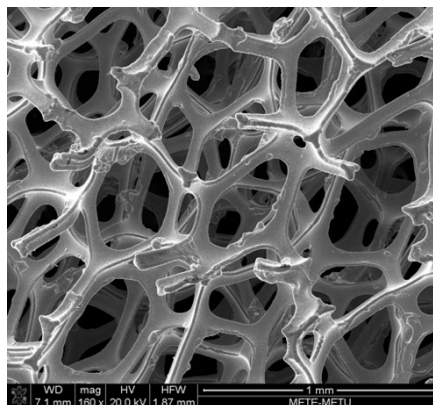


Figure 2.16: SEM micrograph of Ni foam

The preparation of the negative and positive electrode and the other battery components is followed by the cell assembly. The capacity is an important parameter. Therefore, after choosing the active material, weight of the active material is determined that will be necessary to satisfy the capacity requirement. The active material is then placed in the negative electrode by methods discussed previously. A sequence of negative electrode, separator soaked in electrolyte and the positive electrode is followed and repeated depending on the the voltage and/or capacity requirements by establishing series or parallel connections. The stack is put in a metal case. The cell can be in cylindrical, prismatic, button, pouch and flooded configurations.

Stempel et al. (1998) summarized electrode preparation process used in Ni/MH batteries of the HEVs in Ovonic Battery Company (OBC). According to their approach, alloy that is used in negative electrode undergone mechanical milling or hydriding-dehydriding method to obtain them in powder form. The powder in desired size is either roll-compacted directly or a slurry prepared using the mixture of powder and a binder which is then applied on the perforated or expanded substrate. They point out that a dry route, i.e. free from binder material and other additives should be preferred. In the positive electrode, a slurry formed using Ni(OH)₂ powder, cobalt compounds for performance enhancement was applied to highly porous substrates. The electrode stack is welded to terminals. Considering the nominal voltage of each cell, a battery with the desired voltage is formed connecting the cells.

2.3.2 Architecture of negative electrodes for electrochemical measurements

Both approaches; pasting and pellet making by pressing, i.e. sintered electrodes, are used in the literature for electrochemical testing.

Soria et al. (2001) investigated sintered electrode architectures on the performance of the Ni/MH battery electrodes. They compared nickel fibre mats of 700 g/m² and 950 g/m² densities together with nickel foam of 500 g/m² regarding capacity of the resulting electrode. They observed that the performance is highly affected by the substrate type. The fibrous substrates provide higher capacities due to closer contact

of the active powder with the current collector. Also the high rate performance of the electrodes on nickel fibre substrates were better with the use of the substrate with higher density of Ni.

In the same study, the performance of pasted electrodes was also investigated. Different fractions of additives, PTFE, PVA, CMC and arabic gum, were used for this purpose. It was reported that a mixture of PTFE and PVA with 8:1 ratio provides adequate paste viscosity thus optimum mechanical properties. A preparation method involving; 3.2 wt. % conductive carbon, 1.6 wt. % PTFE, 0.2 wt. % PVA added to powders with 0.095 g/cm^2 active material rolled and pressed on nickel fiber was recommended as optimum for the negative electrode. Active materials containing La and Mm were mixed with carbon black, PTFE, nickel and cobalt compound powders, applied onto a nickel foam to be used for electrochemical measurements (Soria et al., 2001).

The use of binder material is sometimes preferred to enhance the mechanical integrity of the electrode during charging and discharging cycles. The amount of binder material would be just sufficient to establish a network between the powders, as otherwise the binder will not work effectively. If the amount is more, this time rather than active material, it would be the binder material which will be determinant in electrical conductivity and hydrogen permeation (Cuscueta et al., 2010).

The electrode performance may be improved by copper or nickel coating that can be applied to electrode after pressing the powder on the substrate. In this way, the electrical conductivity of the electrode is increased, as a result, a more active surface is obtained by establishing a better contact between the active material and the substrate. Instead of coating, powder additions of copper or nickel, or sometimes carbon, can be made to obtain similar effects.

For electrochemical measurements the negative electrodes are tested against a positive electrode, i.e. in two electrode configuration. In cases where the electrode will be tested in the absence of a positive electrode three electrode configuration is normally used. This configuration involves a negative electrode as working electrode, a

reference electrode and a counter electrode. Metallic nickel is a widely used counter electrode in three-electrode cell set-ups.

Selective examples of electrode architecture used in the literature for electrochemical measurements are reported in Table 2.4. Although the table covers a variety of methods, some selective examples are summarized below.

Willems (1984) used an AB₅ alloy as the active material and mixed it with copper powder without the use of any binder material. The mixture was pressed under 400 MPa in order to obtain a pellet 8 mm in diameter. Gamboa et al. (2001, 2002), in their study, used 30 gr of micron sized AB₅ metal hydride powder that was pressed under 490 MPa on rectangular nickel foam. The resulting piece was sintered at 900⁰C for 10 minutes. For the electrochemical measurements Pt mesh was used as counter electrode. In another study, metal hydride powder was mixed with nickel powder in 1:1 ratio with the addition of 3 wt. % PTFE. Without the use of a substrate, the mixture was pressed under 500 MPa. In both studies Ni(OH)₂/NiOOH sheet was used as a positive electrode.

Tammela (2012) used a paste electrode that is formed by mixing 90 wt. % alloy powder, 5 wt. % carbon black and 5 wt. % PTFE with the addition of a few drops of ethanol. This paste was rolled to 0.3 mm as the final thickness. Electrochemical measurements were done in a three electrode cell that is open to atmosphere but with argon flow through the solution. Hermann et al. (2001) used pasted electrodes prepared with mixing the active powder using ethanol with Ni powder (0.5-1 μm) in 4:1 ratio applying it to nickel foam. They have sintered this electrode at 800°C for 20 minutes under Ar+H₂ (90:10) atmosphere. Hoshino et al. (2001) used hydrogenation-dehydrogenation method to obtain a -38 μm active alloy which was activated by charge-discharge cycles in 6 M KOH. The electrode was prepared by adding 0.74 g spherical (5 μm in diameter) graphite powder and 0.12 g of PVA to the 9 g of active powder and pasting this mixture on a Ni ribbon of an area of 7 cm x 6 cm. As the positive electrode sintered nickel hydroxide was used. The electrodes were connected to the cell via nickel ribbons.

Table 2.4: Electrochemical measurement details from different studies

Active material	Additive	Method	Pressure (MPa)	Counter electrode (RE: Hg/HgO)	Reference
AB₅	5 wt. % PTFE, 5 wt. % C black on Ni foam	Paste	100	Ni mesh	Tammela (2012)
AB₅	17 wt. % PTFE, 33 wt. % C black	Pasted (disk)	300	Ni mesh	Cuscueta et al. (2010)
AB₅	Cu powder (1:2-9)	Pressed	40-400	Pt plate	Willems (1984)
La-Mg-Ni	C powder (1:1), PTFE	Pasted (on Ni sponge)	-	NiOOH	Holm (2012)
Mg₂Ni	20 wt. % PTFE -acetylene black	Pasted (on Ni foam)	-	Ni foam	Cui et al. (1996)
AB₂ (C14)	Ni powder (1:3), 3 wt. % PTFE	Pasted (on Ni mesh)	100	NiOOH	Yang (1996)
AB₂ (C14)	-	Pressed (on Ni net by hot press)	800	NiOOH	Kopczyk et al. (1996)
AB₂ (C14-C15)	Cu powder (1:2), 3 wt. % PTFE	Pressed	100	NiOOH	Yang (1996)
AB₂ (C14-C15)	Cu powder (1:2)	Pressed (in Cu holder)	100	NiOOH	Yang (1996)

Yang (1996) prepared the pasted electrode by mixing powders using 94 wt. % active alloy, 3 wt. % nickel, 1 wt. % carbon, using 2 wt. % binder mixture containing PTFE:CMC weight ratio 3:7 applied onto nickel coated porous steel. After drying of the electrode, it was pressed until the final thickness of the electrode was 0.2 mm. A similar procedure was applied for the positive electrode that has a final thickness of 0.5 μm which is formed by adding CoO, ZnO, TiO₂, Y₂O₃ and Ni to Ni(OH)₂ that is mixed with the same binder material and water.

Tliha et al. (2010) used so called 'latex' technology to prepare both the positive and negative electrodes. For the negative electrode, the alloy was first ground under Ar gas and sieved to above 63 μm . The active powder 90 wt. % was mixed with 5 wt. % PTFE and 5 wt. % carbon black. Two pieces of 0.5 cm² latex were pressed onto the two sides of the nickel grid and the electrochemical measurements were conducted using a three-electrode cell open to atmosphere. Here the nickel grid was used as the counter electrode and Hg/HgO as reference electrode in 7 M KOH.

CHAPTER 3

EXPERIMENTAL

3.1 Materials

AB₂ alloy powder supplied by BASF has a composition of (Ti_{0.36}Zr_{0.64})(V_{0.15}Ni_{0.58}Mn_{0.20}Cr_{0.07})₂. Particle size distribution of powders as supplied is given in Figure 3.1.

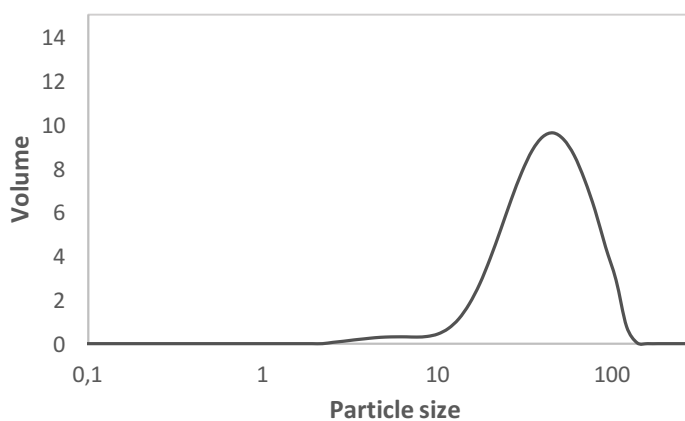


Figure 3.1: Particle size distribution of the unsieved AB₂ alloy

3.2 Processing

In order to study the activation behaviour of AB₂ compound a number of treatments were employed; sieving, ball milling, hot KOH treatment and NiO coating.

3. 2. 1 Sieving

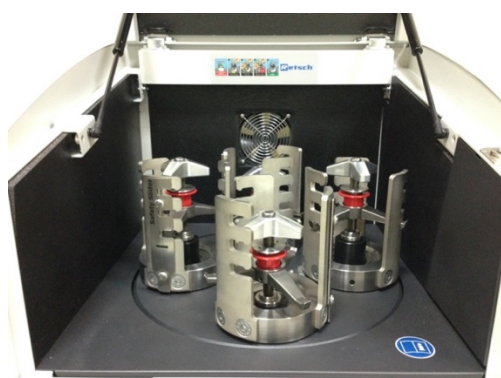
The purpose of sieving was to investigate how particle size affect the activation behaviour of AB₂ compound. For this purpose, typically 100 g powder was sieved using Utest Sieve Shaker. Six sieves (Endecotts) of mesh sizes 38, 45, 53, 63, 75 and 90 μm were used, Figure 3.2.



Figure 3.2: The sieve shaker with the sieves

3.2.2 Ball milling

In order to examine the effect of ball-milling on activation behaviour, AB_2 powder was milled using Retsch planetary ball mill (PM 400 MA type) at 250 rpm, Figure 3.3. Milling was carried out with 50 cc vial using stainless steel balls of 10 mm in diameter with ball to powder ratio of 20:1. The starting powder was between +45 and -53 μm . The milling was carried out for durations of 1 hour, 3 hours and 5 hours.



(a)



(b)

Figure 3.3: (a) Retsch planetary ball mill and the (b) 50 cc vial

3.2.3 KOH treatment

For an effective surface modification, hot KOH treatment was applied to the powders. 5 grams of AB₂ powder was used. A 50 ml 6 M KOH solution was prepared which was continuously stirred and heated just above 100 °C. Powders were poured into boiling KOH solution and kept there for periods of 20, 40, 60, 80 and 100 minutes, Figure 3.4. At the end of the treatment, the solution was poured out of the beaker and the powders were washed for 3-4 times with distilled water. The powders were then left to dry.

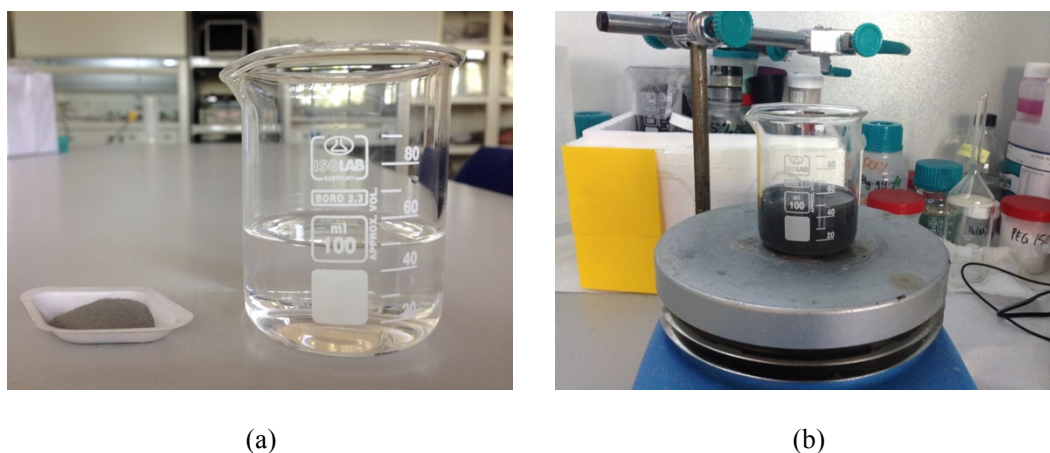


Figure 3.4: (a) AB₂ powder and 6M KOH solution and (b) boiling KOH treatment

3.2.4 NiO coating

NiO coating on AB₂ powders was carried out via two sol-gel methods as described by Suciú et al. (2006) and Bocutti et al. (2001). First route involves the use of pectin as the gelation agent. The process involves mixing of two solutions. One solution was prepared 0.12 g pectin (Alfasol) and 2.38 g sucrose (table sugar) dissolved in 25 ml deionized water. The second solution was a mixture of 0.59 g NiCl₂·6H₂O (Merck EMSURE for analysis), Figure 3.5(a), with 3.55 g of AB₂ powder in 25 ml deionized water. The two solutions were mixed together in a beaker heated to 90 °C while stirring. The stirring was discontinued when the solution was gelled. Following 5 hours of drying the product was heated at a rate of 200 °C/h to 650 °C and calcined at this temperature for 3 hours.

Another route involved the use of ethylene glycol (EG) as solvent and $\text{NiNO}_3 \cdot 6\text{H}_2\text{O}$ as NiO source. In this method, 50 ml EG (Merck EMPLURA purity >99%) together with 2.5 mmole (0.7270 g) of $\text{NiNO}_3 \cdot 6\text{H}_2\text{O}$ (Riedel de Haën purity 96%), Figure 3.5(b), was put in a beaker and stirred while heating to 90 °C. When the temperature of the solution reaches 90 °C, 3.5 grams of AB_2 powder is added to the solution. Here the amount of NiO and AB_2 was adjusted so as to keep NiO not less than 5 wt. % of AB_2 . The mixture was stirred and temperature was maintained at 90 °C until the solution is vaporized, i.e. approximately 12 hours. The mixture was then transferred into a crucible and put into the furnace. The furnace was heated at a rate of 2 °C/min to 200 °C and held at this temperature for 24 hours (Bocutti et al., 2001).



Figure 3.5: (a) $\text{NiCl}_2 \cdot 6\text{H}_2\text{O}$ and (b) $\text{NiNO}_3 \cdot 6\text{H}_2\text{O}$ which were used in the first and second routes respectively.

3.3 Electrochemical Measurements

Electrochemical measurements were carried out in two different cells; one was quite narrow container housing working, counter and reference electrodes, Figure 3.6. The other was a two compartment cell, one compartment housing working and reference electrode and the other housing the counter electrode joined together with a frit (porosity #5), Figure 3.7. Both cells were open to atmosphere.

Working electrodes were prepared by mixing the active powder with copper powder (150 μm) in 1:3 weight ratio. The powder mixture was pressed in a stainless steel die under 400 MPa pressure into a 10 mm-diameter pellet. The pellet was tightly wrapped in a nickel mesh (100 mesh) of 20 mm by 30 m size. The envelope produced was spot welded to a 100 mm long-nickel wire of 1.5 mm in diameter used for connection (Figure 3.8).

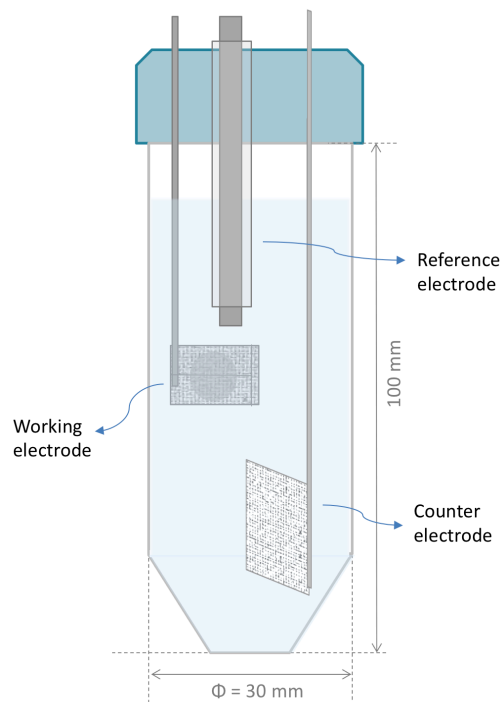


Figure 3.6: Illustration of single compartment cell. Note that the working electrode is a pressed electrode, counter electrode is a Ni mesh and reference electrode is a Zn rod.

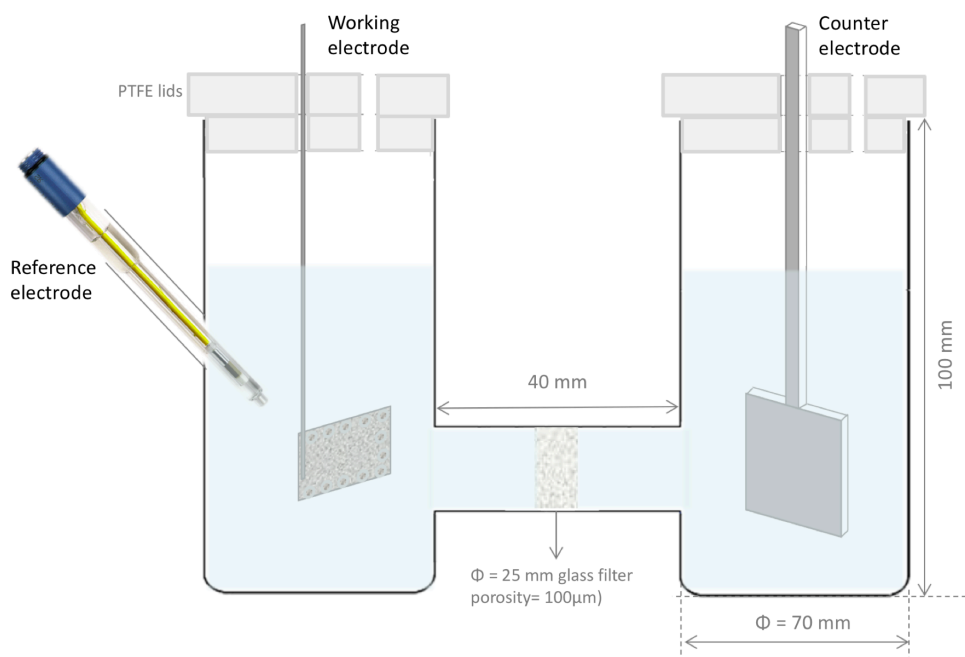


Figure 3.7: Illustration of double compartment cell. Note that the working electrode is a foam electrode, counter electrode is a Ni sheet and reference electrode is a Hg/HgO.

In a similar manner, the counter electrode was prepared using a thicker nickel mesh (20 mesh) with surface area larger than the working electrode. For the reference electrode zinc rod (4 mm-diameter, purity 99.995%) was used. Electrolyte was 6M KOH (Sigma-Aldrich, pellets) in distilled water (conductivity $<0.2 \mu\text{S}$) solution. Electrochemical measurements were carried out with Lanhe CT 2001A battery tester, Figure 3.9, in galvanostatic mode. Charging was carried out at a current density of 50 mA/g for 8 hours. Discharging was carried out at the same rate until the cut-off voltage of -0.75 V vs. Zn electrode.

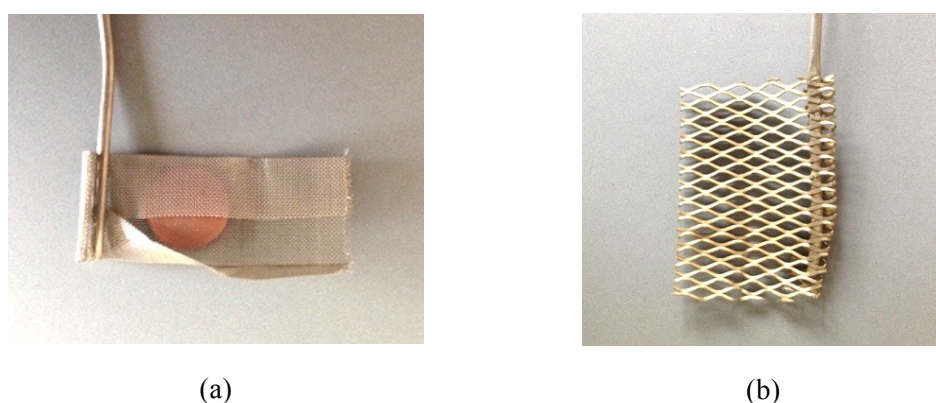


Figure 3.8: Photographs of (a) negative electrode prepared with pellet and mesh and (b) corresponding counter electrode for electrochemical measurements.

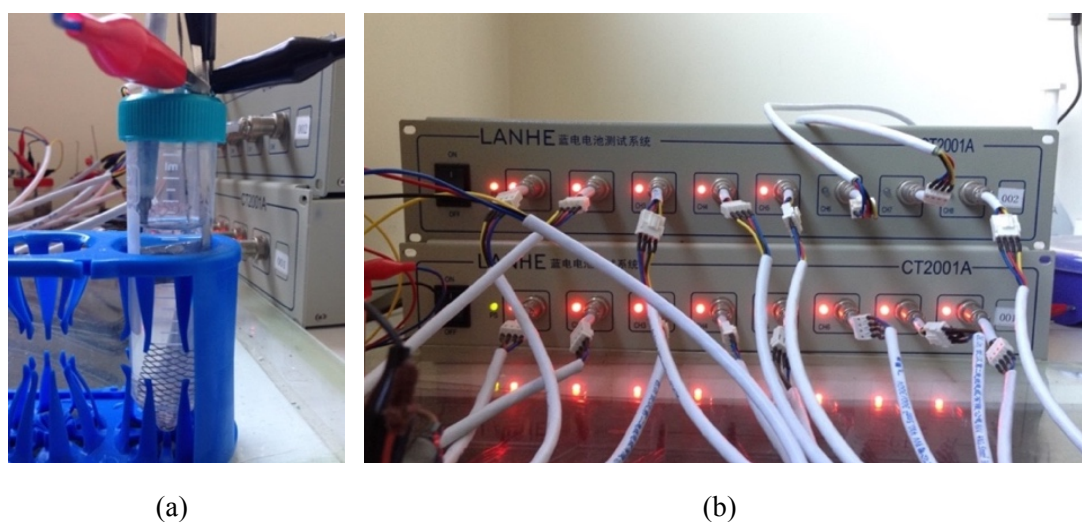


Figure 3.9: Photographs of (a) cell used in the electrochemical charge-discharge measurement for electrode prepared by pellet and mesh and b) Lanhe CT2001A battery tester.

The pressed electrode used in the above configuration was quite satisfactory for most purposes. However, one problem faced with this electrode was a powder drop-out. In order to prevent this, an alternative method was used in preparing the electrode. Here, rather than pressing, electrodes were pasted in an enclosed foam. In this approach, 2 wt. % polyvinyl alcohol (PVA) solution was prepared. For this purpose, PVA (Alfa Aesar, 98-99% hydrolysed) of typically 0.4 g was added to 20 ml distilled water and heated up to 80°C under continuous stirring kept at this temperature for one hour. The treatment was stopped when the solution was thickened. Having prepared the solution, the active powder was mixed with nickel powder at 1:3 weight ratio. A paste was prepared by adding PVA solution with 2 wt. % of the powder mixture plus a few drops of ethanol. The mixture was mixed with a spatula and applied onto 1.6 mm thick nickel foam (MTI) of 40 mm by 40 mm size. Another piece of nickel foam of the same size was placed above the foam and the periphery of the sandwich was spot welded as shown in Figure 3.10. For circuit connection this sandwich was spot welded to a 0.25 mm thick and 100 mm long nickel ribbon (rolled from Ni ingot). In this measurement, nickel sheet with dimensions of 35 mm by 35 mm was used as the counter electrode. Electrolyte was the same as above, i.e. 6 M KOH. Measurements were conducted this time using a Hg/HgO reference electrode with the same rates stated above where cut-off voltage was -0.6 V vs. Hg/HgO. Gamry Interface 1000 Potentiostat/Galvanostat/ZRA was used in galvanostatic mode, Figure 3.11.



Figure 3.10: Photographs of (a) negative electrode prepared with paste and foam and (b) corresponding counter electrode for electrochemical measurements.



Figure 3.11: Photographs of (a) the electrochemical charge-discharge measurement setup for electrode prepared by paste and foam and (b) Gamry Interface 1000 potentiostat/galvanostat/ZRA.

3.4 Material Characterization

Initial powders as well as those resulting from the various processing routes were examined by a variety of techniques. Powder size and distribution were determined by laser diffraction using Malvern Mastersizer 2000. Water was used as dispersing media. Where necessary, crystal structure of powders together with phases present was analysed with X-ray diffraction using Bruker Diffractometer (Cu-K α). The XRD pattern obtained was Rietveld refined using MAUD to determine the lattice parameters of phases present. The crystallite sizes were estimated using Popa Rules as size-strain model in MAUD (Popa, 1998).

Morphology of the powders especially those resulting from KOH treatment was examined with FEI Nova NanoSEM operated at 20 kV. The powder samples were examined by attaching them to double sided carbon tape.

For KOH treated powders near-surface concentration of elements was examined using electron probe micro analyser (EPMA) using an accelerating voltage of 20 kV and a probe current of 0.02 μ A.

CHAPTER 4

RESULTS AND DISCUSSION

This section deals with experimental study carried out on activation behaviour of AB₂ alloy. Since there are a number of AB₂ alloys used as negative electrode material, the alloy used in this study will be characterized first. This will be followed by various processing techniques employed to activate the alloy. These techniques fall into two groups namely activation via increased surface area and activation via surface modifications.

4.1 Characterization of AB₂ Alloy

In order to chemically characterize the alloy, a sample was prepared from the starting powder and characterized by EMPA. The result of this analysis is given in Table 4.1. Since in AB₂ alloys, A is associated with Ti and Zr and B is associated with V, Ni, Mn and Cr elements present in the alloy may be grouped together with a chemical formula of (Ti_{0.36}Zr_{0.64})(V_{0.15}Ni_{0.58}Mn_{0.20}Cr_{0.07})₂.

XRD pattern of this AB₂ alloy is given in Figure 4.1. Here the pattern was Rietveld refined using MAUD (Materials Analysis Using Diffraction). It is seen that many of the peaks in the diffractogram is compatible with C14 phase typified by ZrMn₂ which has hexagonal crystal structure. Rietveld refinement yields lattice parameters of a= 4.9589 Å and c= 8.0917 Å.

Table 4.1: Composition of the alloy according to the results of the EPMA analysis.

Element	Amount (at. %)
Ti	11.89
Zr	20.69
V	11.50
Ni	35.34
Mn	14.58
Cr	5.97

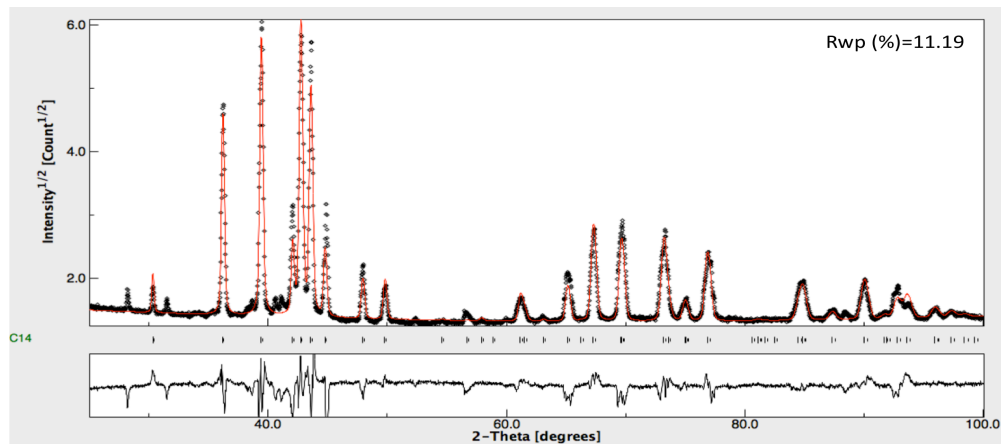
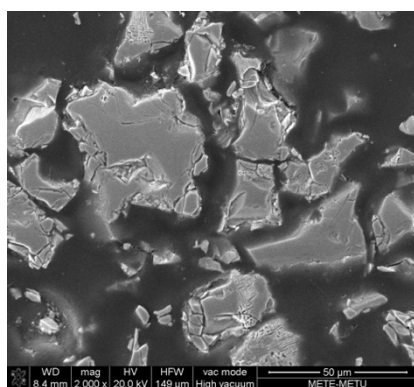
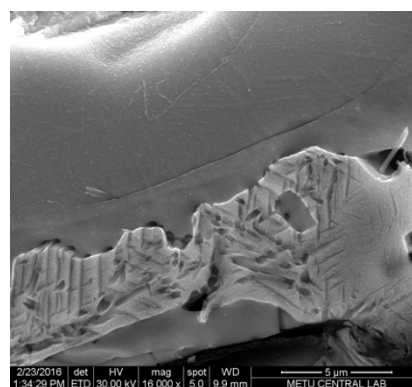


Figure 4.1: Fitted XRD pattern of AB₂ powder. Note that the alloy contains a secondary phase besides predominant C14 phase.

Although the alloy has predominantly C14 phase, the diffractogram do contain additional peaks not accounted for by C14 phase. This implies that the alloy is not a single phase C14. In order to check this, a sample was prepared metallographically, i.e. representative powders were embedded in epoxy mount and ground, polished and finally etched with 10 vol. % HF- 10 vol. % HCl in ethanol. A SEM micrograph of a representative powder is given in Figure 4.2. Here it is seen that the powders are quite homogenous except for certain regions where there is a lamellar like structure, Figure 4.2 (b). EDS analysis of this lamellar region is given in Table 4.2. This region where there are secondary phases comply with the composition of (Ti_{1.3}Zr)Ni_{2.5}.



(a)



(b)

Figure 4.2: Phase distribution in AB₂ alloy under SEM (powder mounted in epoxy, polished and etched) at (a) 2000x and (b) 16000x.

Table 4.2: EDS analysis of a lamellar region in AB₂ alloy

Element	Lamellar region (at. %)
Zr	19.47
Ti	25.38
V	1.46
Ni	49.51
Mn	3.68
Cr	0.49

The PCI curve of the AB₂ alloy obtained at 30°C is given in Figure 4.3. From this figure it can be seen that the alloy shows a single sloping plateau. At 0.1 MPa pressure, the alloy absorbs/desorbs 1.2 wt. % hydrogen. The value can be converted into electrochemical storage capacity using the following formula:

$$Capacity (wt. \% H) \times \frac{96500 C}{3.6} = Capacity \left(\frac{mAh}{g}\right) \quad \text{Equation 4.1}$$

The capacity of 1.2 wt. % hydrogen therefore corresponds to 320 mAh/g electrochemical capacity. With a similar approach the gas phase capacity at 1 MPa of 1.6 wt. % matches with 428 mAh/g.

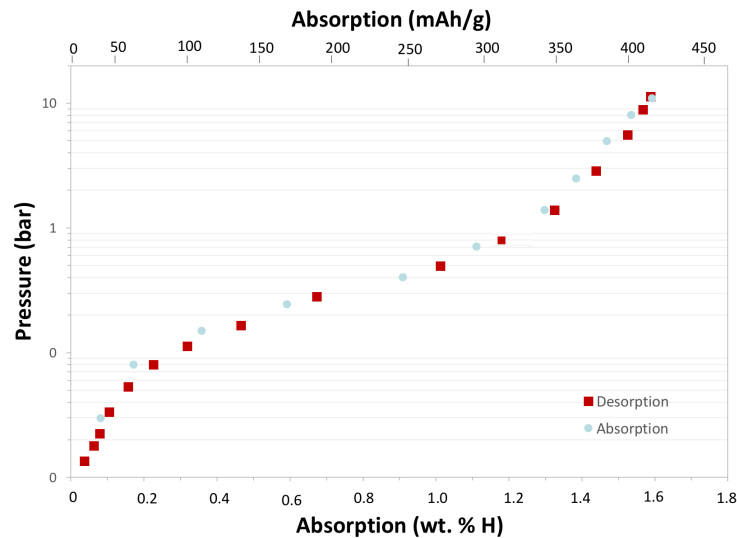


Figure 4.3: Pressure-composition isotherm of pristine AB₂ alloy at 30°C. Note that the alloy shows 1.2 wt. % gaseous phase hydrogen storage capacity at 1 atm which corresponds to 320 mAh/g (Young, personal communication, May 19, 2015).

4.2 Activation via Increased Surface Area

Two methods were used to study the effect of increased surface area on activation. One was ball milling of starting powder, and the other was sieving of powders so that powders of different surface area were obtained from the same starting powder.

4.2.1 Ball milling

In order to study the effect of surface area on activation, the starting powder AB_2 (particle size between 45-53 μm) were ball milled for 1, 3 and 5 hours. SEM images of milled powders are given in Figure 4.4.

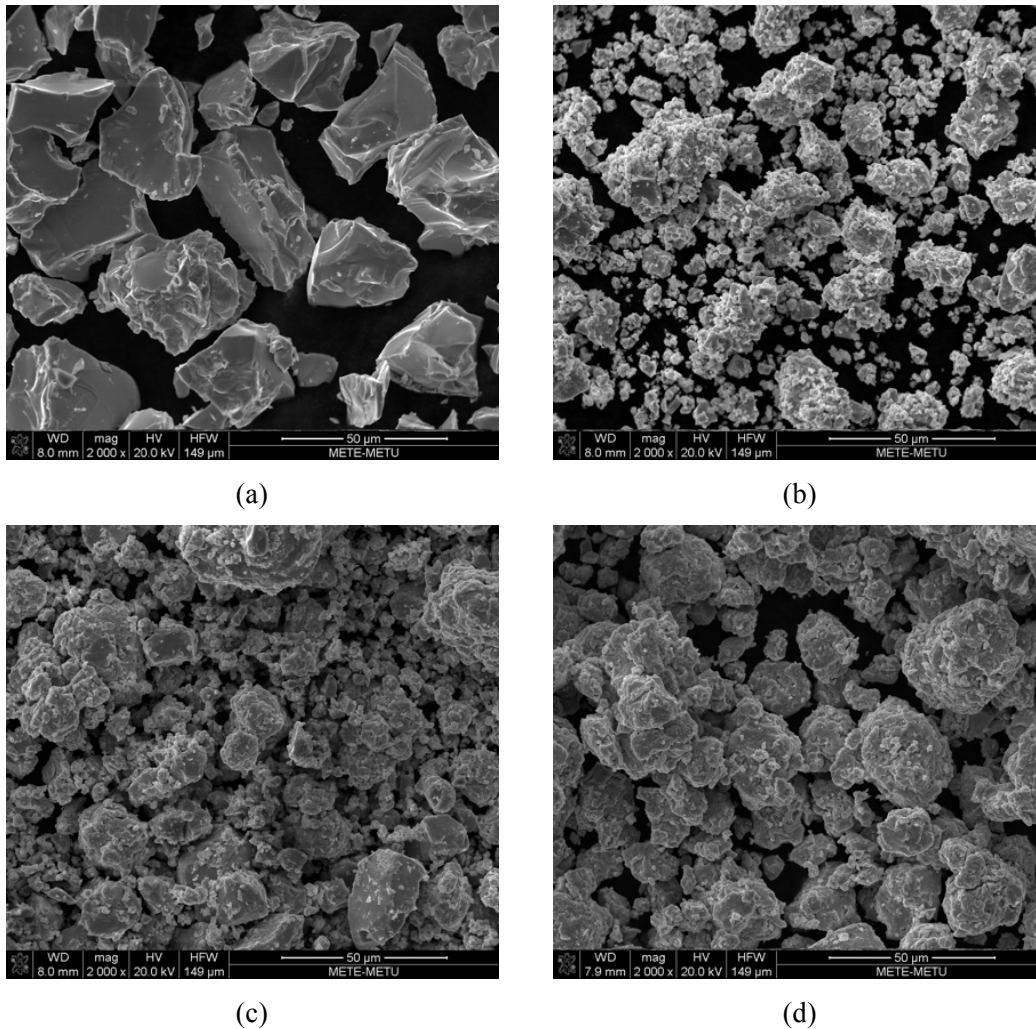


Figure 4.4: SEM images of (a) unmilled and ball milled AB_2 powder after (b) 1, (c) 3 and (d) 5 hours of milling.

It is seen that the particles were pulverized as a result of milling. However, degree of pulverization does not follow a simple pattern with milling time. With 1-hour milling, particles were fragmented into pieces, Figure 4.4(b). As milling time increases, particles do agglomerate with the resultant increase in particle size. The $d(0.5)$ values were 27, 26 and 29 μm for 1, 3 and 5 hour milling durations respectively. Although $d(0.5)$ values are quite close to each other, it should be noted that with increased milling there is a decrease at the finer end of the distribution.

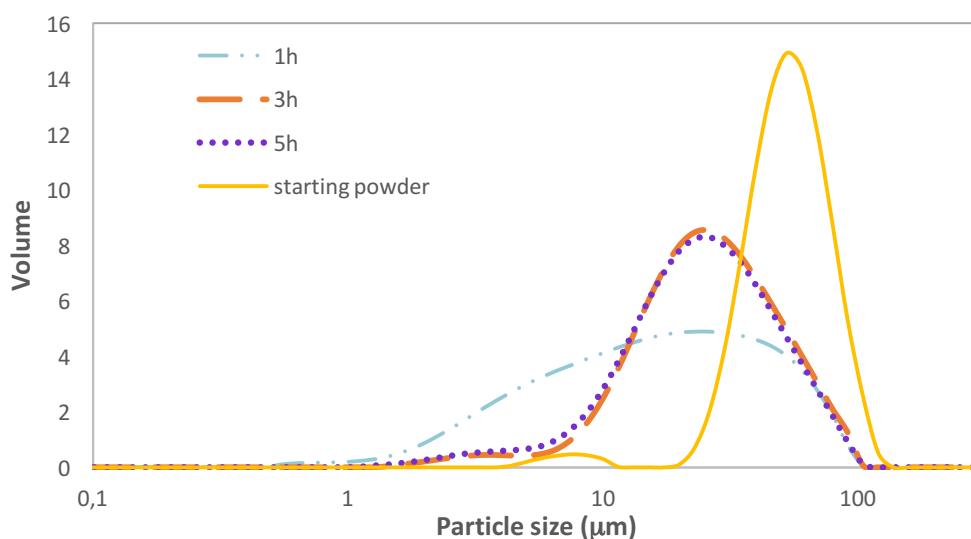


Figure 4.5: Particle size distribution of powders resulting from 1h, 3 h and 5 h milling. The distribution of starting powder was also included for comparison.

Pellets prepared from milled powders were tested electrochemically using a single compartment cell. Discharge capacities vs. cycle number are given in Figure 4.6 for milled as well as unmilled samples. It can be seen that ball milling for all durations provide improved activation. The pressed electrode prepared from the starting powder reached its maximum capacity after 12-13 cycles. With milled samples only 5-6 cycles were enough to obtain the maximum capacity each exhibiting similar activation behaviour.

The saturation capacities of powders varied with different milling durations. While the unmilled powder had a saturation capacity of 220 mAh/g, higher saturation capacities were obtained after 1 and 3 hour-milling durations. The 1 hour-milled sample gave a

saturation capacity of 330 mAh/g. It should be noted that this capacity is above the gas phase capacity of the alloy, Figure 4.3. However, with 3 hour-milled sample saturation capacity dropped down to 265 mAh/g. For 5 hour-milled sample the saturation capacity was lower than the unmilled sample, 214 mAh/g.

It should be mentioned that the maximum capacities obtained dropped by cycling. Even though no capacity drop was seen for 5 hour-milled powders, this case was observed most critically for 1 and 3 hour-milled powders. For 1-hour milled sample the maximum capacity of 330 mAh/g decreased to 280 mAh/g at the end of 20 cycles. 3 hour-milled sample also experienced such a situation and the maximum capacity of 265 mAh/g dropped down to 185 mAh/g after 20 cycles. The drop in capacity by cycling is probably due to particle drop-out. Loss of the active mass is due to the presence of small particles in the active powder disintegrating and leaving the electrode.

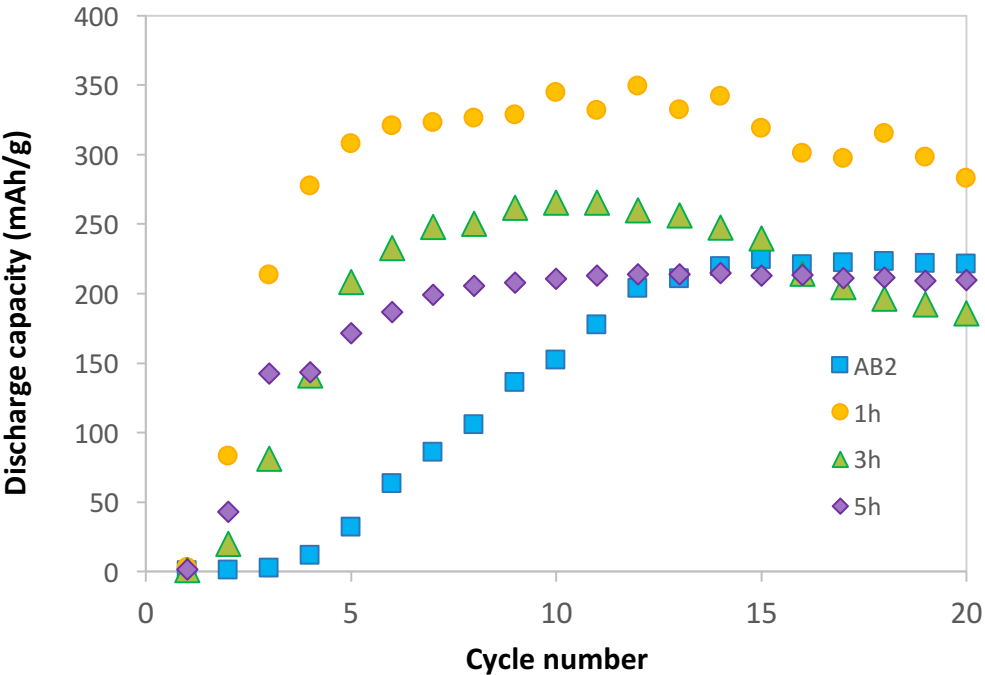


Figure 4.6: Discharge capacity vs. cycle number for pressed electrodes prepared from AB₂ powders milled for 1, 3 and 5 hours. Data for pristine alloy is included for comparison.

4.2.2 Sieving

So as to obtain particles of different surface area, the as-received powder was sieved into separate batches. The size intervals were +38/-45 μm , +53/-63 μm and +75/-90 μm . Particle size distribution of all batches are given in Figure 4.7. The distribution yields average particle sizes $d(0.5)$ of 37.3 μm , 62.7 μm and 82.5 μm .

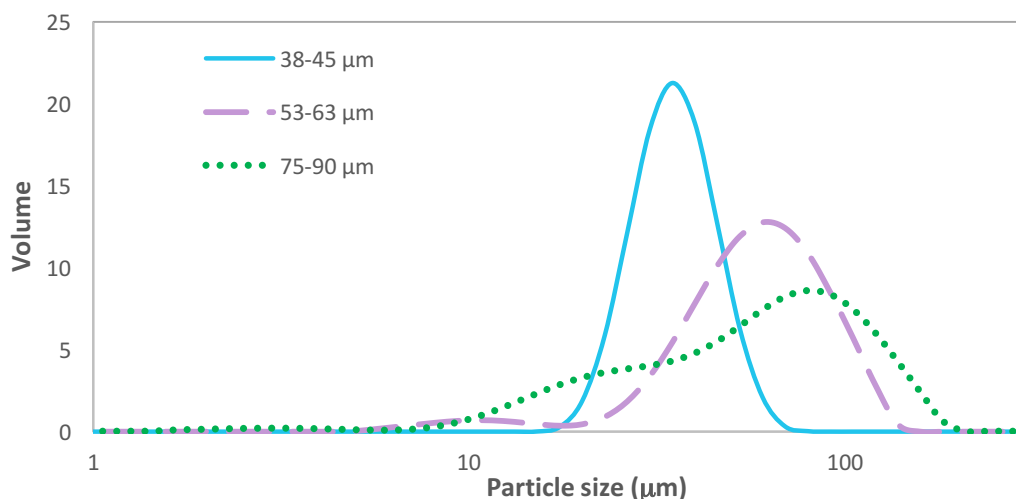


Figure 4.7: Particle size distributions for AB_2 particles: +38/-45 μm , +53/-63 μm and +75/-90 μm . Note that $d(0.5)$ values for these intervals are 37.3 μm , 62.7 μm and 82.5 μm respectively.

Pellets prepared from sieved powders were tested electrochemically using a single compartment cell. Discharge capacities vs. cycle number are given in Figure 4.8 for sieved as well as unsieved samples. The behaviour of the fine powder, i.e. $d(0.5) = 37.3 \mu\text{m}$, was quite similar to that of the unsieved powder. The maximum capacity was reached and saturated at that value after 15 cycles. The coarse powder, i.e. $d(0.5) = 62.7 \mu\text{m}$ and $82.5 \mu\text{m}$, on the other hand, got activated faster. After 7-8 cycles a maximum capacity of 245 mAh/g was reached.

It should be noted that, the coarse powder having reached its maximum exhibits a decrease in the capacity with continued cycling, Figure 4.8. This phenomenon is similar to what was observed for the ball milled powder, but more pronounced. It should also be mentioned that the fine powder does not show such a capacity decline with continued cycling.

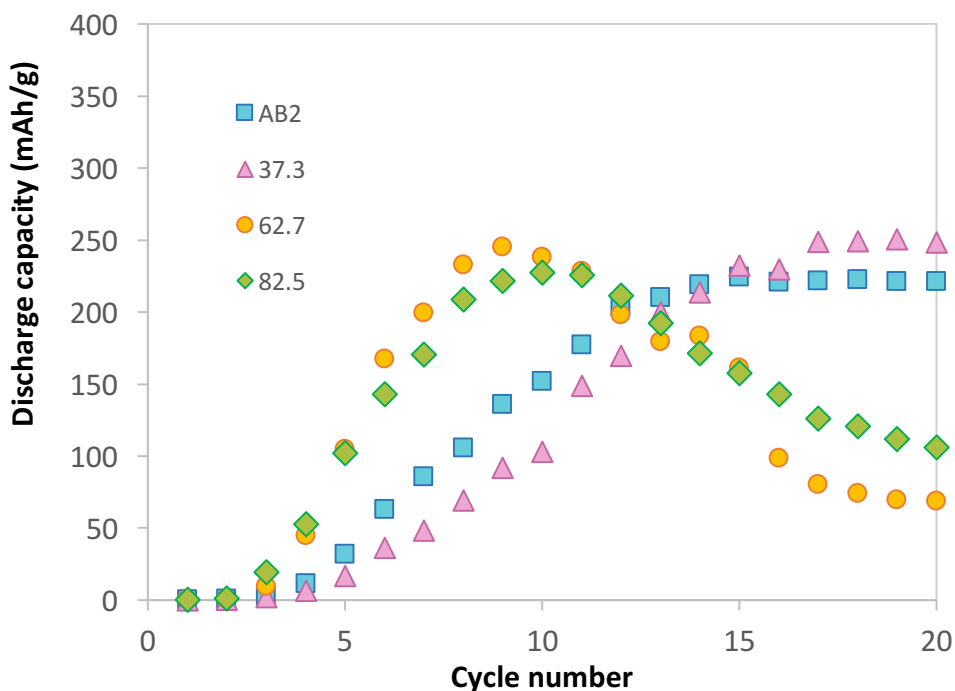


Figure 4.8: Discharge capacity-cycle number plot of pressed electrodes of powders sieved into separate batches yielding average particle sizes of $d(0.5)$ of 37.3, 62.7 and 82.5 μm . Data for the unsieved powder is also included for comparison.

The decrease in capacity with continued cycling is probably due to particle drop-out as discussed above. So as to eliminate the complications arising from particle drop-out a new electrode configuration was used. As described in Section 3.3, the active powder was applied to a Ni foam with the use of PVA binder in such a manner that the active powder was totally enveloped in the foam, preventing the particle drop-out.

The foam electrodes described above were electrochemically tested in a double compartment cell. Discharge capacity versus cycle number obtained with foam electrode is given in Figure 4.9. It is seen that with foam electrodes the capacity saturates and does not decrease by cycling. It can be inferred that the use of foam electrode is useful in preventing the particle drop-out.

In terms of activation behaviour, foam electrodes activate faster than the pressed electrodes. The sample with slowest activation is the one prepared with finest powder, i.e. $d(0.5) = 37.3 \mu\text{m}$. The behaviour of other samples is similar in that they reach their saturation capacity after 3-5 cycles.

A major difference in foam electrodes is their saturation capacity. The capacity of the fine powder, $d(0.5) = 37.3 \mu\text{m}$, saturates at 350 mAh/g. With the coarse powder, $d(0.5) = 82.5 \mu\text{m}$ the saturation capacity was even higher and has a value of 370 mAh/g. It should be mentioned that this value is the highest capacity encountered so far and it is higher than that obtained with 1 hour- ball milled powder which had a value of 330 mAh/g. It may be worth restating both cells were open to atmosphere and therefore the capacity expected from the powders, according to PCI curve, Figure 4.3, should not be more than 320 mAh/g.

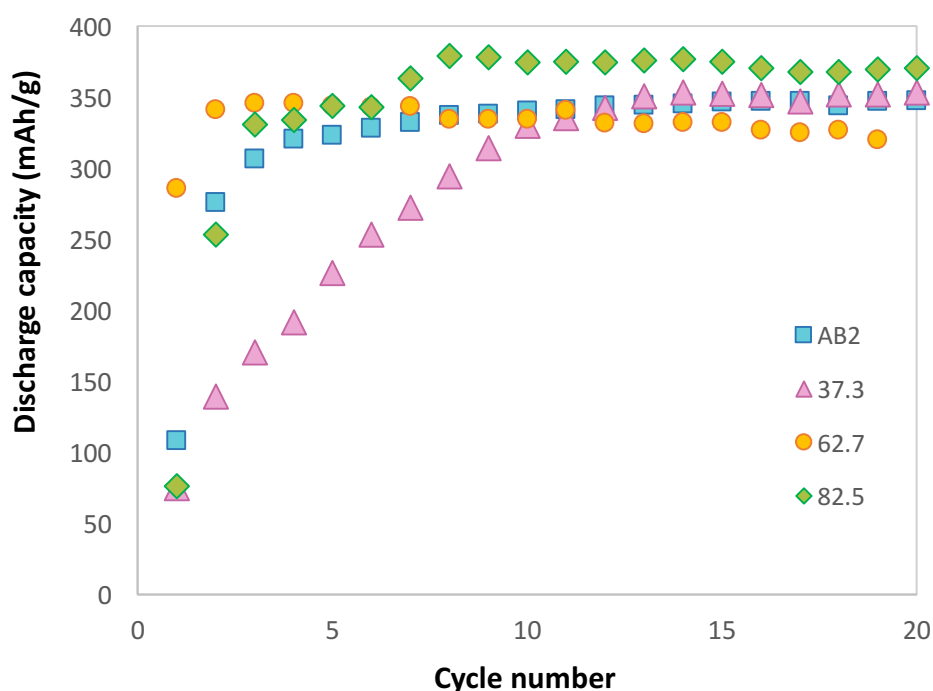


Figure 4.9: Discharge capacity-cycle number plot of foam electrodes of powders sieved into separate batches yielding average particle sizes of $d(0.5)$ of 37.3, 62.7 and 82.5 μm . Data for the unsieved powder is also included for comparison.

4.3 Activation via Surface Modification

Two methods were used to study the effect of surface modification on activation. One was KOH treatment applied on the starting powder, and the other was NiO coating of the AB_2 powders.

4.3.1 KOH treatment

In order to modify the surface of the AB₂ alloy, boiling KOH solution treatment was carried out for durations of 20, 60, 80 and 100 minutes. SEM micrographs of the resulting powder surfaces are given in Figure 4.10. The smooth surface of the untreated particle becomes decorated first with needle like features and as duration of the treatment increases these fine features become coarser and takes up plate-like configurations.

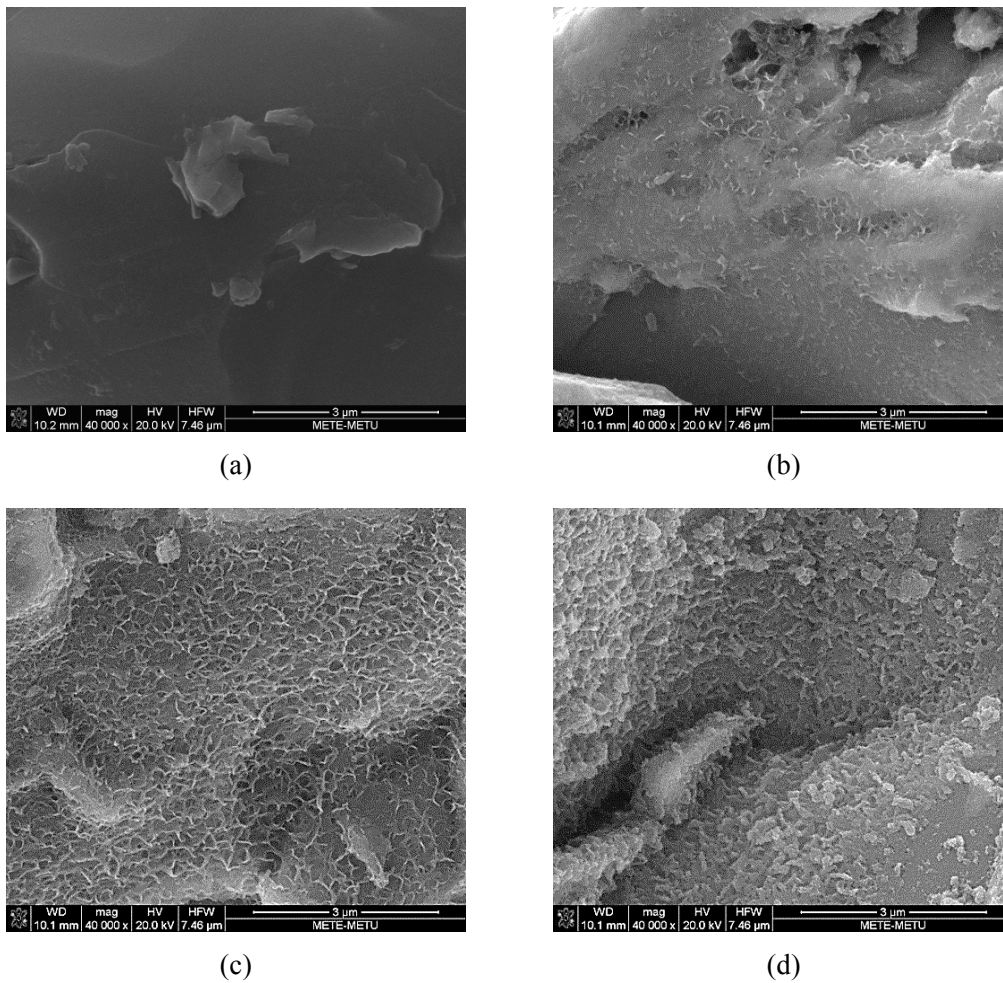


Figure 4.10: SEM images of the surfaces of (a) untreated powder and powders subjected to hot KOH treatment for (b) 20, (c) 60 and (d) 80 minutes.

The activation behaviour of powders treated for different periods of time; 20, 60 and 80 minutes were studied by Tan et al. (2016) and were reproduced in Figure 4.11. The test refers to pressed electrodes with a single compartment cell. It can be seen that the

activation performance of the powder is enhanced with the KOH treatment. While with 20-minute treatment, the maximum capacity was obtained after 4 cycles, this value was reduced to 2 cycles after 60-minute treatment. However, the best activation performance was attained with 80-minute treated powder where the powder was ready to give its maximum capacity at the second cycle.

The maximum capacities attained with pellets prepared from powders treated for 20 and 60 minutes, were nearly the same and were equal to the expected capacity of 315 mAh/g. With 80 minute treated powder, maximum capacity of 411 mAh/g was attained quickly and maintained thereafter. Here it should be mentioned that this capacity is very much higher than the expected capacity of these powders in the open cell.

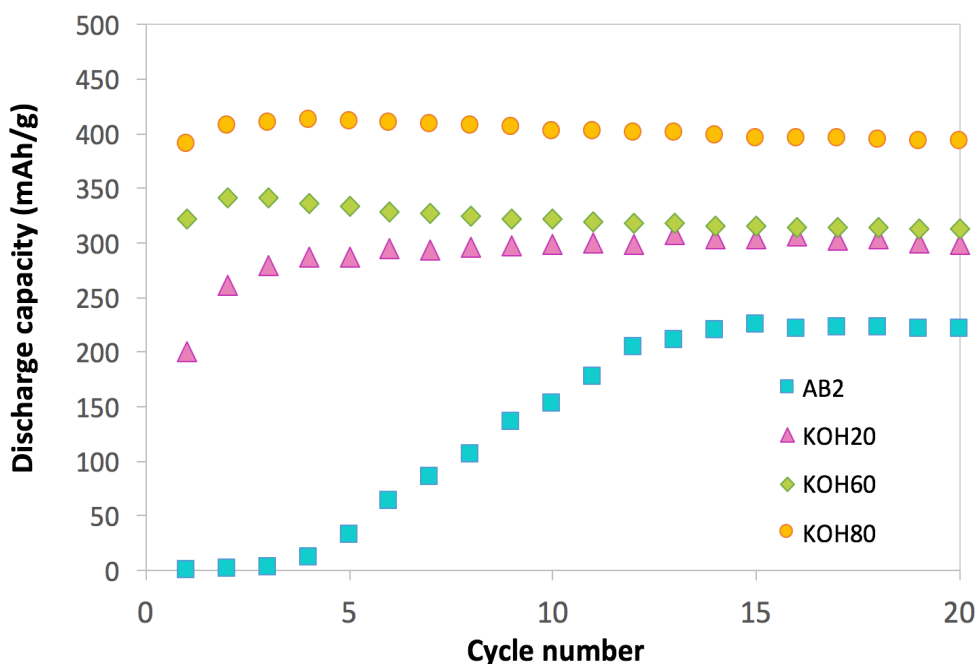


Figure 4.11: Discharge capacity vs. cycle number plot of the pressed electrodes prepared from powders treated in boiling KOH solution for 20, 60 and 80 minutes. Data of pristine powder is also included for comparison (Tan et al., 2016).

To check whether further increase was possible with this treatment, a new sample was prepared, where the powder was boiled 100 min in KOH. SEM micrograph of resulting powder surface is given in Figure 4.12. The capacity dropped, however, to 320 mAh/g, i.e. similar to those obtained with 20 or 60 minute-treatments.



Figure 4.12: SEM image of the surface of AB₂ powder subjected to hot KOH treatment for 100 minutes.

It should be noted that even though electrode configuration used in the above samples were of the pressed type, there was no decrease in the saturation capacity with continued cycling. This implies that with KOH treated powders particle drop-out somehow did not take place.

In order to examine how KOH treatment improves the activation behaviour of AB₂ powders, the treated samples were subjected to a detailed surface characterization. The pristine powder was mounted in epoxy and the KOH treatments were applied to the mounted samples for 20, 40, 60, 80 and 100 minutes. Treated samples were then characterized by Electron Probe Microanalyzer (EPMA) for their surface compositions.

Results obtained with EPMA are shown plotted in Figure 4.13. Here the variation of major elements making up AB₂ powder are shown as a function of the treatment time. It is seen that with the increased duration of KOH treatment, the relative proportion of Ni increases at the expense of other elements, most notably Zr. This enrichment of Ni on the surface could also be confirmed with attraction of the treated powder to a permanent magnet.

In order to investigate the surface features formed as a result of boiling KOH treatment, particles forming at the surface were collected by ultrasonication in ethanol. Figure 4.14 shows SEM image of the particle mixture which refer to a sample treated 80 minutes in KOH. It is seen that those features are quite fine as reported before. The

powder mixture was further investigated by XRD, Figure 4.15(b). The XRD pattern contain extremely broad peaks together with three peaks emerging from the broad spectrum. Two of these peaks are compatible with Ni(OH)_2 with broadened peaks of AB_2 . This was expected as the powder contain fine particles of AB_2 together with Ni(OH)_2 .

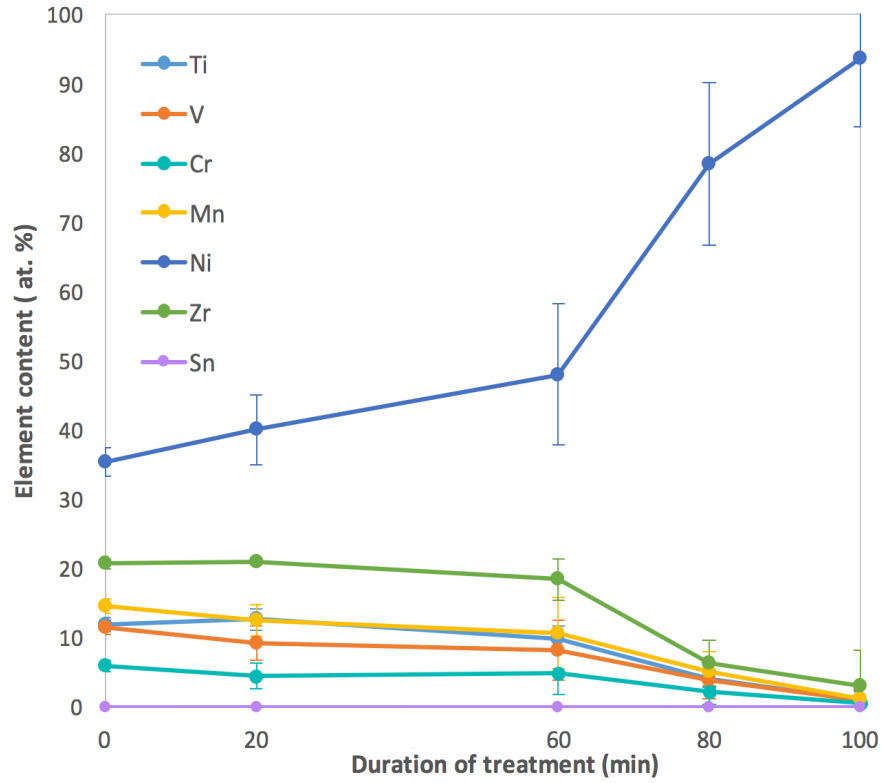


Figure 4.13: Change in amount of present elements by increasing KOH treatment duration obtained by EPMA.

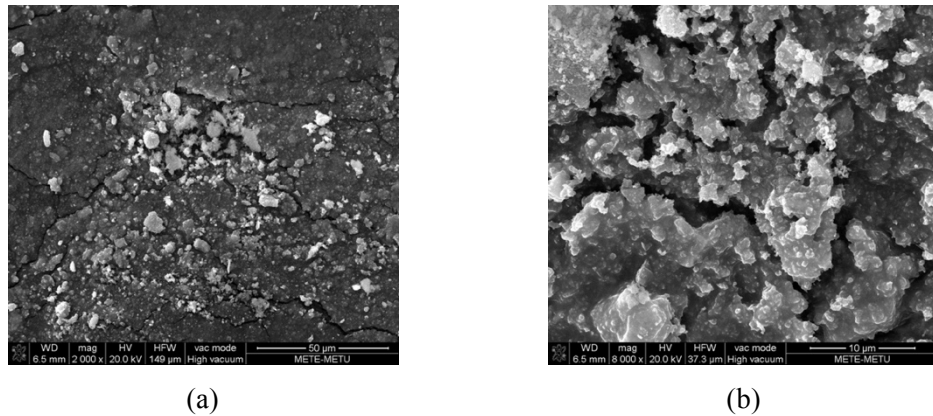
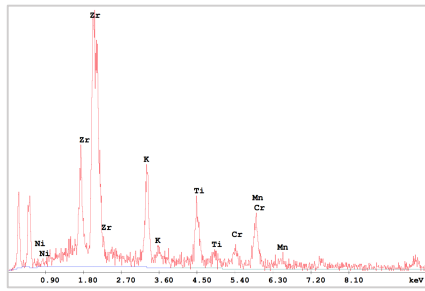
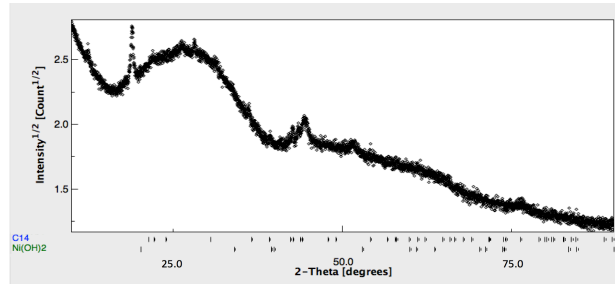


Figure 4.14: SEM images of the mixture collected over 80 minute KOH treated AB_2 powders observed at (a) 2000x and (b) 8000x. Note that mixture also contains some AB_2 particles.



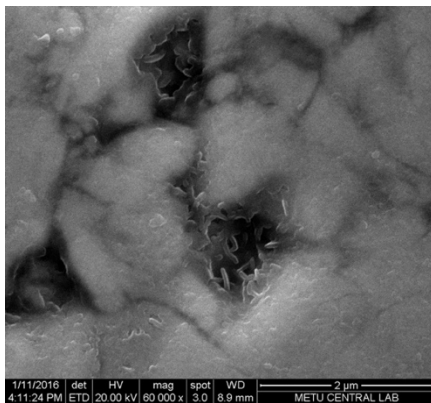
(a)



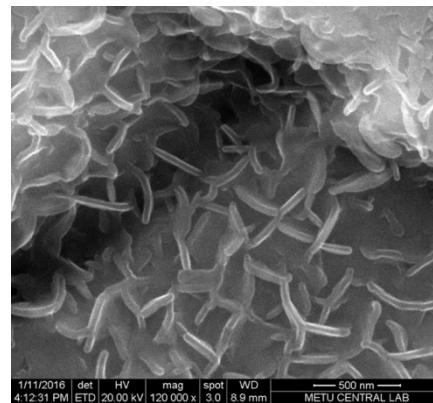
(b)

Figure 4.15: (a) EDS analysis and (b) XRD pattern of the mixture collected over 80 minute KOH treated AB_2 powders. Note that the angles at which $Ni(OH)_2$ peaks and C14 peaks are given on the XRD pattern.

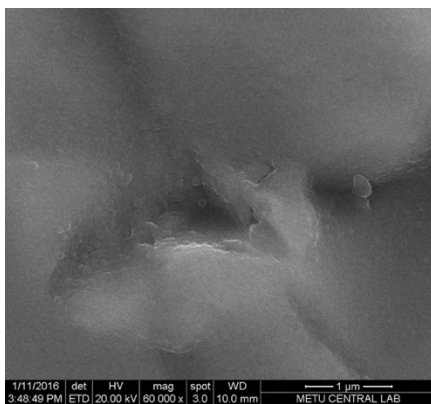
SEM micrographs of the samples characterized with EPMA are shown in Figure 4.16. In 20 minute treated sample, there is a growth of some features, finer than 100 nm, in the small pits on the powder surface Figure 4.16(b). These features coarsen with the duration of treatment. In 100 minutes, the features exceed 1 μm in size, Figure 4.16(h). With this prolonged treatment deep cracks do develop in the powders. (such cracks were not observed in free, i.e. unmounted powders)



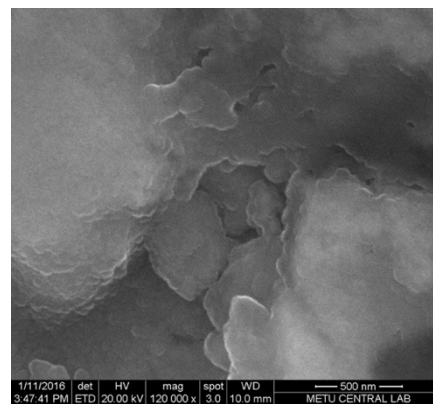
(a)



(b)



(c)



(d)

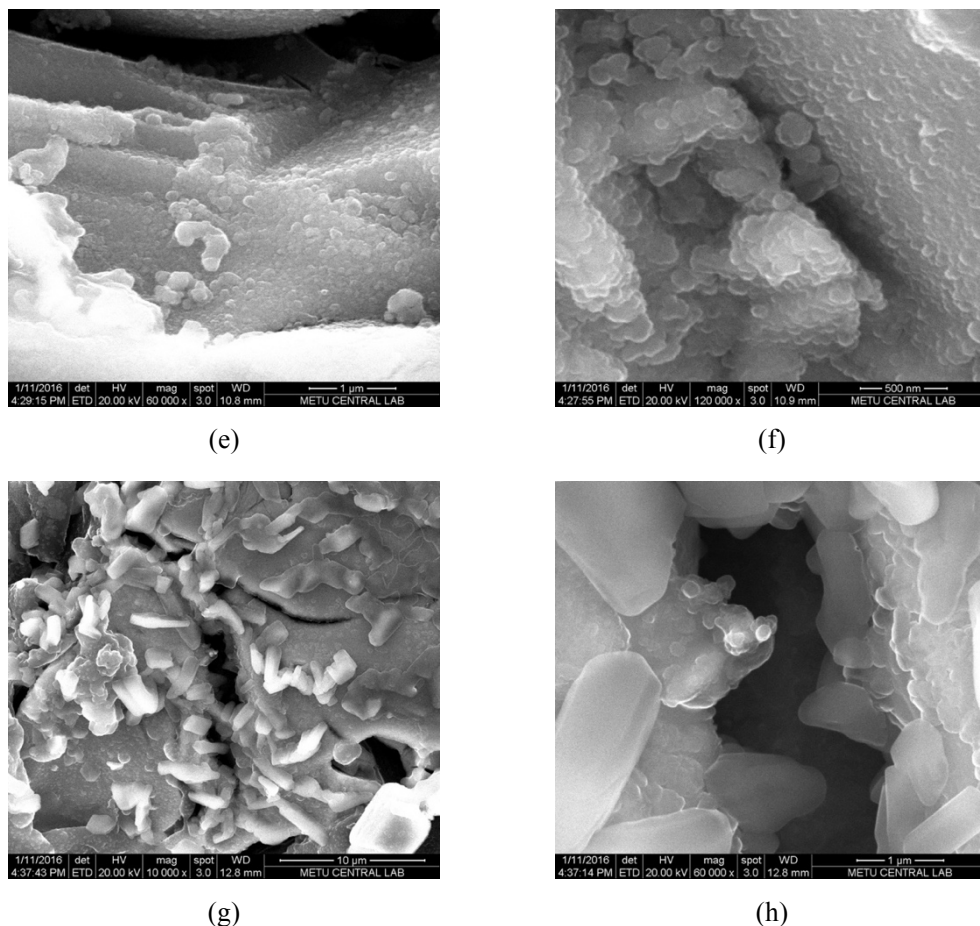


Figure 4.16: SEM images of AB_2 powders mounted in epoxy and KOH treated for (a and b) 20 minutes, (c and d) 60 minutes, (e and f) 80 minutes and (g and h) 100 minutes. Note that the images for 100 minute treated powders are at 10000x and 60000x magnification and the rest is at 60000x and 120000x.

Returning to the electrochemical results, it would be useful to mention that the results given in Figure 4.11 refer to pressed samples tested in single compartment cell as reported by Tan et al. (2016). It is useful to add that these electrochemical measurements were repeated using the foam electrodes also. The results of these measurements are given in Figure 4.17, which however yielded unexpected results. There was no improvement in the activation behaviour of treated powders, as could be seen in Figure 4.17. The reason for this is not clear though, special surfaces generated by KOH treatment may be negatively affected by PVA addition.

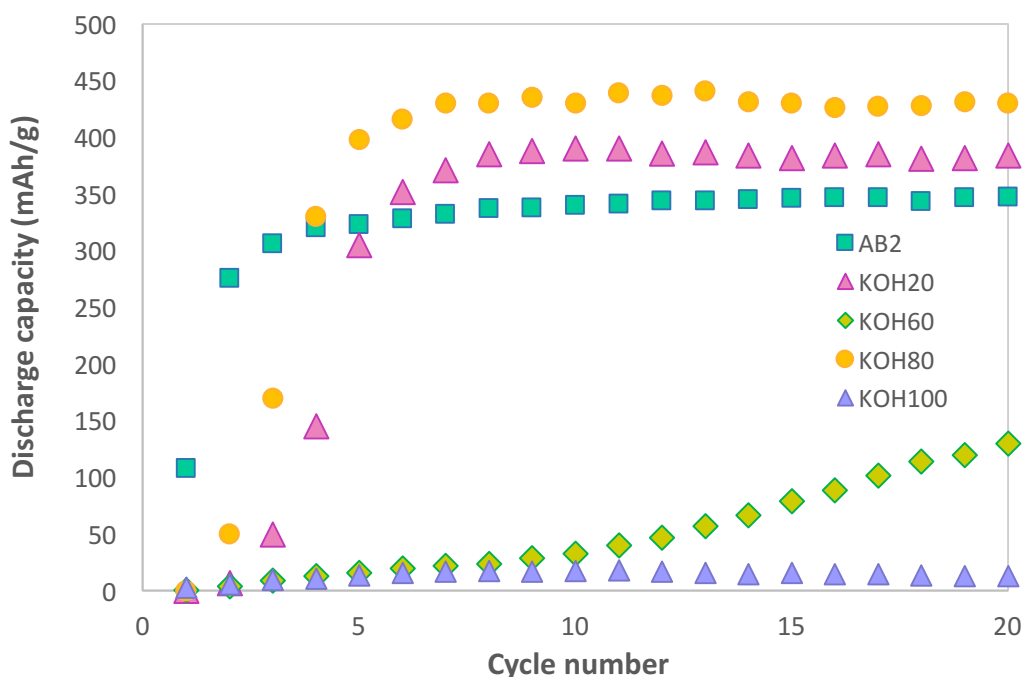


Figure 4.17: Discharge capacity vs. cycle number plot of the foam electrodes prepared from powders treated by boiling KOH solution for 20, 60 and 80 minutes. Note that the data of pristine powder is also included for comparison.

4.3.2 NiO coating

Following a successful result obtained by KOH treatment, an alternative approach would be to produce a Ni rich surface through alternative means. One approach would be to coat AB₂ powders with NiO which could be reduced to Ni later on.

In order to coat AB₂ powders with NiO, two sol-gel routes were followed. The first route involved the use of aqueous solution of NiCl₂ and sucrose while the second route made use of NiNO₃ and EG.

First, NiO in the absence of AB₂ material was obtained using the two procedures mentioned above. For this purpose, using the first route (Suciu et al., 2006), two solutions; one solution 0.12 g pectin (Alfasol) and 2.38 g sucrose (table sugar) dissolved in 25 ml deionized water and the other solution containing 0.59 g NiCl₂.6H₂O (Merck EMSURE for analysis) with 25 ml deionized water were mixed together in a beaker and heated to 90 °C while stirring. The stirring was discontinued when the solution was gelled. Following 5 hours of drying, the product was heated to 650 °C at a rate of 200 °C/h and calcined at this temperature for 3 hours.

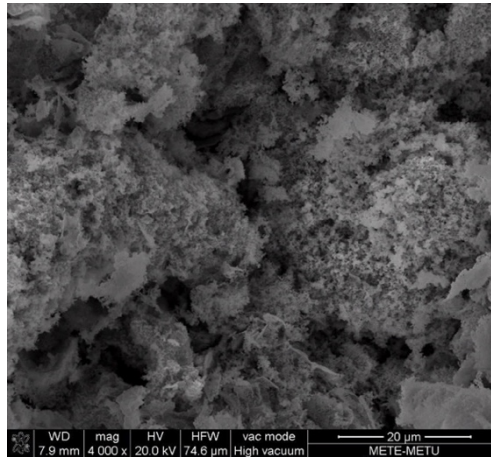


Figure 4.18: SEM image of NiO coating in the absence of AB₂ powders using NiCl₂ precursor.

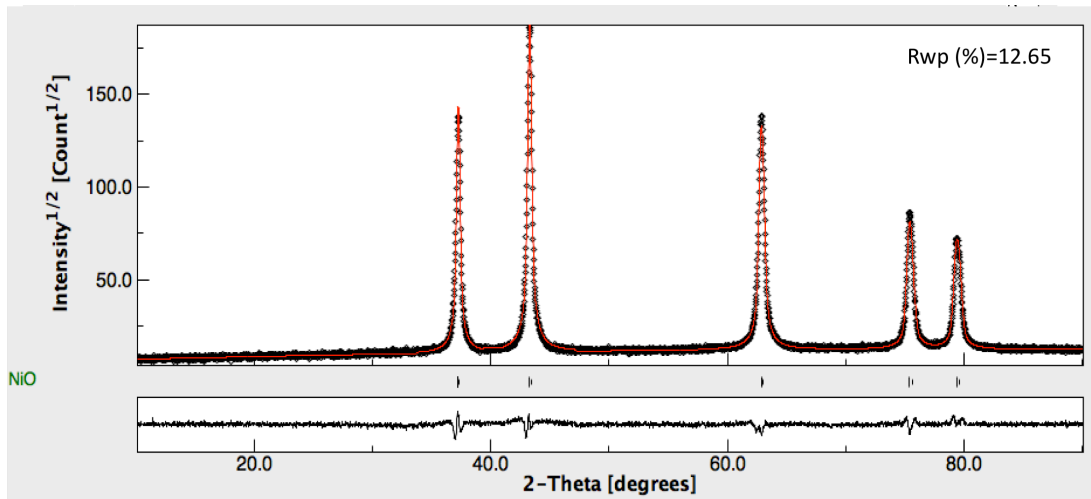


Figure 4.19: XRD pattern of NiO coating by sucrose and NiCl₂ precursors. Note that the pattern is compatible with NiO.

Resulting product, as shown in Figure 4.18, is in the form of very fine powder. XRD pattern of this powder is given in Figure 4.19, which is compatible with NiO.

In order to coat AB₂ particles with NiO, the route was repeated but this time with the addition of 3.55 g of AB₂ powder to the NiCl₂ solution. The product was examined under SEM, Figure 4.20. It can be seen that the treatment leads to the coating of AB₂ powders with fine particles.

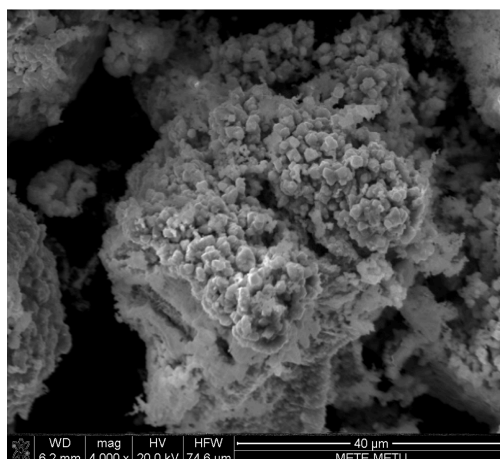


Figure 4.20: SEM image of AB₂ powder coated using NiCl₂ precursor. The gelled mixture was calcined at 650°C.

The pellet prepared from AB₂ powders NiO coated by this route was tested electrochemically in a single compartment cell. No capacity could be obtained from the powder. In addition to this, charging was not successful which is an indication of inability of current flow through the electrode.

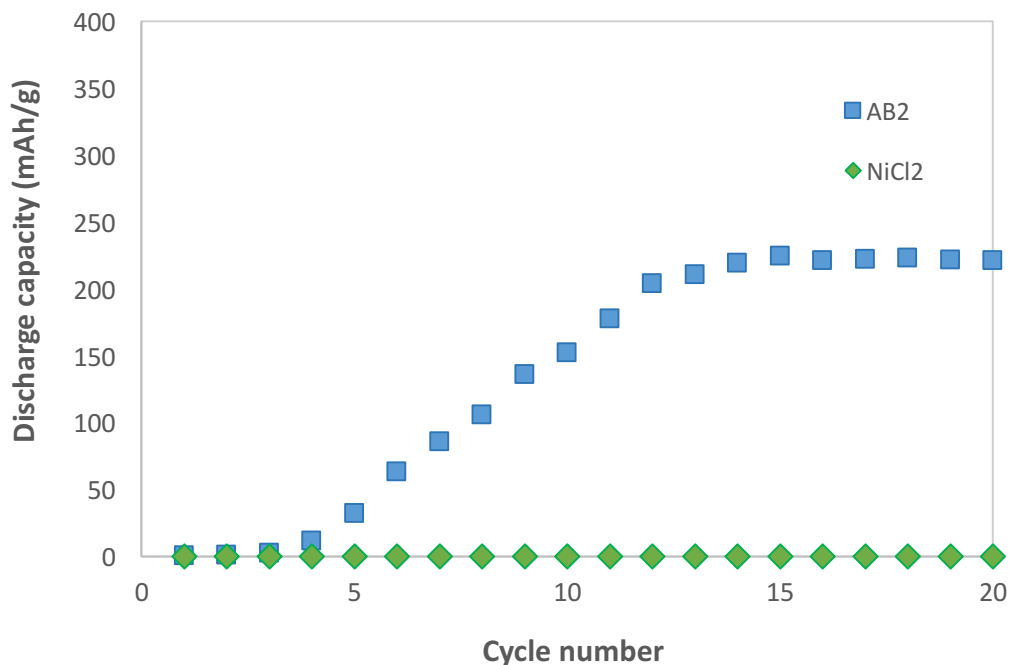


Figure 4.21: Discharge capacity vs. cycle number plot of the pressed electrodes prepared from powders coated by sol-gel methods that use NiCl₂ as precursor. Data of pristine powder is also included for comparison.

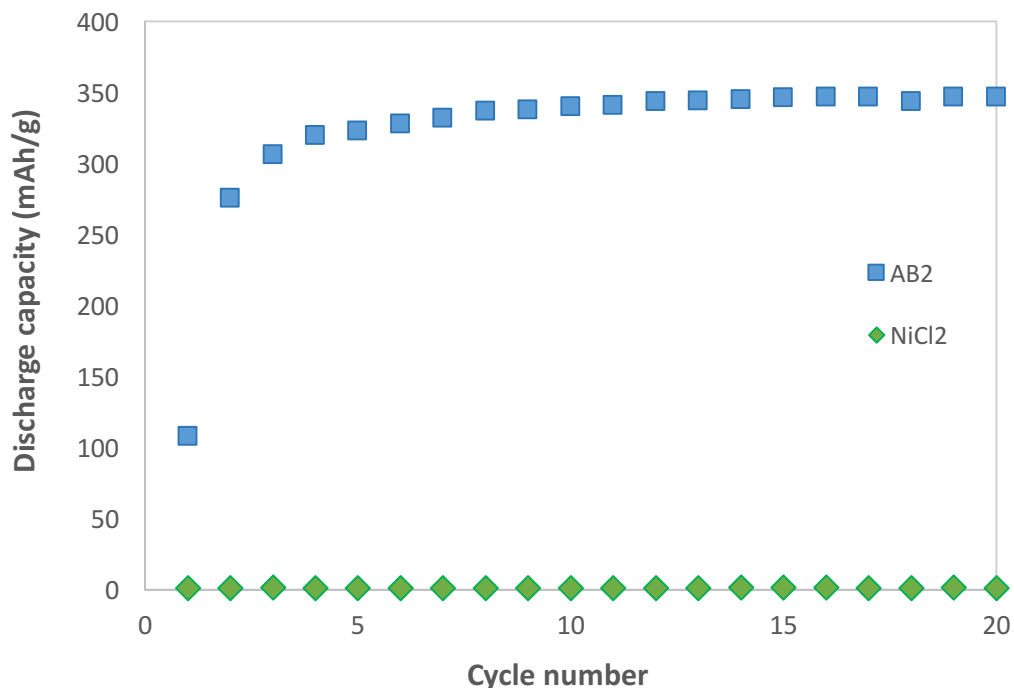


Figure 4.22: Discharge capacity vs. cycle number plot of the foam electrodes prepared from powders coated by sol-gel methods that use NiCl_2 as precursor. Data of pristine powder is also included for comparison.

In the second route, the process was first carried out in the absence of AB_2 powder. The route involved the use of ethylene glycol (EG) as solvent and $\text{NiNO}_3 \cdot 6\text{H}_2\text{O}$ as NiO source (Bocutti et al., 2001). In this method, 50 ml EG together with 2.5 mmole $\text{NiNO}_3 \cdot 6\text{H}_2\text{O}$ was put in a beaker and stirred while heating to 90°C . The mixture was stirred and temperature was maintained at 90°C until the solution is vaporized, i.e. approximately 12 hours. The mixture was then transferred into a crucible and put into the furnace. The furnace was heated to 200°C at a rate of $2^\circ\text{C}/\text{min}$ and held at this temperature for 24 hours.

Resulting product, Figure 4.23, resembles a cracked shell rather than a fine powder. XRD pattern of the product is given in Figure 4.24. As a result of Rietveld analysis on the pattern it was observed that the pattern is compatible with NiO with some additional Ni (0.95 wt. %).

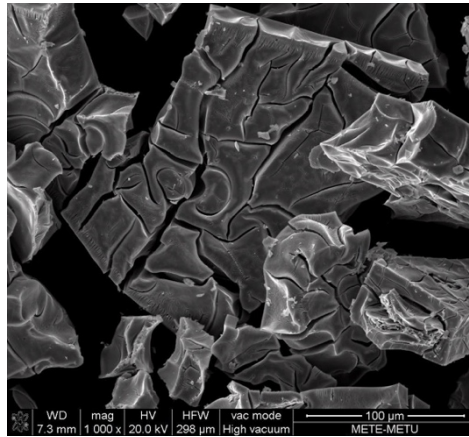


Figure 4.23: SEM image of NiO coating in the absence of AB₂ powders using NiNO₃ precursor.

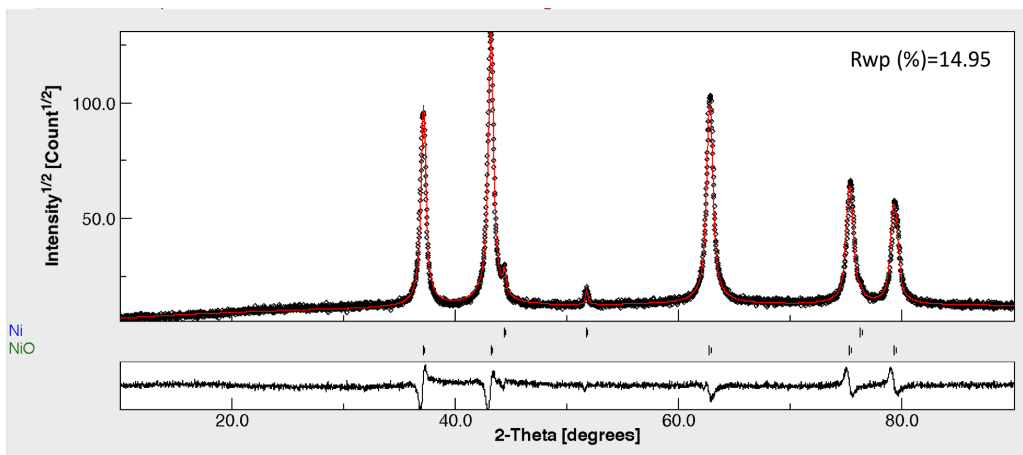


Figure 4.24: XRD pattern of NiO coating by EG and NiNO₃ precursors. Note that the material contains Ni peaks.

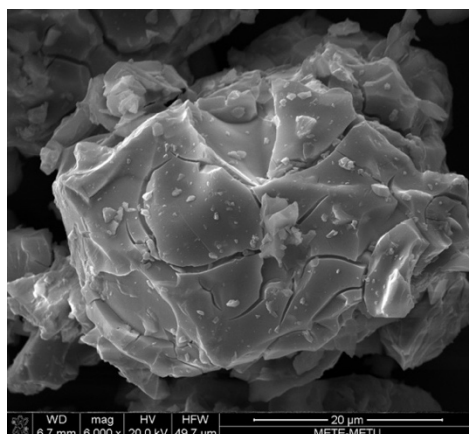


Figure 4.25: SEM image of AB₂ powder coated using NiNO₃ as precursor. The gelled mixture was calcined at 200°C.

In order to coat AB₂ particles via this route, 3.5 g of AB₂ particles were added to the mixture described above before the gelation starts. Here the amount of AB₂ powder was adjusted so as to keep NiO not less than 5 wt. % of AB₂ powder. SEM micrograph of the product is given Figure 4.25 where fine particles can be detected at the surface of AB₂ powder.

The pellet prepared from AB₂ powders coated via the second route was tested electrochemically with pressed electrode in a single compartment cell. The electrode, yield a maximum capacity of 37 mAh/g Figure 4.26. It is seen that this capacity has not yet saturated after 20 cycles, which imply a higher attainable capacity. It is obvious that the activation performance of the electrode is not better than the uncoated alloy.

The experiments with NiO coatings were repeated with pasted electrodes. The capacity reached with these electrodes were significantly higher. The coated powder reaches a capacity of 270 mAh/g after tenth cycle. However, NiO coating has not provided any advantage. The capacity was lower as compared to bare powder and the cycle number for saturation capacity was higher, i.e. no improvement in activation.

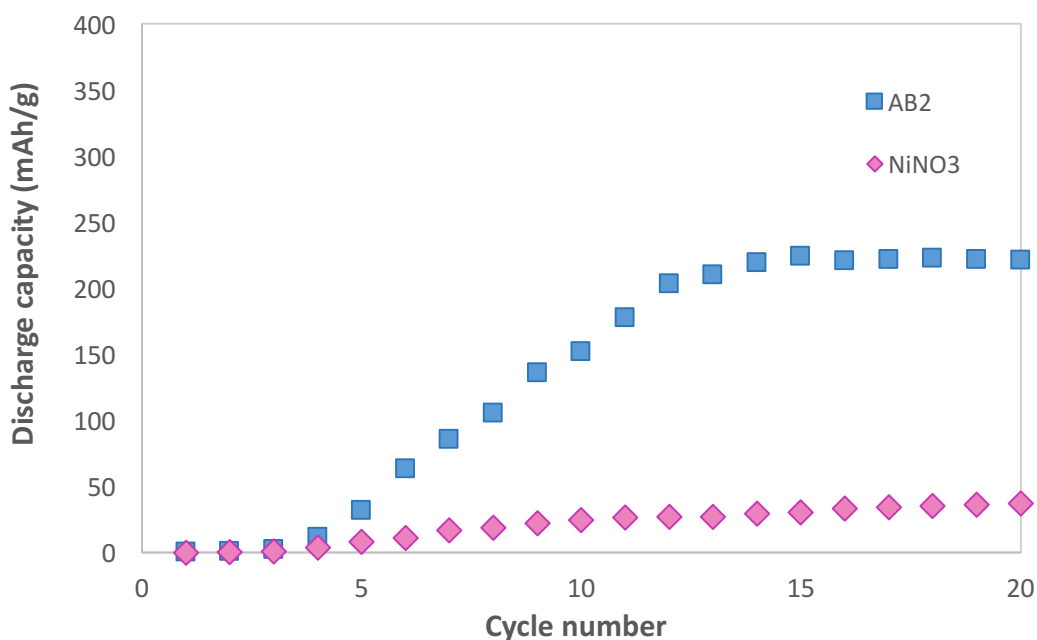


Figure 4.26: Discharge capacity vs. cycle number plot of the pressed electrodes prepared from powders coated by sol-gel methods that use NiNO₃ as precursor. Note that the data of pristine powder is also included for comparison.

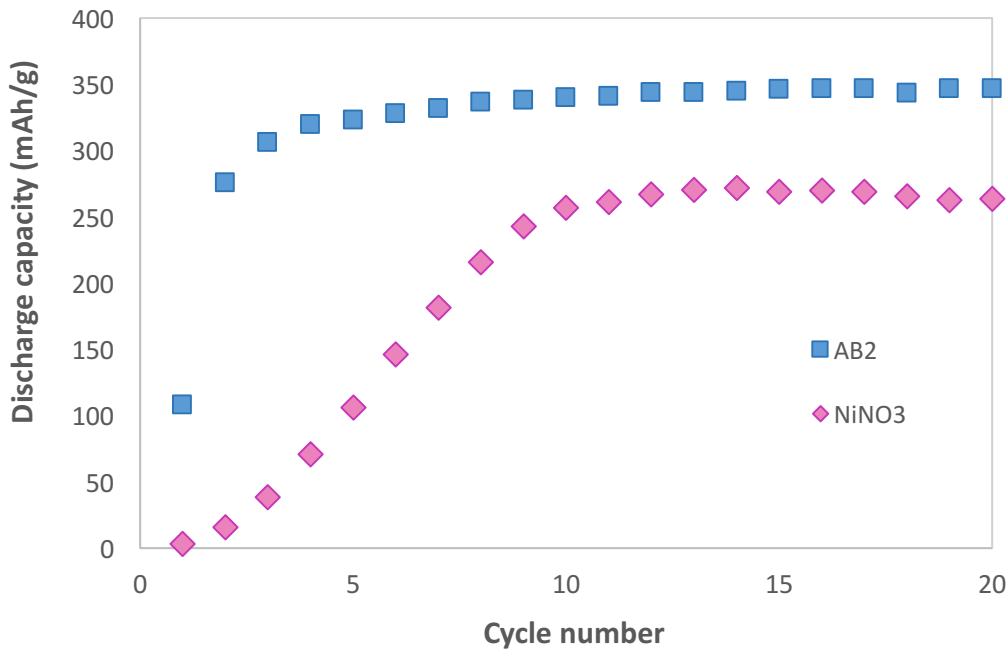


Figure 4.27: Discharge capacity vs. cycle number plot of the foam electrodes prepared from powders coated by sol-gel methods that use NiNO₃ as precursor. Note that the data of pristine powder is also included for comparison.

4.4 Discussion

There are several aspects that could be discussed further. First C14 alloy in question will be evaluated and its place in the group of AB₂ alloys will be given. Then methods of electrochemical characterization will be concentrated upon so as to reliably characterize the performance of the electrodes. Methods of activation which is the main subject of this thesis will then be evaluated so as to identify the method best suited for the purpose. One important finding in this study is that the saturation capacity in the current alloys could well be above that expected from the PCI curve. Reasons how this could arise will also be discussed.

The current alloy is an AB₂ type (Ti_{0.36}Zr_{0.64})(V_{0.15}Ni_{0.58}Mn_{0.20}Cr_{0.07})₂ alloy that has C14 crystal structure. As mentioned previously AB₂ alloys have Laves phase crystal structures. There are three types of Laves phases: hexagonal C14, cubic C15 and again hexagonal C36 (intergrowth of C14 and C15). The hexagonal layers are differently stacked in each of these structures. C14 (prototype MgZn₂) and C15 (prototype

MgCu₂) are the most frequently observed structures in AB₂ alloys (Huot et al., 1995). Due to difficulties in production, AB₂ alloys most of the time cannot be monophasic in the as-cast condition. Therefore, secondary phases are almost always present in AB₂ alloys. According to Young et al. (2008) when the r_A/r_B ratio is less than 1.225, the crystal structure is C14-dominated. C14-dominated alloys were observed to have superior high rate dischargeability, i.e. little drop in capacity with high rate of discharge, when compared to C15-dominated alloys (Huot et al., 1995, Young et al., 2010).

The prototype of C14 AB₂ alloys, ZrMn₂, is a representative of the flexibility of C14 structure in AB₂ alloys. The wide solubility range of ZrMn₂ enables formation of multi component AB₂ alloys. The current alloy comprises elements such as Zr, Ti, V, Ni, Mn, Cr and Sn. With varying amount and type of alloying elements, performance could be adjusted to a large extent. According Young and Nei (2013), Zr, Ti and Ni are considered as the main elements in AB₂ alloys, i.e. (Zr,Ti)Ni₂. They found, experimentally that the replacement of certain fraction of Ni by V and Sn are beneficial in enhancing bulk diffusion coefficient and the high rate dischargeability. Cr increases the battery shelf life while adversely affecting the high rate discharge performance. Mn, while decreasing cycle life, is preferred in most of the AB₂ alloys as it increases the capacity and improves the activation behaviour of the alloy.

As reported above, the current alloy comprises a certain fraction of second phase, (Ti_{1.3}Zr)Ni_{2.5} which is not more than 5 wt. %. The function of these second phases in (Zr,Ti)Ni₂ negative electrode materials is quite controversial (Zhu et al., 2001). The second phases have low plateau pressures and they are not likely to play a useful role in functioning of the electrodes. Cuevas and Joubert (2001), on the other hand, indicate that these second phases can function like a gate/pump that charges and discharges the Laves phase thus catalysing the process due to this low plateau pressure. Thus, it might be that the second phases present in the current alloy, (Ti_{1.3}Zr)Ni_{2.5}, could play quite a crucial role in charge-discharge process.

The original plan was to characterize the negative electrode material made out of AB₂ alloy with the use of pressed electrode. This simply involves mixing the alloy powder

with copper powder and pressing the mixture to a 10 mm diameter pellet. In electrochemical measurements it was noted that with pressed electrodes prepared with milled powder (ball milled for 1 hour and 3 hours) and most critically with sieved powder (especially with coarse powders), there was a decay in capacity with continued cycling. This was attributed to the loss of active material by drop-out i.e. certain fraction of powder drops from the electrode resulting in the loss of active material. Therefore, a new electrode configuration was employed. Using PVA binder and Ni foam in electrochemical measurements, particle drop-out was prevented. Therefore, the use of this foam electrode configuration was useful in providing more reliable measurements on the saturation capacity (compare Figure 4. 8 and 4. 9). It should be pointed out that the use of PVA may prevent the particle drop-out, so the saturation capacity could be measured more reliably, but its presence may affect the activation behaviour of the alloy so this aspect should be kept in mind.

Activation behaviour of the AB_2 alloy was examined regarding the two aspects namely surface area and surface modifications. In order to examine the effect of surface area on activation, ball milling and sieving was used to obtain particles of different surface area. According to the results given above, coarse particles activate relatively fast. Thus electrode with coarse particles ($d(0.5) = 82.5 \mu\text{m}$ and $62.7 \mu\text{m}$), attain their maximum capacities after 7-8 cycle. On the other hand, electrode prepared with fine powders, i.e. $d(0.5) = 37.3 \mu\text{m}$, a cycle number of more than 15 was necessary to obtain a similar capacity. It is well-known that active powders are usually coated with oxide layers and the role of activation is to generate new surfaces free from oxides. The probable cause for the fast activation with coarse particles is the ease of their fragmentation. A similar explanation was advanced by Liu et al. (1996) where there was also a clear difference in the activation behaviour of the powders with different particle sizes. The fragmentation brings fresh uncontaminated surfaces into contact with electrolyte thus including them in the charge-discharge process. It should be mentioned that if fragmented pieces could not be kept within the electrode, this would lead to the particle drop-out.

When there is particle drop-out, discharge capacity versus cycle number often show a maximum beyond which the capacity decreases with the loss of active particles. It can

be inferred from the results reported above that the maximum occurs with coarse powders and in the case of fine powders such maxima is absent. In fact, in the case of fine powders, the value at which the capacity saturates is lower than those obtained with coarse particles (compare Figure 4.8 and 4.9). This could be attributed to ineffective distribution of conductive additive which leaves a certain portion of fine powders not contact with the electrode. Liu et al. (1996), have used the same argument and explained that this situation leads to inefficient utilization of the active powders thus yielding a lower saturation capacity.

An alternative method of activation is surface modification on AB₂ powders. For this purpose, alloy powders were processed for different durations in hot 6 M KOH solution. According to electrochemical measurements, this method is quite effective in activating the alloy. With 80 minute-treatment, quite a high saturation capacity (390 mAh/g) was attained in the first cycle.

While investigating the reason for the enhanced activation behaviour, surface composition and morphology were examined by EPMA and SEM. In near surface examinations, leaching of elements most notably Zr was observed yielding a Ni-rich surface layer. Selective dissolution of elements and formation of Ni-rich surface layer by KOH treatment was also observed by Gao et al. (1996) , Jung et al. (1998) and Young et al. (2010). According to the latter workers, the first elements leaching out from the AB₂ alloy through this corrosion process are Zr and V.

In KOH treated powders, the surfaces are roughened to various degrees. According to Liu et al. (1996) this roughened surface contributes to fast activation by facilitating the charge acceptance. A result of this roughening there is an increase in surface area. Underlying mechanism for improved kinetics is therefore similar to the one observed in the powders undergone for instance milling where there is also an increase in the surface area.

Originating from the advantage of Ni-rich surface on activation behaviour, the AB₂ powder, an alternative method was employed whereby AB₂ powders were coated with NiO powders. Unfortunately, this approach was not successful, most probably coating achieved was not optimized. For instance, using NiCl₂, the electrode prepared from

NiO coated powder had no capacity at all. Using NiNO₃ on the hand gave a capacity of 271 mAh/g. More work is needed to optimize the coating and establish the role of NiO coatings on fast activation.

An important observation made in this study is that saturation capacity observed in some of the activated powders is higher than that expected from gas phase hydrogen storage. According to the PCI of the alloy given in Figure 4.28, at 1 bar, the expected hydrogen storage capacity of the alloy is 1.2 wt. %. This value corresponds to electrochemical storage capacity of 320 mAh/g. In the results reported above, there are cases where the capacity was below or above this value.

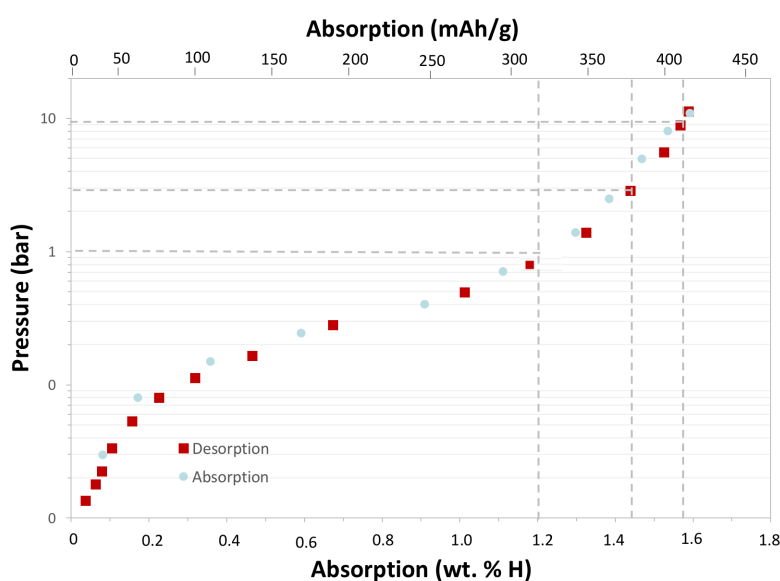


Figure 4.28: PCI curve of the AB₂ alloy. Note that at 1 bar the alloy gives a gas phase capacity of 1.2 wt. % hydrogen which corresponds to 320 mAh/g electrochemical storage capacity.

One example where the discharge capacity was higher than 320 mAh/g was observed in foam electrodes prepared from the sieved powder as given in Figure 4.29. The capacity was 378 mAh/g with the sieved ($d(0.5) = 82.5 \mu\text{m}$) powder. This value is very much larger than that obtained with pressed electrode where the value was 220 mAh/g. This difference in capacity might be due to the use of nickel foam in the former electrode. If the surface was smooth as in the case of pressed electrode, bubbles could form on/escape from the surface which would limit the equilibrium pressure close to that of atmospheric value. However, in case of foam electrode, pressed foam where

pores 3D in structure collapses into 2D, Figure 4.31, may stabilize the bubbles creating pressures greater than atmospheric before they could escape from the surface. According to Figure 4.28 so as to obtain a discharge capacity of 378 mAh/g, local pressure achieved should be as high as 3 bar.

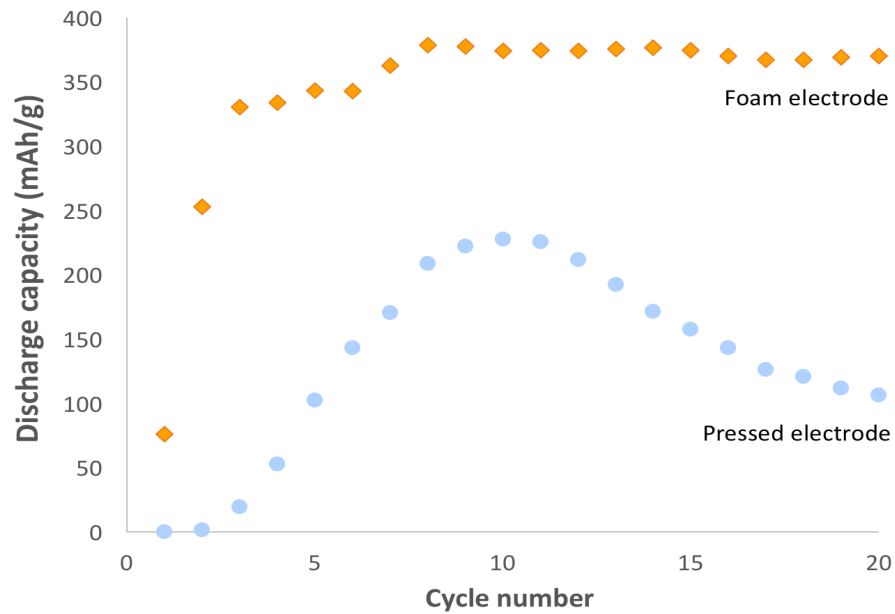


Figure 4.29: Discharge capacity vs. cycle number of the foam and pressed electrodes prepared from coarse powders.

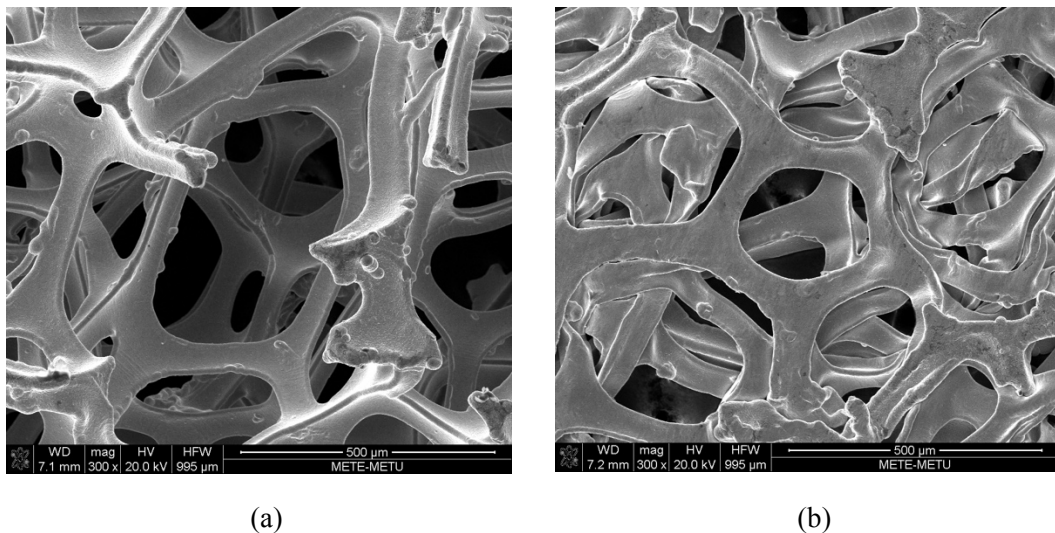


Figure 4.30: 3D structure of (a) unpressed nickel foam and (b) resulting 2D structure after pressing.

One of the highest capacities attained in this study, as reported by Tan et al. (2016), was obtained with 80 minute-KOH treated powders, 411 mAh/g. The powders were tested electrochemically using pressed electrode configuration, i.e. without any binder material. Young et al. (2012), studying $ZrV_{0.5}Ni_{4.0}$ alloy observed the same effect with KOH treatment, i.e. electrochemical discharge capacity was much higher than that of gas phase storage capacity at 1 bar pressure. Young et al. (2012) advances an argument stating that this was made possible because the equilibrium pressure decreases in electrochemical environment. Secondary phases present in the alloy with their interfaces was thought to be the reason for this reduced pressure.

It should be noted that, as reported above, KOH treatment yields a rough surface Figure 4.10. As discussed above for the foam electrode, a similar mechanism might be responsible for the observed high capacity. Thus, the rough surface generated by the treatment may create small pits which would allow pressure to increase locally well above 1 atmosphere. The value of 411 mAh/g requires a local pressure value of 10 bar, see Figure 4.28. Therefore, the origin of high capacity may be due totally to the rough surface generated by KOH treatment. If this is the case, then there is no special role played by the second phases present in the alloy. More detailed study would be needed to clarify the role of second phases in AB_2 alloys.

CHAPTER 5

CONCLUSIONS

A study was carried out on activation behaviour of a Laves phase AB₂ alloy of composition (Ti_{0.36}Zr_{0.64})(V_{0.15}Ni_{0.58}Mn_{0.20}Cr_{0.07})₂ using two groups of methods; one aiming for an increase in the surface area and the other aiming for surface modifications.

In order to examine the effect of an increase in the surface area on activation behaviour two processes were employed; sieving of powders into different sizes and ball milling. As a result of this study the following conclusions can be made:

- i) The alloy with coarse particle sizes (> 60 μm) activates faster. This was attributed to the ease of fragmentation of coarse powders which leads to the generation of new fresh surfaces whereby leading to fast activation. A saturation capacity of 245 mAh/g was reached in electrode made up of d(0.5) = 62.7 μm powders after 8 cycles.
- ii) The alloy with fine particle sizes (e.g. d(0.5) = 37.3 μm) yields low saturation capacities which was attributed to ineffective utilization of the active powders, i.e. certain fraction of powders are not in contact with the electrode.
- iii) Milling of powders leads initially to a decrease in particle size. But with prolonged milling the particles do agglomerate yielding particles sizes similar to the initial ones. For all durations milling provides fast activation. Saturation capacity, however, is adversely affected by extended milling.

The conclusions made above rely on electrochemical measurement made on pressed electrode. It may be useful to mention that when pressed electrode is used there is a capacity decay with cycling which is caused by particle drop-out.

The use of foam electrode, i.e. encapsulation of pasted electrode inside a foam, was useful in preventing this particle drop out whereby enabling reliable measurement of capacity with continued cycling.

In order to study the effect of surface modification on AB₂ powders, two treatments were employed; hot KOH treatment and NiO coating of AB₂ powders. The following can be deduced from the study on surface modifications:

- iv) Hot alkaline treatment, i.e. treating AB₂ powder in boiling 6 M KOH solution, appears to be the most efficient method of activation. This treatment leads to preferential leaching of elements in the powders producing surface layers rich in Ni. The treatment with a duration of 80 minutes yields powders that are already active and ready to be used as is. In addition, the treatment yields a capacity of 390 mAh/g, which is higher than those obtained with other methods used in the current study.
- v) NiO coating aimed to develop Ni rich surfaces similar to those obtained with KOH treatment. The coatings produced in the current study was not useful in activating the alloy.

The most noteworthy result obtained in the current study is the high capacity obtained in AB₂ alloy with KOH treatment. In literature this increase was explained to be the result of a special role played by the second phases present in the structure. However, this increase in capacity could solely be attributed to the rough surface generated by the alkaline treatment. Such rough surfaces could stabilize the hydrogen bubbles. This would allow high hydrogen pressures to be reached locally in the surface.

REFERENCES

- Adzic, G. D., Johnson, J. R., Reilly, J. J., McBreen, J., Mukerjee, S., Sridhar Kumar, M. P., Srinivasan, S. (1995). Cerium Content and Cycle Life of Multicomponent AB₅ Hydride Electrodes. *Journal of The Electrochemical Society*, 142(10), 3429.
- Akiba, E. (1999). Hydrogen-absorbing alloys. *Current Opinion in Solid State and Materials Science*, 4(3), 267–272.
- Akiba, E., & Iba, H. (1998). Hydrogen absorption by Laves phase related BCC solid solution. *Intermetallics*, 6(6), 461–470.
- Akiba, E., & Okada, M. (2002). Metallic Hydrides III : Cubic Solid-Solution Alloys. *MRS Bulletin*, 27(September), 699–703.
- Akyıldız, H., Özenbaş, M., & Öztürk, T. (2006). Hydrogen absorption in magnesium based crystalline thin films. *International Journal of Hydrogen Energy*, 31(10), 1379–1383.
- Bocutti, R., Saeki, M. J., & Angelo, A. C. D. (2001). A surface modification for hydrogen storage intermetallic particles by sol-gel method. *Journal of New Materials for Electrochemical Systems*, 4(2), 77–81.
- Bocutti, R., Saeki, M. J., Florentino, A. O., Oliveira, C. L. F., & Angelo, A. C. D. (2000). The hydrogen evolution reaction on codeposited Ni-hydrogen storage intermetallic particles in alkaline medium. *International Journal of Hydrogen Energy*, 25, 1051–1058.
- Chandra, B. D., Chien, W., & Talekar, A. (1996). Metal Hydrides for NiMH Battery Applications. *Material Matters*, 6(2), 48–53.
- Choi, W.-K., Yamataka, K., Guo Zhang, S., Inoue, H., & Iwakura, C. (1999). Effects of Surface Treatment with Boiling Alkaline Solution on Electrochemical and Physicochemical Properties of the Zr_{0.9}Ti_{0.1}Ni_{1.1}Co_{0.1}Mn_{0.6}V_{0.2} Alloy Electrode. *Journal of The Electrochemical Society*, 146(1), 46–48.
- Cuevas, F., & Joubert, J. (2001). Intermetallic compounds as negative electrodes of Ni/MH batteries. *Applied Physics A*, 238, 225–238.
- Cui, N., Luan, B., Liu, H. K., & Dou, S. X. (1996). Discharge behaviour of MgNi-type hydrogen-storage alloy electrodes in 6 M KOH solution by electrochemical impedance spectroscopy. *Journal of Power Sources*, 63(2), 209–214.

- Cuscueta, D. J., Ghilarducci, A. A., & Salva, H. R. (2010). Design, elaboration and characterization of a Ni-MH battery prototype. *International Journal of Hydrogen Energy*, 35(20), 11315–11323.
- Du, Y. L., Yang, X. G., Zhang, Q. A., Lei, Y. Q., & Zhang, M. S. (2001). Phase structures and electrochemical properties of the Laves phase hydrogen storage alloys $Zr_{1-x}Ti_x(Ni_{0.6}Mn_{0.3}V_{0.1}Cr_{0.05})_2$. *International Journal of Hydrogen Energy*, 26, 333–337.
- Gamboa, S. A., Sebastian, P. J., Feng, F., Geng, M., & Northwood, D. O. (2002). Cyclic Voltammetry Investigation of a Metal Hydride Electrode for Nickel Metal Hydride Batteries. *Journal of The Electrochemical Society*, 149(2), A137.
- Gamboa, S. A., Sebastian, P. J., Geng, M., & Northwood, D. O. (2001). Temperature, cycling, discharge current and self-discharge electrochemical studies to evaluate the performance of a pellet metal-hydride electrode. *International Journal of Hydrogen Energy*, 26(12), 1315–1318.
- Gao, X. P., Zhang, W., Yang, H. B., Song, D. Y., Zhang, Y. S., Zhou, Z. X., & Shen, P. W. (1996). Electrochemical properties of the $Zr(W_{0.4}Ni_{0.6})_{2.4}$ hydrogen storage alloy electrode. *Journal of Alloys and Compounds*, 235, 225–231.
- Hermann, A. M., Ramakrishnan, P. A., Badri, V., Mardilovich, P., & Landuyt, W. (2001). Metal hydride batteries research using nanostructured additives. *International Journal of Hydrogen Energy*, 26(12), 1295–1299.
- Holm, T. (2012). Synthesis and characterisation of the nanostructured magnesium-lanthanum-nickel alloys for Ni-metal hydride battery applications, PhD Thesis. Norwegian University of Science and Technology.
- Homma, H., Saitoh, H., Misawa, T., & Ohnishi, T. (2002). Effect of Laves Phase on Hydrogen Behavior in V–Zr–Ti–Ni Hydrogen Absorption Alloys. *Materials Transactions*, 43(5).
- Hoshino, H., Uchida, H., Kimura, H., Takamoto, K., Hiraoka, K., & Matsumae, Y. (2001). Preparation of a nickel-metal hydride (Ni-MH) rechargeable battery and its application to a solar vehicle. *International Journal of Hydrogen Energy*, 26(8), 873–7.
- Huot, J., Akiba, E., Ogura, T., & Ishido, Y. (1995). Crystal structure, phase abundance and electrode performance of Laves phase compounds $(Zr, A)V_{0.5}Ni_{1.1}Mn_{0.2}Fe_{0.2}$ (A:Ti, Nb or Hf). *Journal of Alloys and Compounds*, 218(1), 101–109.
- Iwakura, C., Kim, I., Matsui, N., Inoue, H., & Matsuoka, M. (1995). Surface modification of laves-phase $ZrV_{0.5}Mn_{0.5}Ni$ alloy electrodes with an alkaline solution containing potassium borohydride as a reducing agent. *Electrochimica Acta*, 40(5), 561–566.

- Jiansheng, C., Xueping, G., Dongfeng, L., & Xingdi, Z. (2001). Activation behavior of the Zr-based Laves phase alloy electrode. *Journal of Power Sources*, 93, 141–144.
- Joubert, J.-M., Latroche, M., Percheron-Guégan, A., & Bouet, J. (1996). Improvement of the electrochemical activity of Zr-Ni-Cr Laves phase hydride electrodes by secondary phase precipitation. *Journal of Alloys and Compounds*, 240(1-2), 219–228.
- Jung, J.-H., Liu, B.-H., & Lee, J.-Y. (1998). Activation behavior of Zr Ti Cr Mn V Ni alloy electrode modified by the hot-charging treatment. *Journal of Alloys and Compounds*, 264, 306–310.
- Jurczyk, M., Okonska, I., Nowak, M., & Jarzebski, M. (2008). Mg-based nanomaterials for energy storage. *Journal of Optoelectronics and Advanced Materials*, 10(4), 907–912.
- Jurczyk, M., Smardz, L., Okonska, I., Jankowska, E., Nowak, M., & Smardz, K. (2008). Nanoscale Mg-based materials for hydrogen storage. *International Journal of Hydrogen Energy*, 33(1), 374–380.
- Kaabi, A., Khaldi, C., & Lamloumi, J. (2016). Thermodynamic and kinetic parameters and high rate discharge-ability of the AB₅-type metal hydride anode. *International Journal of Hydrogen Energy*, 41(23), 9914–9923.
- Kim, S., Lee, J., & Park, H. (1994). A study of the activation behaviour of ZrCrNiLa metal hydride electrodes in alkaline solution. *Journal of Alloys and Compounds*, 205, 225–229.
- Kim, S. Y., Chourashiya, M. G., Park, C. N., & Park, C. J. (2013). Electrochemical performance of NAFION coated electrodes of hydriding combustion synthesized MgNi based composite hydride. *Materials Letters*, 93, 81–84.
- Kopczyk, M., Wojcik, G., Mlynarek, G., & Siercznska, A. (1996). Electrochemical absorption-desorption of hydrogen on multicomponent Zr-Ti-V-Ni-Cr-Fe alloys in alkaline solution. *Journal of Applied Electrochemistry*, 26, 639–645.
- Kuriyama, N., Endo, Y., Sakai, T., & Uehara, I. (1996). Activation behavior of AB₂-type metal hydride electrodes. *Journal of Alloys and Compounds*, 238, 128–140.
- Landi, B. J., Ganter, M. J., Cress, C. D., DiLeo, R. a., & Raffaele, R. P. (2009). Carbon nanotubes for lithium ion batteries. *Energy & Environmental Science*, 2(6), 638.
- Li, Y., Wang, A., Li, J., & Chen, Q. (2013). A Brief Analysis of Global Rare Earth Trade Structure, *Advanced Materials Research* 737, 3324–3331.

- Li, Z. P., Higuchi, E., Liu, B. H., & Suda, S. (1999). Electrochemical properties and characteristics of a fluorinated AB₂-alloy, *295*, 593–600.
- Linden, D., & Reddy, T. B. (2011). *Handbook of Batteries*. (T. B. Reddy, Ed.) (4th ed.). McGraw-Hill.
- Liu, B.-H., Jung, J. H., Lee, H.-H., Lee, K.-Y., & Lee, J.-Y. (1996). Improved electrochemical performance of AB₂-type metal hydride electrodes activated by the hot-charging process. *Journal of Alloys and Compounds*, *245*(96), 132–141.
- Liu, B.-H., & Lee, J.-Y. (1997). The electrochemical activation and surface properties of Zr-based AB₂ metal hydride electrodes. *Journal of Alloys and Compounds*, *255*(1-2), 43–49.
- Liu, Y., Pan, H., Gao, M., & Wang, Q. (2011). Advanced hydrogen storage alloys for Ni/MH rechargeable batteries. *Journal of Materials Chemistry*, *21*(13), 4743.
- Ma, H., Cheng, F., & Chen, J. (2012). Nickel-Metal Hydride (Ni-MH) Rechargeable Batteries. In *Electrochemical Technologies for Energy Storage and Conversion* (pp. 175–237). Wiley.
- Martinez, P. S., Ruiz, F. C., & Visintin, A. (2013). Influence of Different Electrolyte Concentrations on the Performance of an AB₂-Type Alloy. *Journal of The Electrochemical Society*, *161*(3), A326–A329.
- Matsuoka, M., & Tamura, K. (2007). Effects of mechanical grinding on initial activation and rate capability of Zr–Ti based Laves phase alloy electrode. *Journal of Applied Electrochemistry*, *(37)*, 759–764.
- McCormack, M., Badding, M. E., Vyas, B., Zahurak, S. M., & Murphy, D. W. (1996). The Role of Microcracking in ZrCrNi Hydride Electrodes. *Journal of The Electrochemical Society*, *143*(2), L31–L33.
- Nishimura, K., Takasaki, T., & Sakai, T. (2013). Introduction of large-sized nickel-metal hydride battery GIGACELL for industrial applications. *Journal of Alloys and Compounds*, *580*, 353–358.
- Oesterreicher, H., & Bittner, H. (1980). Hydride formation in La_{1-x}Mg_xNi₂. *Journal of the Less Common Metals*, *73*(2), 339–344.
- Okada, M., Kuriwa, T., Kamegawa, A., & Takamura, H. (2002). Role of intermetallics in hydrogen storage materials. *Materials Science and Engineering A*, *329-331*, 305–312.

- Peng, X., Liu, B., Zhou, Y., Fan, Y., Yang, Y., & Li, Q. (2013). Microstructures and Electrochemical Hydrogen Storage. *Int. J. Electrochem. Sci*, 8, 2262–2271.
- Popa, N. C. (1998) The (hkl) Dependence of Diffraction-Line Broadening Caused by Strain and Size for all Laue Groups in Rietveld Refinement. *Journal of Applied Crystallography*, 31, 176-180.
- Roscher, M. A., Bohlen, O., & Vetter, J. (2011). OCV Hysteresis in Li-Ion Batteries including Two-Phase Transition Materials. *International Journal of Electrochemistry*, 1–6.
- Ruggeri, S., & Roué, L. (2003). Correlation between charge input and cycle life of MgNi electrode for Ni–MH batteries. *Journal of Power Sources*, 117(1-2), 260–266.
- Sakai, T., Uehara, I., & Ishikawa, H. (1999). R&D on metal hydride materials and Ni-MH batteries in Japan. *Journal of Alloys and Compounds*, 293, 762–769.
- Schüler, D., Buchert, M., Liu, R., Dittrich, S., & Merz, C. (2011). Study on Rare Earths and Their Recycling. *Öko-Institut e , Abschlussbericht*, 49(January), 30–40.
- Shen, H., Bendersky, L. A., Young, K., & Nei, J. (2015). Fine Structure in Multi-Phase $Zr_8Ni_{21}-Zr_7Ni_{10}-Zr_2Ni_7$ Alloy Revealed by Transmission Electron Microscope, *Materials* 8(7), 4618–4630.
- Soria, M. L., Chacón, J., & Hernández, J. C. (2001). Metal hydride electrodes and Ni/MH batteries for automotive high power applications. *Journal of Power Sources*, 102(1-2), 97–104.
- Stein, F., Palm, M., & Sauthoff, G. (2004). Structure and stability of Laves phases. Part I. Critical assessment of factors controlling Laves phase stability. *Intermetallics*, 12(7-9), 713–720.
- Stempel, R. C., Ovshinsky, S. R., Gifford, P. R., & Corrican, D. A. (1998). Nickel-metal hydride: ready to serve. *IEEE SPECTRUM*, November, 29-34.
- Suciu, C., Gagea, L., Hoffmann, A. C., & Mocean, M. (2006). Sol–gel production of zirconia nanoparticles with a new organic precursor. *Chemical Engineering Science*, 61, 7831–7835.
- Sun, D., Enoki, H., Gintl, F., & Akiba, E. (1999). New approach for synthesizing Mg-based alloys. *Journal of Alloys and Compounds*, 285(1-2), 279–283.
- Sun, D., Latroche, M., & Percheron-Guegan, A. (1997). Activation behaviour of mechanically Ni-coated Zr-based Laves phase hydride electrode. *Journal of Alloys and Compounds*, 257, 302–305.

- Sun, J. C., Zhang, Y. J., Ji, S. J., & Yu, Z. W. (2002). The Effects of Pretreatment on Activation Performance of ZrCr_{0.7}Ni_{1.3} Alloys. *Journal of New Materials for Materials for Electrochemical Systems Journal of New Materials for Electrochemical Systems*, 5, 31–34.
- Tammela, P. (2012). Preparation and characterization of a metal hydride electrode. PhD Thesis. Uppsala University.
- Tamura, T., Kazumi, T., Kamegawa, A., Takamura, H., & Okada, M. (2003). Protium absorption properties and protide formations of Ti-Cr-V alloys. *Journal of Alloys and Compounds*, 356-357, 505–509.
- Tan, S., Shen, Y., Onur Şahin, E., Noréus, D., & Öztürk, T. (2016). Activation behavior of an AB₂ type metal hydride alloy for NiMH batteries. *International Journal of Hydrogen Energy*, 41(23), 9948–9953.
- Taniguchi, A., Fujioka, N., Ikoma, M., & Ohta, A. (2001). Development of nickel/metal-hydride batteries for EVs and HEVs. *Journal of Power Sources*, 100(1-2), 117–124.
- Tliha, M., Boussami, S., Mathlouthi, H., Lamloumi, J., & Percheron-Guégan, A. (2010). Electrochemical characteristics of AB₅-type hydrogen storage alloys. *Journal of Alloys and Compounds*, 506(2), 559–564.
- Tsukahara, M., Takahashi, K., Mishima, T., Isomura, A., & Sakai, T. (1996). V-based solid solution alloys with Laves phase network: Hydrogen absorption properties and microstructure. *Journal of Alloys and Compounds*, 236(1-2), 151–155.
- Uehara, I., Sakai, T., & Ishikawa, H. (1997). The state of research and development for applications of metal hydrides in Japan. *Journal of Alloys and Compounds*, 253-254, 635–641.
- Wang, X.-L., Suda, S., & Wakao, S. (1994). Improved Surface Properties of Zr-M-Ni Hydride Electrodes by Oxidation Treatment. *Zeitschrift Fur Physikalische Chemie*, 183, 297–302.
- Willems, J. (1984). *Metal Hydride Electrodes Stability of LaNi₅-Related Compounds*. PhD Thesis. Philips Research Laboratories.
- Wu, M. S., Wu, H. R., Wang, Y. Y., & Wan, C. C. (2000). Surface treatment for hydrogen storage alloy of nickel/metal hydride battery. *Journal of Alloys and Compounds*, 302(1-2), 248–257.
- Yan, D., & Cui, W. (1999). Preparation and properties of no-binder electrode Ni/MH battery, *Journal of Alloys and Compounds*, 293-295, 780–783.

- Yan, D., Sandrock, G., & Suda, S. (1995). Activation of $Zr_{0.5}Ti_{0.5}V_{0.75}Ni_{1.25}$ alloy electrodes by hot alkaline solutions. *Journal of Alloys and Compounds*, 216(2), 237–242.
- Yang, H. W. (1996). Studies of Electrochemical Properties of $Ti_{0.35}Zr_{0.65}Ni_xV_{(2-x-y)}Mn_y$ Alloys with C14 Laves Phase for Nickel/Metal Hydride Batteries. *Journal of The Electrochemical Society*, 143(2), 429.
- Yartys, V., Noreus, D., & Latroche, M. (2016). Metal hydrides as negative electrode materials for Ni-MH batteries. *Applied Physics A: Materials Science and Processing*, 122(1), 1–11.
- Ye, Z., Noréus, D. & Howlett III, J., R. (2013). Metal hydrides for high-power batteries, *MRS Bulletin* 38(6), 504–508.
- Young, K., Chao, B., Bendersky, L. a., & Wang, K. (2012). $Ti_{12.5}Zr_{21}V_{10}Cr_{8.5}Mn_xCo_{1.5}Ni_{46.5-x}$ AB₂-type metal hydride alloys for electrochemical storage application: Part 2. Hydrogen storage and electrochemical properties. *Journal of Power Sources*, 218, 487–494.
- Young, K., Fetcenko, M. A., Li, F., & Ouchi, T. (2008). Structural, thermodynamic, and electrochemical properties of $Ti_xZr_{1-x}(VNiCrMnCoAl)_2$ C14 Laves phase alloys. *Journal of Alloys and Compounds*, 464(1-2), 238–247.
- Young, K., Huang, B., Regmi, R. K., Lawes, G., & Liu, Y. (2010). Comparisons of metallic clusters imbedded in the surface oxide of AB₂, AB₅, and A₂B₇ alloys. *Journal of Alloys and Compounds*, 506(2), 831–840.
- Young, K., & Nei, J. (2013). The Current Status of Hydrogen Storage Alloy Development for Electrochemical Applications. *Materials*, 6(10), 4574–4608.
- Young, K., Nei, J., Huang, B., & Fetcenko, M. A. (2011). Studies of off-stoichiometric AB₂ metal hydride alloy: Part 2. Hydrogen storage and electrochemical properties. *International Journal of Hydrogen Energy*, 36(17), 11146–11154.
- Young, K., Nei, J., Ouchi, T., & Fetcenko, M. A. (2011). Phase abundances in AB₂ metal hydride alloys and their correlations to various properties. *Journal of Alloys and Compounds*, 509(5), 2277–2284.
- Young, K., Ouchi, T., & Fetcenko, M. A. (2009). Roles of Ni, Cr, Mn, Sn, Co, and Al in C14 Laves phase alloys for NiMH battery application. *Journal of Alloys and Compounds*, 476(1-2), 774–781.
- Young, K., Ouchi, T., Huang, B., Chao, B., Fetcenko, M. A., Bendersky, L. A., Chiu, C. (2010). The correlation of C14/C15 phase abundance and electrochemical properties in the AB₂ alloys. *Journal of Alloys and Compounds*, 506(2), 841–848.

- Young, K., Ouchi, T., Nei, J., & Wang, L. (2016). Annealing effects on Laves phase-related body-centered-cubic solid solution metal hydride alloys. *Journal of Alloys and Compounds*, 654, 216–225.
- Yu, B., Chen, L., Wen, M., Tong, M., & Chen, D. (2001). Surface modification of AB₂ and AB₅ hydrogen storage alloy electrodes by the hot-charging treatment. *Journal of Materials Science and Technology*, 17(2), 247–251.
- Yuan, X., & Xu, N. (2001). Determination of hydrogen diffusion coefficient in metal hydride electrode by cyclic voltammetry, *Journal of Alloys and Compounds* 316(1-2), 113–117.
- Zhang, Q. A., Lei, Y. Q., Yang, X. G., Ren, K., & Wang, Q. D. (1999). Annealing treatment of AB₂-type hydrogen storage alloys: I. Crystal structures. *Journal of Alloys and Compounds*, 292(1-2), 236–240.
- Zhao, X., & Ma, L. (2009). Recent progress in hydrogen storage alloys for nickel/metal hydride secondary batteries. *International Journal of Hydrogen Energy*, 34(11), 4788–4796.
- Zhu, M., Lu, Y., Ouyang, L., & Wang, H. (2013). Thermodynamic tuning of Mg-based hydrogen storage alloys: A review. *Materials*, 6, 4654–4674.
- Zhu, Y. F., Pan, H. G., Wang, G. Y., Gao, M. X., Ma, J. X., Chen, C. P., & Wang, Q. D. (2001). Phase structure, crystallography and electrochemical properties (M = Fe; Al; Cr; Co), 26, 807–816.
- Züttel, A., Meli, F., & Schlapbach, L. (1995). Surface and bulk properties of the Ti_yZr_{1-y}(V_xNi_{1-x})₂ alloy system as active electrode material in alkaline electrolyte. *Journal of Alloys and Compounds*, 231(1-2), 645–649.

APPENDICES

APPENDIX A

EFFECT OF PLASMA PROCESSING ON ELECTROCHEMICAL BEHAVIOUR OF AN AB₂ ALLOY

A.1 Introduction

Plasma processing is a technique that can be used for nanopowder production (Aktekin et al., 2014), surface coating (Bystrzejewski et al., 2011) and sphereoidisation of powders (Girshick et al., 1993). The technique involves feeding of precursors, usually a powder, into a plasma torch where the temperature is normally in excess of 10000 K. In this study, effect of plasma processing on electrochemical behaviour of a Laves phase AB₂ alloy of composition (Ti_{0.36}Zr_{0.64})(V_{0.15}Ni_{0.58}Mn_{0.20}Cr_{0.07})₂ was investigated.

A.2 Experimental

A photograph and a schematic representation of plasma system used in the current study is given in Figure A.1 and A.2 respectively. The apparatus used in the study is a 30 kW thermal induction plasma system (Tekna Plasma Systems Inc.). The system was operated at 15 kW under the starting pressure of 0.97 bar where the plate current was 2.6 A and the plate voltage was 5.9 kV. This plasma power is considered low, but the power was kept low in order to minimize the evaporation of the precursor powder. The conditions were as follows: sheath gas Ar: 60 slpm, H₂: 6 slpm, central gas (plasma forming gas) Ar: 20 slpm, carrier gas Ar: 5 slpm. The quenching gas was N₂ at a rate of 150 slpm. AB₂ powder was fed into the plasma from the top injector at a rate of 29 g/min.

Electrochemical measurements were carried out in a quite narrow container housing working, counter and reference electrodes. The cell was open to atmosphere.



Figure A.1: Photograph of induction plasma system

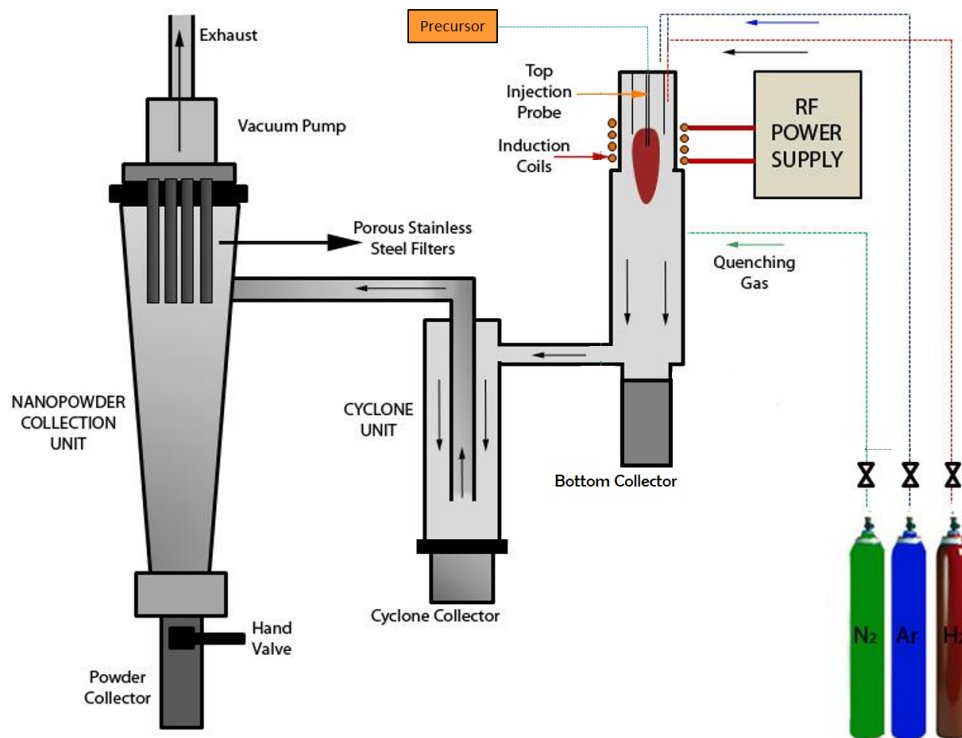


Figure A.2: Schematic of the induction plasma system (Adapted from Aktekin, 2013)

Working electrodes were prepared by mixing active powder with a copper powder (150 μm) in 1:3 weight ratio. The mixture was pressed in a stainless steel die under 400 MPa pressure into a 10 mm-diameter pellet. The pellet was wrapped in a nickel mesh (100 mesh) of 20 mm by 30 mm size. The envelope was spot welded to a 100 mm long-nickel wire of 1.5 mm in diameter used for connection. Similarly, the counter electrode was prepared by a thicker nickel mesh (20 mesh) with surface area larger than the working electrode. As the reference electrode, zinc rod (4 mm-diameter, purity 99.995%) was used. Electrochemical measurements were carried out in 6M KOH electrolyte prepared by dissolving KOH pellets (Sigma-Aldrich) in distilled water (conductivity $<0.2 \mu\text{S}$). Measurements were made using Lanhe CT 2001A battery tester. During the measurements charging was carried out at a current density of 50 mA/g for 8 hours while discharging rate varied over a total of 40 cycles. In the first 20 cycles, the discharge rate was 50 mA/g, while in the last 20 cycles the rate was quite high and had a value of 320 mA/g. Discharge was carried out until the cut-off voltage of -0.75 V vs. Zn electrode.

The crystal structure of powders together with phases present was analysed with X-ray diffraction using Bruker Diffractometer ($\text{Cu-K}\alpha$). Morphology of powders was examined with FEI Nova NanoSEM at 20 kV by attaching the powders to double sided carbon tape.

A.3 Results and Discussion

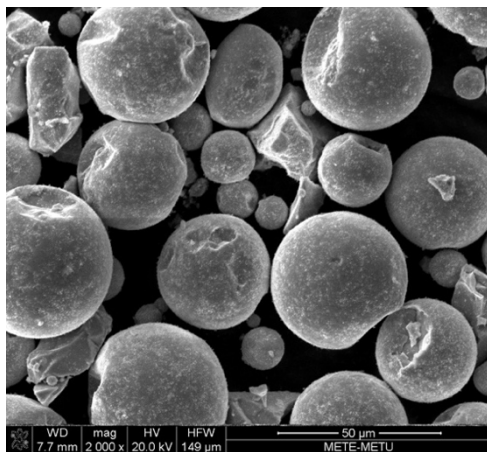
AB_2 alloy powder was fed into the plasma at approximately 29 g/min rate. The powder placed in the feeder was weighed before and after the experiment in order to estimate the powder yield obtained from plasma processing. From 110 g powder fed, 39.8, 38.8 and 5.75 g powders were collected from bottom collector, cyclone and powder collector respectively. This corresponds to 76 % efficiency which is considered to be high considering that the experiment was rather short.

Morphologies of the powders collected from bottom collector, cyclone and powder collector are given in Figures A.3, A.5 and A.6 respectively. It is seen that powders collected from the bottom collector were spheroidised. It was also observed that the

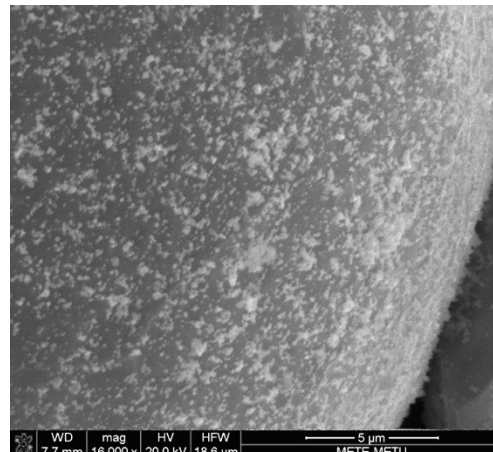
surface of the particles was decorated with nanoparticles condensed from the gas phase. Based on the SEM images, the average particle size of the powders in the bottom collector was $35 \pm 15 \mu\text{m}$. It should be mentioned that plasma gas-flow just above the bottom collector make a 90° turn and powders that are collected in the bottom container are those which could not follow the gas flow due to their relatively high mass.

Figure A.4 shows the EDS analyses of the general composition AB_2 powders collected from the various collectors in the plasma system. It was observed that the composition of the powder collected from the bottom collector did not change significantly. The composition was $\text{Ti}_{12.5}\text{Zr}_{25.5}\text{Ni}_{33.5}\text{V}_9\text{Mn}_{14.6}\text{Cr}_{4.9}$. This should be compared to the original powder which had the composition of $\text{Ti}_{11.9}\text{Zr}_{20.7}\text{Ni}_{35.3}\text{V}_{11.5}\text{Mn}_{14.6}\text{Cr}_{5.9}$.

SEM images of powders collected from the cyclone is given in Figure A.5. It is seen that the powders collected in the cyclone is much smaller. It should be mentioned that here the gas flow makes a 180° turn and that leaves behind particles that have intermediate mass. The average particle size in the cyclone was $17 \pm 6 \mu\text{m}$.



(a)



(b)

Figure A.3: SEM images of plasma processed particles: from bottom collector at (a) 2000x and (b) 16000x magnification.

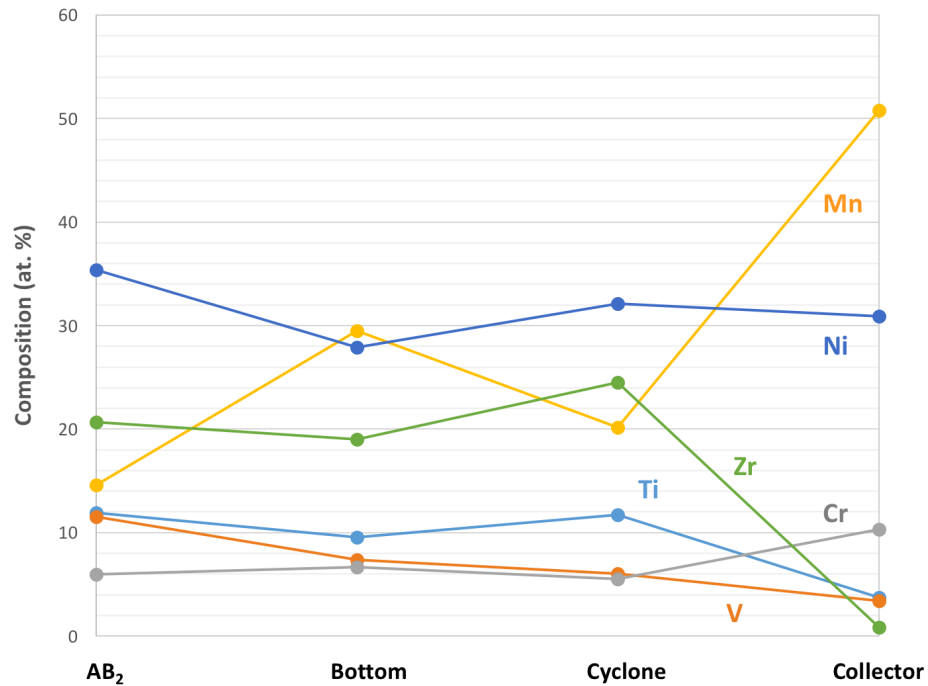


Figure A.4: Compositional change in plasma processed AB₂ powder. Note that the composition of the unprocessed alloy was calculated as Ti_{11.9}Zr_{20.7}Ni_{35.3}V_{11.5}Mn_{14.6}Cr_{5.9} according to EDS results.

Degree of spheroidisation of the particles from the cyclone section is higher, as can be seen in Figure A.5. These powders are covered with smaller particles as was the case in bottom collector.

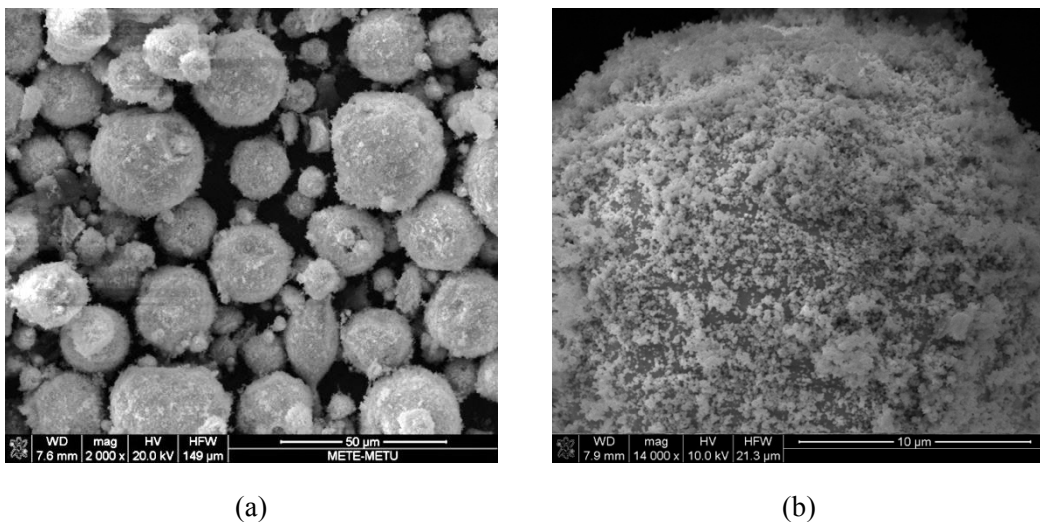


Figure A.5: SEM images of plasma processed particles: from cyclone section at (a) 2000x and (b) 14000x magnification.

The composition of the powder collected from the cyclone is different than that in the bottom collector or starting powder Figure A.6. Powders are poorer in terms of Zr, V and Ni, and richer regarding Ti, Mn and Cr. The general composition is $Ti_{8.4}Zr_{17.2}Ni_{26.3}V_7Mn_{33.5}Cr_{7.4}$.

Powders collected from powder collector are extremely small in size, Figure A.6. SEM images yield an average particle size of 95 ± 21 nm.

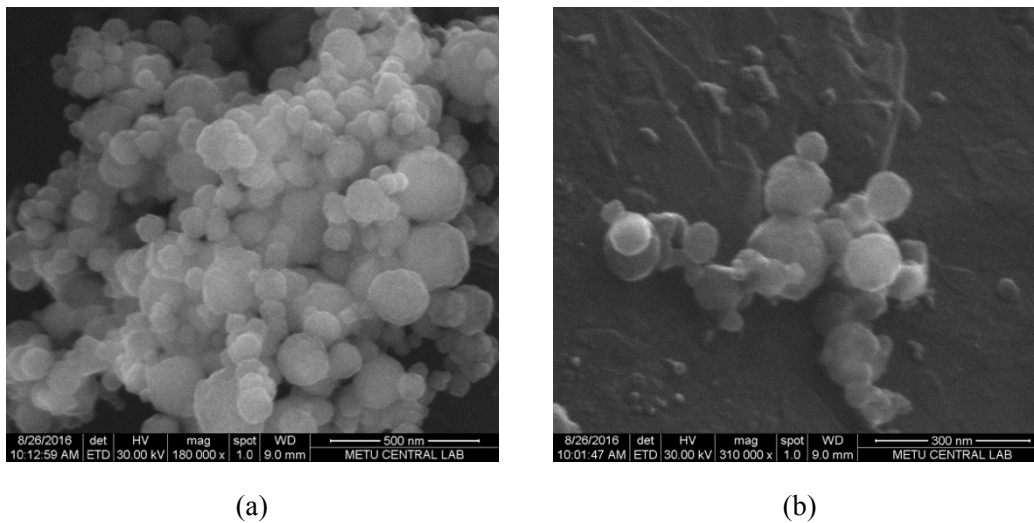


Figure A.6: SEM images of plasma processed particles: from powder collector section at (a) 180000x and (b) 310000x magnification.

The composition of the powder from the powder collector is significantly different than that of the original powder. Nearly 50.8 at. % of the powder composition is Mn. The overall composition is $Ti_{3.9}Zr_1Ni_{21.7}V_{3.2}Mn_{59.9}Cr_{10.3}$. It is seen that the nanopowders obtained from the powder collector are rich in Mn and Cr and poor in terms of Ti and Zr. Thus in the original composition AB_2 alloy A elements are adversely affected by plasma processing.

XRD patterns obtained from bottom collector, cyclone and powder collector are given in Figure A.7. The pattern from powders in bottom collector and cyclone are almost the same as the starting powder. XRD pattern from powders from powder collector is however drastically affected as there are no well-defined peaks in the pattern. This is compatible with nanosized particles which leads to extreme broadening of peaks. Most

broad peaks are compatible with those of original powder except for the one at $2\theta=50^\circ$. This is probably due to the formation of ZrO_2 .

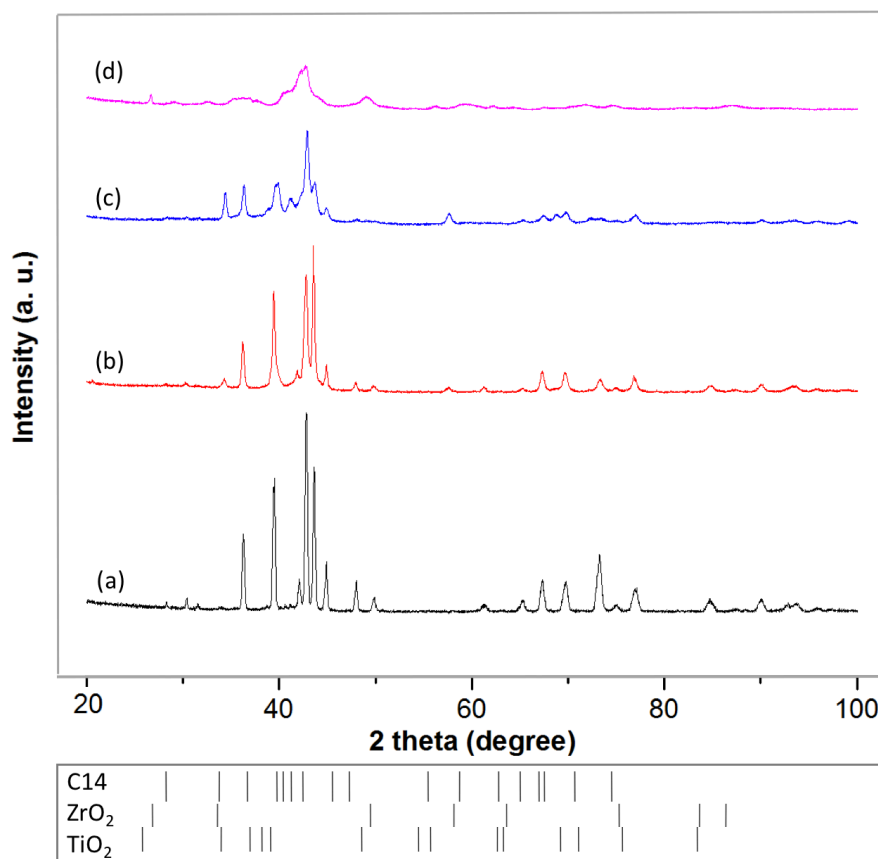


Figure A.7: XRD patterns of (a) unprocessed, and plasma processed AB_2 powders collected from (b) bottom collector, (c) cyclone and (d) nanopowder collector sections.

Powders were characterized electrochemically using pressed electrode. discharge capacity vs. cycle number obtained from powders are given in Figure A.8. The curve for starting powder was included for comparison. The powder from the bottom collector as well as from cyclone does not give any significant capacity over the two discharge regimes.

Nanopowders collected from the powder collector display an interesting behaviour. No capacity was detected in the first regime where the discharge rate was 50 mA/g. In the second regime of high discharge rate (320 mA/g), the capacity is observed starting from 26th cycle and steadily increased to 140 mAh/g.

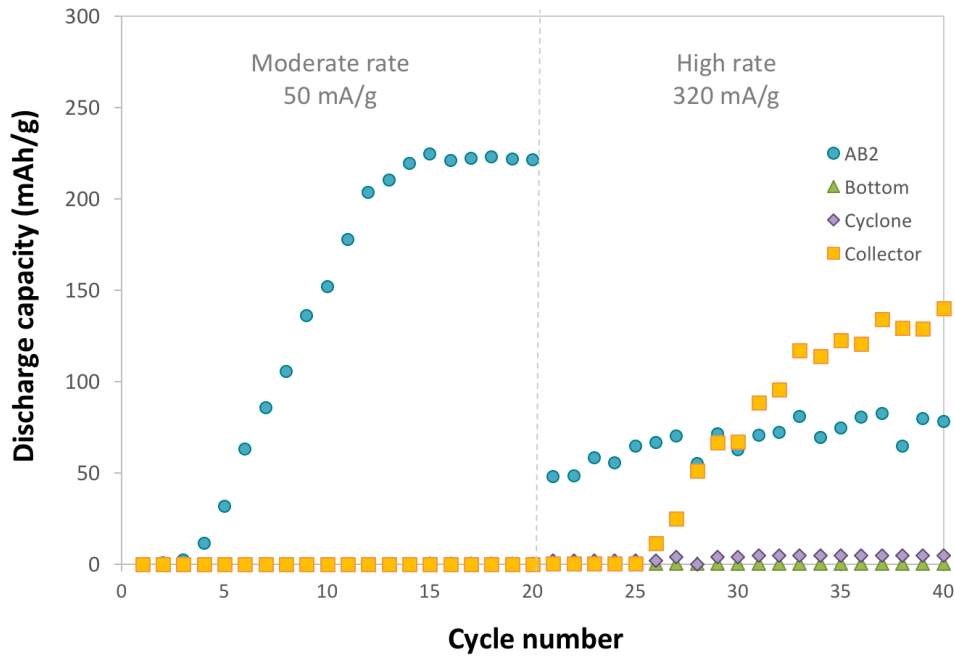


Figure A.8: Discharge capacity vs. cycle number plot of the electrodes prepared from plasma processed AB₂ powders. Note that there are two discharge regimes of 20 cycles each.

A.4 Conclusions

From the current study on electrochemical performance of plasma processed AB₂ powder following conclusions can be made:

- i) Powders collected from 90° turn of plasma gases have the same composition as the starting powder and have an average size of $35 \pm 15 \mu\text{m}$.
- ii) Powders collected from 180° turn of plasma gases are $17 \pm 6 \mu\text{m}$ in size and therefore much finer than the starting powder. The composition in these powders are overall the same as the starting powder.
- iii) Powders collected from powder collector are much finer and has a size of $95 \pm 21 \text{ nm}$. The particles are richer in Mn and Cr and poorer in Ti and Zr elements.
- iv) Electrochemical tests have shown that only nanopowders collected from powder collector develop any significant capacity. It is observed that nanopowders obtained with plasma processing has significantly improved performance in high discharge rate. Nanopowder in high discharge rate had a

capacity of 140 mAh/g. The capacity of original powder under the same condition was 78 mAh/g.

The study reported above indicates that nanopowders could have a significant advantage in applications requiring fast discharge rate.

A.5 References

- Aktekin, B., Çakmak, G., Öztürk, T. (2014) Induction thermal plasma synthesis of Mg₂Ni nanoparticles, *International Journal of Hydrogen Energy*, 39(18), 9859–9864
- Aktekin, B. (2013) Induction Plasma Synthesis of Mg-Ni Nanoparticles. Master's Thesis. Middle East Technical University.
- Bystrzejewski, M., Károly, Z., Szépvölgyi, J., Huczko, A., & Lange, H. (2011). Continuous synthesis of controlled size carbon-encapsulated iron nanoparticles. *Materials Research Bulletin*, 46(12), 2408-2417.
- Girshick, S., Chiu, C., & McMurry, P. (1990). Time-dependent aerosol models and homogeneous nucleation rates. *Aerosol Science and Technology*, 13(4), 465-477.

APPENDIX B

Mg-Cu ALLOYS AS NEGATIVE ELECTRODES FOR Ni/MH BATTERIES

B.1 Introduction

Mg based alloys are attractive materials for hydrogen storage alloys due to their low density, abundance, and their high hydrogen storage capacity (7.6 wt. % with MgH_2). Thermodynamic and kinetic properties of Mg-alloys are unfavourable for their use as hydrogen storage alloys for batteries as they require high desorption temperatures around 300°C at atmospheric pressure (Zhu et al. 2013).

Since pure Mg is highly stable, Mg-based alloys that are considered as negative electrode materials have A_2B form which are known to have significantly lower stability (Reilly and Wiswall, 1967). The most important representatives are Mg_2Ni (Iwakura et al., 1998; Szajek et al., 2007; Kim et al., 2013) and Mg_2Cu (Reilly and Wiswall, 1967; Arcot et al., 1994; Sun et al., 1999; Akyıldız et al., 2006; Jurczyk et al., 2007; Szajek et al., 2007)

One of the earliest studies on the Mg-Cu alloy was carried out by Reilly and Wiswall (1967). The Mg-Cu alloy prepared by induction melting was reported to contain high amount of Mg_2Cu with small amount of MgCu_2 . It was stated that from the phases that are present in the cast alloy only Mg_2Cu reacted with hydrogen. In the study, several alloy compositions were studied in order to maximize the gas phase hydrogen storage capacity. Starting from 44.1 wt. % to 90.5 wt. % Mg content, it was seen that the wt. % hydrogen storage capacity increased from 2.72 to 6.62. In another study by Sun et al. (1999) it was reported that the hydrogen storage capacity of composition Mg_2Cu is 2.72 wt. % whereas for higher Mg content this value increases up to 6.62 wt. % H with 90.5 wt. % Mg and 9.5 wt. % Cu. Again a high hydrogen storage capacity in this alloy system was obtained by Akyıldız et al. (2006) thin films. In their study 5.9 wt. %

hydrogen capacity obtained with thin film of $\text{Mg}_{90}\text{Cu}_{10}$ composition where the desorption temperature was around 100°C .

Jurczyk et al. (2007), used mechanical alloying in order to prepare the nanocrystalline Mg_2Ni and Mg_2Cu alloys with the average crystallite size of 20 nm. They found that the milled alloy had 25 mAh/g of discharge capacity. This was despite that fact that the alloy had a gas-phase storage capacity of 2.6 wt. %. Szajek et al. (2007) in a similar study reported a discharge capacity of 26.5 mAh/g.

Another problem limiting the usage of Mg-alloys in batteries is corrosion in the alkaline environment. MgO or $\text{Mg}(\text{OH})_2$ layer formation due to corrosion of the alloy inhibits H_2 dissociation at the surface and H diffusion to the bulk. The irreversible oxidation of the Mg-based alloy operating in relatively concentrated KOH is inevitable unless the necessary precautions are taken. This causes a decrease in active material amount and therefore lowers the capacity (Ruggeri & Roue, 2003).

One approach to prevent the corrosion of Mg is NAFION coating. NAFION solution (perfluorosulfonic acid-PTFT copolymer) may be used to coat the powders or the whole electrode. It forms a rough but continuous film on the surface whereby preventing the direct contact of Mg-alloy with alkaline medium. Kim et al., (2013) coated pellets of Mg-Ni with NAFION and obtained a capacity of 408 mAh/g which was much higher than the bare electrode (156 mAh/g). The increase in discharge capacity is attributed due to protection of the alloy powders that included all the active mass in hydrogenation process.

In this study the aim is to develop a Mg-Cu alloy with high electrochemical capacity. Also the effect of NAFION coating on the electrode will be examined.

B.2 Experimental

Mg-Cu alloy was prepared by induction melting using a Linn High Therm vacuum/pressure induction melting furnace. For this purpose, pieces of 235 g Mg and 314 g Cu were prepared and placed in a graphite crucible. Even though the resulting composition was aimed as Mg_2Cu , Mg was added in excess so as to compensate the

evaporation of Mg. The furnace was taken to vacuum down to 2×10^{-2} mbar twice, being flushed to 1 bar of Ar inbetween. Melting was then carried out under 7 bar Ar pressure.

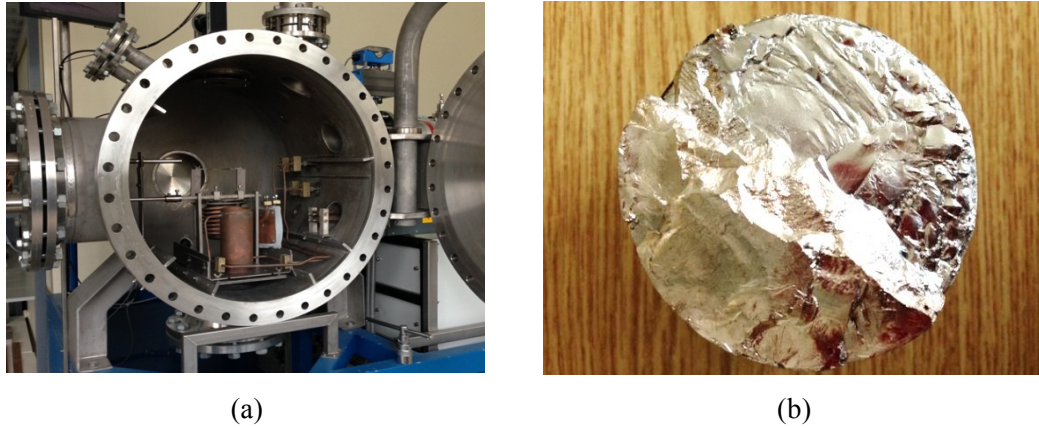


Figure B.1: (a) the induction melting furnace and (b) fracture surface of as-cast Mg-Cu alloy

Following melting, the alloy was crushed into powder. XRD pattern of the alloy obtained as a result of this melting is given in Figure B.2. It shows that the alloy is composed of two phases one of which was Mg_2Cu as aimed, and the other is $MgCu_2$. The result of the Rietveld analysis yields 81 wt. % Mg_2Cu and 19 wt. % $MgCu_2$, Table B.1. The two phase structure was confirmed by SEM examination, Figure B.3.

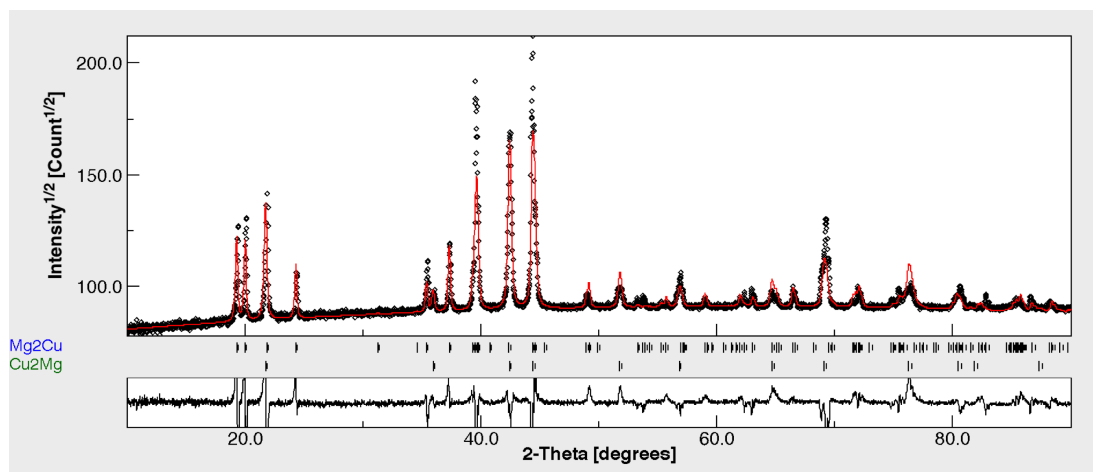


Figure B.2: Fitted XRD pattern of Mg-Cu alloy

Table B.1: Phases present in Mg-Cu alloy and their lattice parameters according to Rietveld analysis

Phase	wt. %	Crystal structure	Lattice parameters (Å)		
			a (Å)	b (Å)	c (Å)
Mg ₂ Cu	81	Orthorhombic	5.260	9.036	18.312
Cu ₂ Mg	19	Cubic	7.052	7.052	7.052

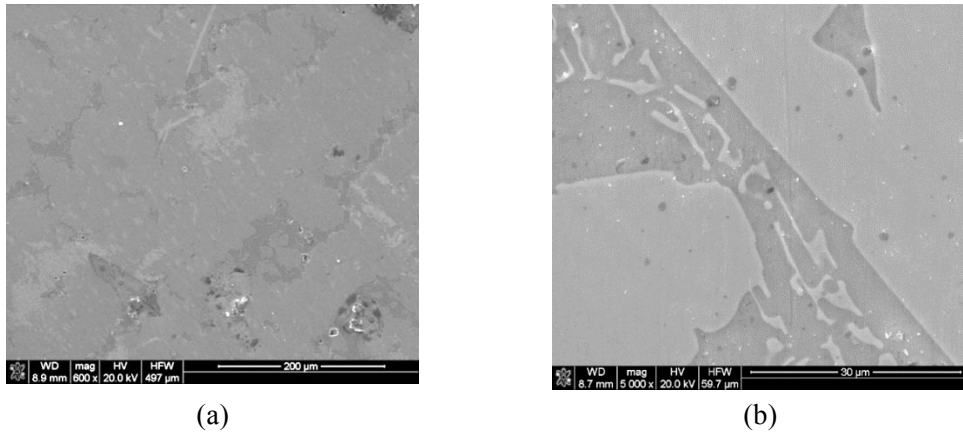


Figure B.3: Microstructure of the as-cast alloy under SEM at 600x (a) and 5000 (b).

Thus it was observed that the alloy contains MgCu₂ besides Mg₂Cu. The Cu content in the alloy was considered relatively high. This might be due to evaporation of Mg which was higher than expected.

Therefore, in the first milling process the alloy powder was milled with the addition of Mg aiming Mg₂Cu. The alloy was milled in Retsch MA 400 planetary ball mill with addition of Mg powder to have Mg-50 wt. %Cu under 10 bar Ar-35 vol. % H₂. The ball to powder ratio was 10:1 in a 50 cc stainless steel vial. The milling was carried out at 250 rpm and a sequence of 5 minute-revolution and 2 minute-break was followed for 50 hours of total milling time.

Another milling operation on the as-cast alloy without any additive was processed in H₂ atmosphere. The alloy was milled this time under 10 bar pure H₂ in a 50 cc stainless

steel vial with 10:1 ball to powder ratio. The powder was milled for total of 80 hours with 20 minute-periods with 5 minute-break at the same rpm with the previous milling operation.

Electrochemical measurements were carried out in a double compartment glass cell, one compartment housing working and reference electrode and the other housing the counter electrode joined together with a glass frit (100 μm pore size). The pellet was prepared using Mg-Cu alloy was mixed with nickel powder (1:3 ratio) and pressed into 10 mm diameter pellets under 400 MPa. The pellets were coated with NAFION using the solution prepared by 5 % NAFION in isopropyl alcohol. Coating was applied for 5 times on each side by applying drops on each surface. The pellet was dried between each application. The prepared pellet was wrapped with the nickel mesh (100 mesh) 20 mm by 30 mm in size. The envelope was spot welded to a 100 mm long-nickel wire of 1.5 mm in diameter. Nickel sheet with dimensions of 35 mm by 35 mm was used as the counter electrode. Radiometer XR400 Hg/HgO electrode was used as the reference electrode. The measurements were carried out in 6M KOH electrolyte prepared by dissolving KOH pellets (Sigma-Aldrich) in distilled water (conductivity $<0.2 \mu\text{S}$). Measurements were made using Lanhe CT 2001A battery tester. Charging was carried out at a current density of 50 mA/g for 8 hours. Discharging was carried out at the same current density until -0.6 V vs. Hg/HgO reference.

B.3 Results and Discussion

Milling of powders were carried out in two different conditions; milling under Ar-35 vol. % H_2 for 50 hours and milling under pure H_2 for 80 hours. The XRD patterns of the powders obtained after the two milling processes together with the pattern for the as-cast alloy are given in Figure B.4. It is seen that the as-cast alloy is crystalline with well-defined peaks. The XRD pattern obtained from the alloy milled with Ar-35 % H_2 has broad peaks implying that crystallite size is much finer with milling. In milling under hydrogen, the pattern again contains broad peaks but probably crystallite size is not as fine as that with milling with Ar-35 % H_2 .

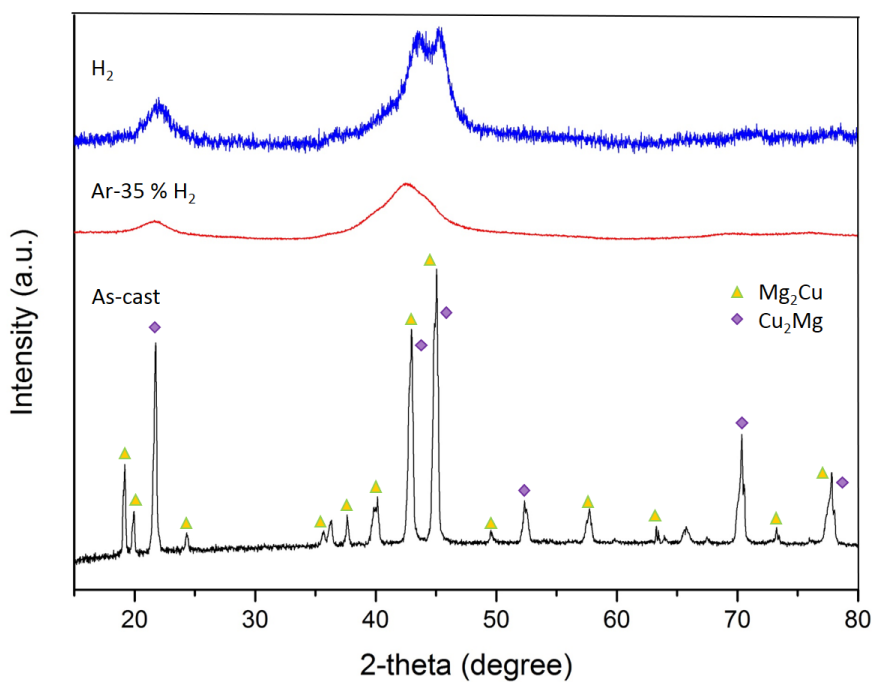


Figure B.4: XRD patterns for Mg-Cu alloy milled in Ar-35 vol. % H₂ and pure hydrogen atmospheres

Electrochemical measurements with electrodes prepared using uncoated pellets did not give discharge capacity. Corrosion were visible in the pellets. Even charging was not possible implying that the electrode was non-conducting.

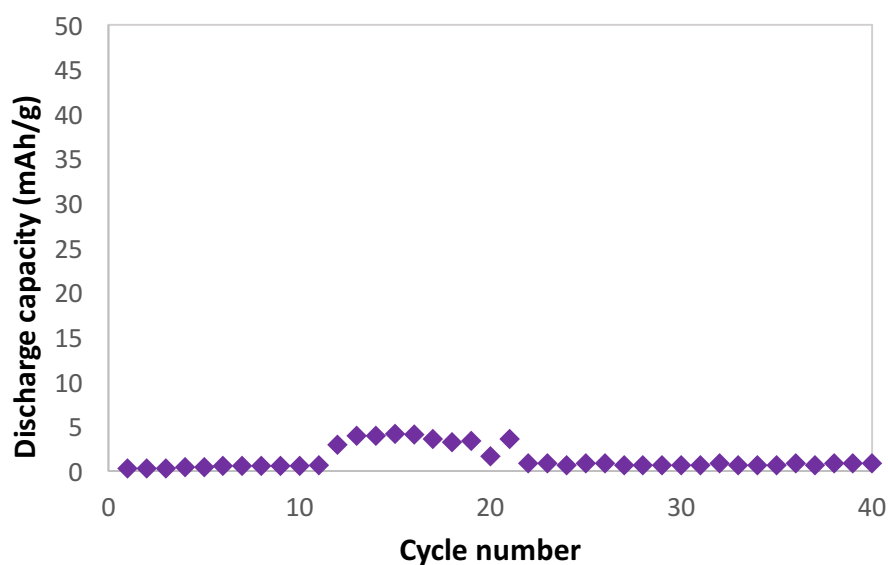


Figure B.5: Discharge capacity vs. cycle number graph for NAFION coated Mg-Cu electrode milled under pure H₂ for 80 hours.

No capacity was observed in the sample milled under Ar-35% H₂ also. Some capacity was detected in powders milled for 80 hours under H₂. The capacity was not more than 4.2 mAh/g, as seen in Figure B.5.

It was seen that the capacity is non-zero after the 11th cycle. The capacity decreases, however, after 21 cycle down to zero. This drop in capacity might be due to corrosion taking place in the pellet. Because with dropping method to coat the pellets with NAFION it is not easy to obtain a smooth and evenly coated surface. It may be suggested that with an improved coating better results could be obtained.

B.4 References

- Akyıldız, H., Özenbaş, M., Öztürk, T. (2006) Hydrogen Storage in Magnesium Based Thin Films, *International Journal of Hydrogen Energy*, 31(10), 1379-1382.
- Arcot, B., Murarka, S. P., Clevenger, L. A., Hong, Q. Z., Ziegler, W., Harper, J. M. E. (1994) Kinetics of Intermetallic Formation in Free Standing Cu/Mg Multilayer Thin Films, *Journal of Applied Physics*, 76(9), 5161.
- Iwakura, C., Inoue, H., Zhang, S. G., Nohara, S. (1998) Hydriding and electrochemical characteristics of a homogeneous amorphous Mg₂Ni-Ni composite, *Journal of alloys and Compounds*, 270, 142-144.
- Jurczyk, M., Okonska, I., Iwansieczko, W., Jankowska, E., Drulis, H. (2007) Thermodynamics and Electrochemical Properties of Nanocrystalline Mg₂Cu-type Hydrogen Storage Materials, *Journal of alloys and Compounds*, 429, 316-320.
- Kalisvaart, W. P., Harrower, C. T., Haagsma, J., Zahiri, B., Lubber, E. J., Ophus, C., Poirier, E., Fritzsche, H., Mitlin, D. (2010) Hydrogen storage in binary and ternary Mg based alloys: A comprehensive experimental study, *International Journal of Hydrogen Energy*, 35, 2091–2103.
- Kim, S.-Y., Chourashiya, M. G., Park, C.-N., Park, C.-J. (2013) Electrochemical performance of NAFION coated electrodes of hydriding combustion synthesized MgNi based composite hydride. *Materials Letters*, 93, 81–84.
- Szajek, A., Jurczyk, M., Okonska, I., Smardz, K., Jankowska, E., Smardz, L. (2007) Electrochemical and electronic properties of nanocrystalline Mg-based hydrogen storage materials, *Journal of Alloys and Compounds*, 436, 345-350.

- Sun, D., Enoki, H., Gintl, F., Akiba, E. (1999) New approach for synthesizing Mg-based alloys. *Journal of Alloys and Compounds*, 285, 279–283.
- Ruggeri, S., Roue, L. (2003) Correlation between charge input and cycle life of MgNi electrode for Ni-MH batteries, *Journal of Power Sources*, 117, 260-266.
- Reilly J. J., Wiswall R. H., 1967, Reaction of hydrogen with alloys of magnesium and copper, *Inorganic Chemistry*, 6(12), 2220.
- Zhu, M., Lu, Y., Ouyang, L., Wang, H. (2013) Thermodynamical Tuning of Mg-Based Hydrogen Storage Alloys: A Review, *Materials*, 6, 4654-4674.